2019

Comparison of two bidirectional atmosphere-surface exchange models for elemental mercury

Jingliang Hao
University of Windsor

Comparison of two bidirectional atmosphere-surface exchange models for elemental mercury

By

Jingliang Hao

A Thesis
Submitted to the Faculty of Graduate Studies
through the Department of Civil and Environmental Engineering
in Partial Fulfillment of the Requirements for
the Degree of Master of Applied Science
at the University of Windsor

Windsor, Ontario, Canada

2019

Comparison of two bidirectional atmosphere-surface exchange models for elemental mercury

by

Jingliang Hao

APPROVED BY:

X. Chen
Department of Electrical and Computer Engineering

N. Biswas
Department of Civil and Environmental Engineering

X. Xu, Advisor
Department of Civil and Environmental Engineering

May 1, 2019

DECLARATION OF ORIGINALITY

I hereby certify that I am the sole author of this thesis and that no part of this thesis has been published or submitted for publication.

I certify that, to the best of my knowledge, my thesis does not infringe upon anyone's copyright nor violate any proprietary rights and that any ideas, techniques, quotations, or any other material from the work of other people included in my thesis, published or otherwise, are fully acknowledged in accordance with the standard referencing practices. Furthermore, to the extent that I have included copyrighted material that surpasses the bounds of fair dealing within the meaning of the Canada Copyright Act, I certify that I have obtained a written permission from the copyright owner(s) to include such material(s) in my thesis and have included copies of such copyright clearances to my appendix.

I declare that this is a true copy of my thesis, including any final revisions, as approved by my thesis committee and the Graduate Studies office, and that this thesis has not been submitted for a higher degree to any other University or Institution.

ABSTRACT

This study compared two bidirectional atmosphere-surface exchange models by Wang et al. (2014) and Wright & Zhang (2015) for one monitoring site in the state of Georgia in the United States of evergreen needleleaf forest and deciduous broadleaf forest in summer and winter. Input data includes observed GEM concentrations and simulated meteorological data from June 2010 to September 2010 and from December 2010 to March 2011. For evergreen needleleaf forest in summer, the net emission flux estimated by Wang's model was greater than that by Wright & Zhang's (0.5 pg $m^{-2}s^{-1}$ vs. 0.18 pg $m^{-2}s^{-1}$). For deciduous broadleaf forest in summer, the net emission flux predicted by Wang's model was smaller than that by Wright & Zhang's (0.1 pg $m^{-2}s^{-1}$ vs. 0.29 pg $m^{-2}s^{-1}$). However, regardless of land cover in winter, the net flux produced by Wang's model was emission flux (0.21 pg $m^{-2}s^{-1}$ for evergreen needleleaf forest and 0.18 pg $m^{-2}s^{-1}$ for deciduous broadleaf forest) while that simulated by Wright & Zhang's model was deposition flux (0.59 pg $m^{-2}s^{-1}$ for evergreen needleleaf forest and 0.49 pg $m^{-2}s^{-1}$ for deciduous broadleaf forest). Additionally, stomata resistance, in-canopy aerodynamic resistance, stomata emission velocity, GEM compensation point concentration in stomata, GEM compensation point concentration in soil, stomata emission flux, soil emission flux, and net flux had large differences (≥100%) between the two models. The dominant factors resulting in these differences were identified. Wright & Zhang's model is more appropriate for simulating GEM exchange flux in winter when a net deposition flux is expected.

DEDICATION

This thesis is dedicated to my parents.

ACKNOWLEDGEMENTS

I am highly thankful to Dr. Che-Jen Lin of Lamar University and Dr. Leiming Zhang of Environment Canada for providing the dry depositing models and the data used in my research, and their help during my research. I would like to thank my supervisor, D. Iris Xiaohong Xu, for her support, encouragement, guidance, and patience. My sincere gratitude also goes to my committee members Dr. Nihar Biswas and Dr. Xiang Chen for their comments and suggestions. I gratefully acknowledge Mr. Tianchu Zhang at University of Windsor for his help in data processing. I would like to thank my family for their continued encouragement and support. Founding of this program is provided by Environment and Climate Change Canada and The Natural Sciences and Engineering Research Council of Canada.

TABLE OF CONTENTS

LIST OF TABLES

LIST OF FIGURES

LIST OF ABBREVIATIONS/SYMBOLS

ANOVA – Analysis of Variance

b_{vpd} – empirical water vapour pressure deficit constant

C – pollutant concentration

coszen – cosine value of zenith angle

D – ambient water vapor pressure deficit

DI – gaseous elemental mercury diffusivity

DV – water vapor diffusivity

f_D – water vapor pressure deficit of air

F_c – gaseous elemental mercury cuticle emission flux

F_d – gaseous elemental mercury deposition flux

f_{fixed} – the fraction of GOM fixed into tissue

F_g – gaseous elemental mercury soil emission flux

f_{oc} – the fraction of organic carbon in topsoil (0-5cm)

f_{rxn} – the fraction of GOM potentially photoreduced to GEM

F_{st} – gaseous elemental mercury stomata emission flux

f_T – correction factor for air temperature

f_ψ – correction factor for water stress of plant

GEM – gaseous elemental mercury

GOM – gaseous oxidized mercury

G_{st}(PAR) – the unstressed canopy stomata conductance

H – Henry's law constant in soil condition

Hg – mercury

k – a constant of 0.4

K_{LA} – gaseous elemental mercury leaf-air partitioning coefficient

K_{oc} – soil organic carbon to water partitioning coefficient

LAI – leaf area index

LAI_{max} – maximum leaf area index in the whole year

LAP – leaf–air partitioning coefficient for GEM

LUC – land cover category

PBM – particulate-bound mercury

$PM_{2.5}$ – particles with size smaller than 2.5μm

$PM_{2.5-10}$ – particles with size between 2.5μm and 10μm

PM_{10} – particles with size larger than 10μm

R_a – aerodynamic resistance

R_{ac} – in-canopy aerodynamic resistance

R_{ac0} – reference value of in-canopy aerodynamic resistance

R_b – qasi-laminar resistance

R_c – canopy resistance

R_{cl} – exposed surfaces in the lower canopy resistance

R_{cut} – cuticle resistance

R_{cutd0} – reference value for cuticle resistance

R_{cutd} – dry cuticle resistance

R_{cutw} – wet cuticle resistance

R_{cutw0} – reference value for wet cuticle resistance

R_{dc} – gas-phase transfer in canopy resistance

R_g – soil resistance

R_{gs} – ground surface resistance

$R_g(O_3)$ – O_3 soil resistance

$R_g(SO_2)$ – SO_2 soil resistance

RH – relative humidity

R_{lu} – cuticle or outer surfaces in the upper canopy resistance

R_m – mesophyll resistance

R_s – surface resistance

R_{st} – stomata resistance

R_t – $\left(\frac{1}{R_a+R_b}+\frac{1}{R_{st}}+\frac{1}{R_{cut}}+\frac{1}{R_{ac}+R_g}\right)^{-1}$

TGM – total gaseous mercury

T – ambient temperature

T_{min} – minimum surface temperature

U – wind speed

u_* – friction velocity

u_{min} – maximum friction velocity when dew occurs

V_{cut} – cuticle emission velocity

V_d – deposition velocity

V_{ds} – surface dry deposition velocity

V_g – soil emission velocity

V_{st} – stomata emission velocity

VI – air diffusivity

Z_R – reference height

Z_0 – roughness height

α – a constant of zero

β – a constant of 0.1

χ_{atm} – gaseous elemental mercury concentration in the air

χ_{cnp} – gaseous elemental mercury concentration above canopy

χ_g – gaseous elemental mercury compensation point concentration in soil

χ_{st} – gaseous elemental mercury compensation point concentration in stomata

Ψ_H – stability correction factor

Γ_{st} – emission potential of stomata

Γ_g – emission potential of soil

[Hg] – total gaseous mercury depositing on foliage

$[Hg^0]_{atm}$ – GEM concentrations at the atmosphere

$[Hg^0]_{st}$ – GEM concentrations in stomata

$[Hg^0]_w$ – GEM concentrations in cuticle

$[Hg^0]_{sl,g}$ – GEM concentrations in soil

$[Hg^0_c]$ – GEM bound to foliar cuticle surface

$[Hg^0_g]$ – GEM bound to organic matter

$[Hg^0_s]$ – dissolved elemental mercury in stomata

$[Hg^{II+}_c]$ – dry deposited GOM loading on cuticle

$[Hg^{II+}_g]$ – GOM content in the soil

$[Hg^{II+}_w]$ – GOM concentration washed-off from leaf

CHAPTER 1 INTRODUCTION

1.1 Background

Mercury (Hg) has been identified as a persistent, bioaccumulative, and toxic pollutant (UNEP, 2013) due to toxicity of most its compounds in aquatic receptors (such as aquatic plants and fish), amphibian (such as frog) and terrestrial receptors (such as terrestrial plants and mammals) (Boening, 2000). Its effects on human health by ingestion and inhalation include nervous system, respiratory system, immune system, and developing fetus (EPA, 1997; EPA, 2017).

Atmospheric Hg is released in the form of gaseous elemental mercury (GEM), gaseous oxidized mercury (GOM), and particulate-bound mercury (PBM) from both natural processes and anthropogenic activities. The natural sources consist of volcano eruption, geothermal activity, and volatilization from soil, plants, and water surfaces (Pirrone et al., 2010; Gaffney and Marley, 2014). Man-made sources include fossil-fuel fired power plants, non-ferrous metals manufacture, and cement production (Zhang et al., 2016a).

During atmospheric Hg is transported, GEM is oxidized to GOM. GOM has low volatility and higher solubility (Fu et al., 2012) compared to GEM. Particulate-bound mercury is formed by adsorption of elemental and GOM on particulate matter. The adsorption of Hg is more likely when particulate matter is rich with element carbon because mercury trends to be adsorbed on element carbon (Pirrone et al., 2000).

Atmospheric Hg is removed via dry and wet depositions. GOM and PBM are removed by both dry and wet deposition. However, the removal of GEM is mostly by dry deposition owing to its low Henry's Law constant (Wang et al., 2014). In monitoring sites, mercury wet deposition is quantified by analysis of precipitation (Wright et al., 2016). Oxidized mercury collected in the solution is reduced to elemental mercury which is removed from the solution and analyzed by dual gold trap amalgamation and cold vapor atomic fluorescence (Prestbo and Gay, 2009). Although dry deposition is difficult to measure due to technical challenges, some methods have been developed such as surrogate surfaces, litterfall, and throughfall (Wright et al., 2016). Surrogate surfaces, such as water-based surfaces, filter-based surfaces, and membrane-based surfaces, are used to simulate surfaces where mercury deposits to (Wright et al., 2016). Uncertainties in the measurement related with selected surrogate surfaces and instrument setup are larger than a factor of two (Wright et al., 2016). Litterfall method is to measure mercury depositing on the leaves (Wright et al., 2016). Throuhgfall method is to monitor the summation of wet-deposited mercury above the canopy and dry-deposited mercury washed off from the canopy (Wright et al., 2016). However, all these measurement methods are time consuming and costly. It is also difficult to select an appropriate monitoring point in complicated terrain and to measure for a long-time period. Therefore, the development of dry deposition models is necessary.

In chemical transport models and at monitor networks, dry deposition is calculated using the inferential approach. The dry deposition flux is a product of atmospheric pollutant concentration and dry deposition velocity. The dry deposition velocity is calculated through multiple resistance analogy scheme, such as those by Wesely (1989), Zhang et al. (2003) and Kerkweg et al. (2006). In addition to dry deposition, GEM has a tendency to emit back to the atmosphere as a result of its high vapor pressure. Thus, GEM exchange flux is estimated by using bidirectional exchange models (Xu et al., 1999; Bash, 2010; Wang et al., 2014; Wright and Zhang, 2015). The net flux is a summation of deposition and emission fluxes.

The first GEM bidirectional exchange model is presented by Xu et al. (1999) for providing lower boundary conditions (mass transfer velocities and GEM exchange fluxes) of regional/global atmospheric transport and deposition models. Bash (2010) introduced another GEM bidirectional scheme. It has been implemented into the Community Multi-scale Air Quality Model (Bash, 2010). An updated bidirectional exchange model is presented by Wang et al. (2014) based on Bash's (2010) scheme with surface resistances from Zhang et al. (2002b, 2003). Another bidirectional exchange model was developed by Wright and Zhang (2015) for air-terrestrial exchange of GEM.

The modeling of dry deposition using various chemical transport models shows inconsistencies between the models, up to a factor of ten, due to different dry deposition algorithms and simulated pollutant concentrations (Wright et al., 2016). Some mercury bidirectional exchange models have been developed; however, no comparison among these models has been conducted. Such a comparison would quantify the magnitude of differences between the models and identify the dominant factors leading to these differences. Knowledge gained from comparison may help researchers to understand what physical and chemical processes need considerations.

1.2 Objective

The objective of this study is to compare two GEM bidirectional exchange models from Wang et al. (2014) and Wright and Zhang (2015). Specific objectives of this study are to

(1) quantify the magnitude of difference in

· Resistances to GEM

· GEM emission and deposition velocities

· GEM compensation point concentrations in soil and stomata

· GEM emission, deposition, and net fluxes

(2) identify the dominant factors causing the differences.

The scope is to run these two models on one site for two land covers under the same meteorological and other conditions in summer from June to September and winter from December to March. This study aims to investigate the difference between the two models, to present the dominant factors resulting in the differences between the two models, and to analyze the significance of land cover and season in the difference between the two models.

CHAPTER 2 LITERATURE REVIEW

2.1 Mercury cycling

Both natural processes and anthropogenic activities are emission sources for atmospheric Hg. GEM is the most common form and accounts for more than 90% of the total Hg in the atmosphere (Zhang et al., 2016a). Atmospheric Hg undergoes local, regional, and global transport in all three forms. PBM is likely to be transported over a long distance on fine particles (<1μm) (Schroeder and Munthe, 1998). In the transport of atmospheric Hg, GEM is oxidized to GOM. The adsorption of GEM and GOM on particulate matters forms particulate-bound mercury.

Atmospheric Hg is removed from the atmosphere by dry and wet depositions. Both GOM and PBM deposit to surfaces through dry and wet processes (Fu et al., 2012). The removal of GEM mostly relies on dry deposition owing to the low Henry's Law constant (Wang et al., 2014). The residence time of GEM is estimated to be several months to over one year (Fu et al., 2012). GOM is captured by droplets and surfaces in the process of dry and wet depositions due to high water solubility. Thus, it has a shorter residence time of hours to weeks (Cole et al., 2014). PBM also has a residence time of hours to weeks.

Mercury in the surface is either emitted to the atmosphere or remained in the plants, soil or water (EPA, 1997). In all three forms of mercury, only GEM is emitted back to the atmosphere as a result of its high vapor pressure. In the soil, mercury forms either complexes with organic matters and mineral colloids or methylmercury through numerous microbial processes (EPA, 1997). The most abundant form of mercury is oxidized mercury complexes followed by methylmercury and elemental mercury (EPA, 1997). Oxidized mercury complexes could account for 97-99% (EPA, 1997). In the water, most of the Hg is bound to organic matters, which could be either dissolved organic carbon or suspended particulate matters (EPA, 1997). Methylmercury is bioaccumulative in fish and the Hg found in fish muscle tissue is almost methylmercury (EPA, 1997). Mercury is transferred to upper food chain through ingestion of fish-consuming wildlife and humans (EPA, 1997).

2.2 Dry deposition models

There are three types of dry deposition models, for particulate pollutants, for gaseous pollutants, and for pollutants that are re-emitted from the surface. Models that have been reviewed are shown in Table 2-1.

Table 2-1. Dry deposition models reviewed.

Categories	Models
Particulate dry deposition models	Slinn (1982)
	Zhang et al. (2001)
	Zhang and He (2014)
Gaseous dry deposition models	Wesely (1989)
	Zhang et al. (2002b)
	Zhang et al. (2003)
GEM bidirectional exchange models	Bash (2010)
	Wang et al. (2014)
	Wright and Zhang (2015)

2.2.1 Particulate pollutants

Dry deposition flux (F) is defined as the product of dry deposition velocity (V_d) and concentration (C) for substances of interest.

$$F = V_d \cdot C \tag{2-1}$$

The concentration of substance is known from measurement in monitor sites or from model computation. The estimation of deposition velocity is crucial. For particulate pollutants, dry deposition velocity is calculated as

$$v_d = v_g + \frac{1}{R_a + R_s} \tag{2-2}$$

where V_g is gravitational settling velocity, R_a is aerodynamic resistance, and R_s is surface resistance. V_g and R_s are related particle size. The deposition velocity should include all collection mechanisms in the process of particle deposition to the surface. There are three steps as particles deposit to surface (Ruijgrok et al., 1995), (1) particles transported from free atmosphere to viscous sublayer by gravitational settling, (2) particles getting across the viscous sublayer by Brownian diffusion, interception, impaction, and gravitational settling, (3) particles getting interaction with the surface and they adhere or rebound. This type of dry deposition models developed as a function of particle size is called process oriented models (Ruijgrok et al., 1995).

Slinn (1982) presented a process oriented model for estimating particle dry deposition velocity to vegetation. His framework was based on the database of wind field in canopies and wind tunnel data of deposition velocity. Gravitational settling, Brownian diffusion, interception, impaction, and particle rebound are all considered. Aerodynamic resistance is calculated by wind speed at reference height and evaluated height and friction velocity. Friction velocity is a parameter that provides a measurement of the vertical flux of horizontal momentum in the surface layer. Larger friction velocity leads to smaller aerodynamic resistance, reflecting that particle deposition is easier with rough surface ground. Surface resistance includes characterizing wind profile in canopy and collection efficiency that is related with Brownian diffusion, interception, impaction, and particle rebound. Brownian diffusion is decided by the property of atmosphere and particle radius. Due to the uncertainty in contribution of interception to overall collection efficiency, Slinn determined to calculate interception as a function of characteristic radius of collectors in the canopy and its fraction in all collectors. For impaction, it only depends on Stokes number. Overall, although Slinn's (1982) model is theoretical, some input parameters may not be available in the regional models.

Based on Slinn's (1982) model, Zhang et al. (2001) presented a size-segregated particle dry deposition model. It has been implemented in Canadian Aerosol Module (Zhang et al., 2001). This model considers gravitational settling, Brownian diffusion, interception, impaction, and particle rebound as in Slinn's model. The difference is the expression of particle growth under humidity. Compared with particle growth not expressed explicitly in Slinn's model, a function of particle growth is included in Zhang's model. The method is that each size bin of particles will increase as a whole and the size distribution of the all particles is fixed at the same time. After growth, the dry particle radius is replaced by the wet particle radius in the calculation of deposition velocity. Additionally, some simplified empirical parameterizations are adopted in Zhang's model because Slinn's model requires detailed canopy information that it is unavailable in regional scale transport models.

In Zhang's (2001) model, the aerodynamic resistance is adopted as the same form as Wesely (1989), which is widely used in many dry deposition models. The surface resistance is more empirical and do not need to consider wind profile in canopy as in

Slinn (1982). It depends on friction velocity, collection efficiency, and particle rebound. As for Brownian diffusion, it becomes more dependent on land cover categories as the parameter varies with land cover categories. Calculation for impaction is adopted from Peters and Eiden (1992) and is modified more dependent on land cover categories. The collection efficiency by interception is calculated as a simpler form from Fuchs (1964) because of the unavailability of data on fraction of collectors in canopy. The results from Zhang's (2001) model are reasonable in the comparison with a variety of measurements. However, it seems that this model overestimates deposition velocity of small particles (e.g. $<0.1\mu m$) over smooth surfaces (Petroff and Zhang, 2010).

Wu et al. (2018a) compared two particulate dry deposition models. One is presented in Petroff and Zhang (2010) and the other is in Zhang et al. (2001). Petroff and Zhang's model has been implemented into the Community Atmospheric Model (Wu et al., 2018a). Through comparison, it is found that the largest difference is velocity of fine particles. Zhang's model (2001) significantly overestimates the velocity for fine particles due to the overestimation of Brownian diffusion effect. After reduction of Brownian diffusion effect in Petroff's and Zhang's model, the velocity decreases substantially and is in better agreement with observations.

There have been numerous monitoring networks established all over the world to quantify atmospheric pollutants deposition. In these networks, bulk aerosol particles of concern are measured. Therefore, an empirical scheme called bulk dry deposition algorithm is needed for estimating deposition velocity of bulk aerosols. Wesely (1985) established an empirical bulk dry deposition model for sulfate particles based on sulfate flux measurement data over grassland. Ruijgrok et al. (1997) derived a bulk dry deposition model for water-soluble inorganic ions based on flux data over forest and Lamaud et al. (1994) and Gallagher et al. (2002) generated formulas for bulk particles. However, none of these models is suitable for any particle species or any type of surfaces. Zhang and He (2014) developed a bulk dry deposition velocity based on the size-segregated model in Zhang et al., (2001).

In Zhang and He (2014), the particle size is grouped into three types, $PM_{2.5}$, $PM_{2.5-10}$, and PM_{10}. In equation 2-2, Vg strongly depends on particle size, slightly on particle density, and not on land cover category. Therefore, in this model, it is assumed as a constant value for a fixed particle size distribution. Considering that Ra has no relation with particle size, there is no change made to it. The inverse of R_s, namely surface deposition velocity (V_{ds}), is fitted into functions for bulk particles. Equation 2-2 becomes

$$v_d = v_g + \frac{1}{R_a + 1/V_{ds}} \tag{2-3}$$

For $PM_{2.5}$, V_{ds} is parameterized as a linear function of friction velocity (u_*).

$$V_{ds} = a_1 u_* \tag{2-4}$$

where a_1 is a constant dependent on land types. As for $PM_{2.5-10}$, V_{ds} is parameterized as a polynomial function of friction velocity for canopies with a constant leaf area index (LAI). LAI is the area of one-sided leaves per unit ground surface area. A correction factor (k) as an exponential function of LAI is added to $PM_{2.5-10}$ over canopies with LAI varying with seasons.

$$V_{ds} = (b_1 u_* + b_2 u_*^2 + b_3 u_*^3) e^{k\left(\frac{LAI}{LAI_{max}} - 1\right)} \tag{2-5}$$

where b_1, b_2, and b_3 are constants for each land type. LAI_{max} is the maximum LAI in the whole year. For PM_{10}, the same method as $PM_{2.5\text{-}10}$ is taken to generate the formula.

$$V_{ds}=(d_1 u_* + d_2 u_*^2 + d_3 u_*^3)e^{k(\frac{LAI}{LAI_{max}}-1)} \quad (2\text{-}6)$$

where d_1, d_2, and d_3 are constants for each land type. Under this model, the estimation of dry deposition velocity for bulk particles is within ±20% compared with original particulate dry deposition model in Zhang et al., (2001).

2.2.2 Gaseous pollutants

As for gaseous substances, the effect of gravitational settling is negligible. There are gaseous substances depositing to leaf stomata and mesophyll. A surface resistance approach called resistance oriented model was developed for dry deposition of trace gases (Ruijgrok et al., 1995). The dry deposition velocity for gaseous pollutants is

$$v_d = (R_a+R_b+R_c)^{-1} \quad (2\text{-}7)$$

where R_a, R_b, and R_c represent the properties of lower atmosphere, canopy, and soil, respectively. R_a corresponds to the aerodynamic resistance of surface boundary layer and makes no difference to all gaseous substances. It depends on the atmospheric stability and friction velocity. R_b represents quasi-laminar resistance to substances when substances are transported through the thin layer related with surface elements. This resistance varies with the molecular diffusivity for the gas of interest. The value of R_b increases as surface becomes rougher as a result of higher friction velocity. R_a and R_b are commonly used in many models and their formulas are similar in various models (Wesely and Hicks, 1977; Padro, 1996). R_c represents canopy resistance to uptake by the surface elements. This resistance is considerable various from model to model and is the most important and complex element for gaseous chemicals in dry deposition models.

Wesely (1989) presented a resistance module for estimation of gaseous dry deposition velocity over regional scales. His approach for R_c is to separate R_c into several components, which is commonly done in the resistance models where parallel and series resistances are set for different parts of the canopy.

$$R_c = 1/\left(\frac{1}{R_s+R_m}+\frac{1}{R_{lu}}+\frac{1}{R_{dc}+R_{cl}}+\frac{1}{R_{ac}+R_{gs}}\right) \qquad (2\text{-}8)$$

where R_m, R_{lu}, R_{cl}, R_{gs}, and R_{ac} are mesophyll resistance, cuticle or outer surfaces in the upper canopy resistance, exposed surfaces in the lower canopy resistance, ground surface resistance, and in-canopy aerodynamic resistance, respectively. These four resistances are input from lookup table for O_3 and SO_2. R_s is stomata resistance and calculated as a function of solar irradiation and ambient temperature, reflecting the effect of the sunlit and temperature on stomata. R_s is artificially set to be a very large value for the closure of stomata when there is no solar irradiation or ambient temperature is too high or too low. R_{dc} is a resistance that reflects a gas-phase transfer affected by the mixing force, which is caused by buoyant convection in canopy. It is expressed as a function of solar irradiation and the slope in radians of the local terrain.

In this model, it is assumed that the concentrations in the plant mesophyll, substrates in the upper canopy, substrates in the lower canopy, and substrates in the ground surface are in equilibrium with the ambient concentration. Under this assumption, all three substrate concentrations are assumed to be zero. It is worth noting that all the resistances in the equation 2-8 correspond to properties or behaviors inferred from measurements of net vertical fluxes from the surface, rather than to a single measurable quantity in the field (Wesely, 1989).

Wesely's model estimates not only the dry deposition velocity of O_3 and SO_2, but also that of other gaseous substances, such as NH_3, H_2O_2, and HCHO. According to the effective Henry's Law constant and chemical reactivity of each gaseous substance, dry deposition velocity for all other gaseous is computed. In addition, he considers the wetting of the surfaces by rain or dew and the covering of the surfaces by snow. However, resistances for many of the additional substances are assumed without the support from observation in field and laboratory. The varying of LAI with seasons is not considered in the model.

The canopy resistance (R_c), in equation 2-7, is separated into two parts—stomatal and non-stomatal resistances. To some extent, separation of these two parts is necessary because stomatal uptake of substances only happens during the daytime for most canopies and dominates over the non-stomatal process (Zhang et al., 2003). As for nighttime, due to the closure of stomata under the darkness environment, non-stomatal uptake will dominate over stomatal uptake (Zhang et al., 2003). Therefore, estimation of dry deposition velocity will have a more accurate representation of diurnal variation after the canopy resistance is separated. For parameterization of stomatal resistance, it varies from a function of solar irradiation, one-big or two-big leaf methods to a multilayer leaf-resistance scheme (Zhang et al., 2003). As for non-stomatal resistance, through analysis of measurement data, it is affected by meteorological conditions, such as relative humidity, wetness of canopy, and friction velocity, as well as the properties of canopy, such as leaf area index and growing period (Zhang et al., 2003).

Zhang et al. (2003) presented an improved gaseous dry deposition model by considering a non-stomatal resistance in Zhang et al. (2002a). This model calculates the dry deposition velocity for 31 gaseous species with resistances scaled to O_3 and SO_2 according to solubility and reactivity. The canopy resistance (R_c) is expressed as

$$\frac{1}{R_c}=\frac{1}{R_s}+\frac{1}{R_{ns}}=\frac{1\text{-}W_{st}}{R_{st}+R_m}+\left(\frac{1}{R_{ac}+R_g}+\frac{1}{R_{cut}}\right) \tag{2-9}$$

where R_c is separated into two parallel paths. One is stomatal part (R_s) with relation to stomata resistance (R_{st}) and mesophyll resistance (R_m) The other one is non-stomatal part (R_{ns}) with respect to in-canopy aerodynamic resistance (R_{ac}), soil resistance (R_g), and cuticle resistance (R_{cut}). Wst stands for the effect of wet conditions on stomatal resistance. It will be zero for dry conditions and be a function of solar irradiation under wet conditions. R_{st} is calculated as sunlit/shaded stomatal resistance in Zhang et al. (2002b). It considers the effect of leaf area index, sunlight, ambient temperature, ambient water vapor pressure, leaf water stress, and molecular diffusivities for pollutants of interest. During nighttime without solar irradiation, R_{st} is assumed to be an infinite value as for the closure of stomata. R_m is mesophyll resistance that input from lookup table. R_{ac} is modified from Erisman et al. (1994) as a function of leaf area index and friction velocity, which is more dependent on diurnal and seasonal variations. R_g is also modified from Erisman et al. (1994) and the soil resistance for SO_2 is considered as different values when surface is dry, when dew occurs, or when rain occurs. R_{cut} is modified from Zhang et al. (2002b) and it considers the effect of relative humidity and friction velocity.

In this model, it is worthwhile mentioning that there are improvements in cuticle and soil resistances in winter. In winter, the effect of temperature below -1^{o}C and the effect of snow cover are considered for cuticle and soil resistances. Although this model is developed to estimate dry deposition velocity for 31 gaseous species, it is not validated for some chemicals by comparisons with measurement because there are few dry deposition velocity measurements for other chemicals except SO_2, O_3, NO_2, HNO_3, and NH_3 (Zhang et al., 2003).

A comparison among five models for O_3 and SO_2 with five years flux database over a temperate mixed forest in southern Ontario, Canada was conducted by Wu et al. (2018b). It was found that substantial differences in the estimations of deposition velocity among gaseous dry deposition models are mainly attributable to the differences in the parameterizations of surface resistances.

2.2.3 GEM

For substances that are re-emitted back to the atmosphere, such as ammonia and GEM, it is inappropriate to only consider deposition process and assume concentrations in canopy and soil to be zero. Instead, deposition should be coupled with emission to create a bidirectional exchange flux. The first GEM bidirectional exchange model is presented by Xu et al. (1999) for providing surface boundary conditions of regional/global atmospheric transport and deposition models. In Xu's model, sources of GEM natural emission are categories into canopy, soil, and water. The GEM emission from the canopy is calculated as a function of evapotranspiration rate and GEM concentration in the surface soil solution. The emission from the soil is parameterized as a function of soil temperature. The GEM deposition on the canopy and soil is calculated as a product of gaseous dry deposition velocity and GEM concentration. A two-film diffusion model was adopted to calculate exchange of GEM between the atmosphere and water.

Bash (2010) presented a GEM bidirectional scheme. It has been implemented into the Community Multi-scale Air Quality Model (Bash, 2010). In this model, GEM exchange is estimated as a function of an atmospheric compensation point, air-biosphere partitioning processes, and atmospheric mixing processes (Bash, 2010). The GEM exchange is categorized into air-terrestrial, air-stomata, air-cuticle, air-soil, and air-water. In air-terrestrial exchange, GEM net exchange flux is calculated as a function of ambient GEM concentration, the compensation point concentration, and aerodynamic resistance. The compensation point ($[Hg^0]_{z0}$) is modeled as a weighted average of resistances and fluxes at the atmosphere, stomata, cuticle, and soil interfaces.

$$[Hg^0]_{z_0} = \frac{\frac{[Hg^0]_{atm}}{r_a} + \frac{[Hg^0]_{st}}{K_{LA}(r_b+r_{st})} + \frac{[Hg^0]_w}{K_{LA}(r_b+r_w)} + \frac{[Hg^0]_{sl,g}}{r_b+r_{ac}+r_{soil}}}{r_a^{-1}+(r_b+r_{st})^{-1}+(r_b+r_w)^{-1}+(r_b+r_{ac}+r_{soil})^{-1}} \quad (2\text{-}10)$$

where $[Hg^0]_{atm}$, $[Hg^0]_{st}$, $[Hg^0]_w$, and $[Hg^0]_{sl,g}$ are GEM concentrations at the atmosphere, stomata, cuticle, and soil, respectively. r_a, r_b, r_{st}, r_w, r_{ac}, and r_{soil} are aerodynamic resistance, laminar boundary layer resistance, stomata resistance, cuticle resistance, in-canopy aerodynamic resistance and soil resistance, respectively. K_{LA} is the leaf-air partitioning coefficient for GEM and is assumed to be the same for mesophyll and cuticle surfaces. For bare land without vegetation, all GEM concentrations related with canopy in equation 2-10 will equal to zero and all resistances related with canopy will become an infinite value.

In air-stomata exchange, GEM net flux depends on GEM concentration at the stomata, the compensation point concentration, laminar boundary layer resistance, and stomata resistance. In air-cuticle exchange, GEM net flux is calculated as a function of GEM concentration at the cuticle, the compensation point concentration, laminar boundary layer resistance, and cuticle resistance. In air-soil exchange, GEM net flux is parameterized as a function of GEM concentration at the soil, the compensation point concentration, in-canopy aerodynamic resistance and soil resistance. It is worth mentioning that GEM concentration in the soil is decided by the partitioning coefficient for GEM and the redox reaction between GEM and GOM. In air-water exchange, though GEM net flux is modeled using the two-film resistance as Xu et al. (1999) did, Bash adopted a different parameterization. In surface water, photo-redox between GEM and GOM is considered.

The results from this model are consistent with the data from isotopic tracer studies (Bash, 2010). However, there are multiple model assumptions in the variables that have not been verified through field data, such as air-vegetation partitioning and surface reduction and oxidation processes. These assumptions could increase the uncertainty of estimation and limit the improvement of the model (Wang et al., 2014).

Based on the Bash's (2010) scheme, an updated bidirectional exchange model is presented by Wang et al. (2014). Wang integrated the bidirectional exchange scheme from Bash with in-canopy aerodynamic, stomata, cuticle, and soil resistances from Zhang et al. (2002b, 2003). The structure of Wang's model is the same as Bash. In air-water exchange, two-film mass transfer model from Poissant et al. (2000) is used to estimate GEM net flux, which depends on wind speed above the water, water temperature, and atmospheric GEM concentration. The photo-redox reaction in the water is not considered by Wang and Bash considered it. In air-terrestrial exchange, compensation point concentration (χ_{cnp}) is also calculated by a weighted average as follows

$$\chi_{cnp}=\frac{\frac{C_{atm}}{R_a+R_b}+\frac{\chi_s}{R_{st}}+\frac{\chi_c}{R_c}+\frac{\chi_g}{R_{ac}+R_{soil}}}{(R_a+R_b)^{-1}+R_{st}^{-1}+R_c^{-1}+(R_{ac}+R_{soil})^{-1}} \tag{2-11}$$

where C_{atm}, χ_s, χ_c, and χ_g are GEM concentrations at the atmosphere, stomata, cuticle, and soil, respectively. R_a, R_b, R_s, R_c, R_{ac}, and R_{soil} are aerodynamic resistance, laminar boundary layer resistance, stomata resistance, cuticle resistance, in-canopy aerodynamic resistance and soil resistance, respectively. In air-soil exchange, GEM net flux is calculated according to bare land or vegetation. For bare land, the concentration gradient is considered between the soil and the atmosphere. For vegetation, the concentration gradient is between the soil and the compensation point (χ_{cnp}). In air-cuticle exchange, the photo-reduction of oxidized mercury is considered and it is not considered by Bash.

The two GEM bidirectional exchange models above are developed for regional models. Wright and Zhang (2015) presented a bidirectional exchange flux model to estimate GEM net flux in monitoring sites. It is a modification of the gaseous dry deposition model in Zhang et al. (2003) and it has the same structure as the ammonia bidirectional exchange model in Zhang et al. (2010). In Wright and Zhang (2015), the GEM net flux is calculated for land and the air-water exchange is not considered. Besides, the mercury soil pool is assumed as unlimited and that is limited in Bash (2010) and Wang et al. (2014). Wright and Zhang did not considered air-stomata, air-cuticle, and air-soil exchange. The GEM emission from the cuticle is assumed to be zero and then emission sources become stomata and the soil.

In Wright and Zhang (2015), the GEM net flux is calculated as a function of atmospheric GEM concentration, compensation point concentration, aerodynamic resistance and laminar boundary layer resistance. The compensation point concentration (χ_c) is parameterized as

$$\chi_c=\left[\frac{\chi_a}{R_a+R_b}+\frac{\chi_{st}}{R_{st}+R_m}+\frac{\chi_g}{R_{ac}+R_g}\right]\cdot\left[\frac{1}{R_a+R_b}+\frac{1}{R_{st}+R_m}+\frac{1}{R_{ac}+R_g}+\frac{1}{R_{cut}}\right]^{-1} \quad (2\text{-}12)$$

where χ_a is atmospheric GEM concentration, R_a, R_b, R_{st}, $R_{m,}$ R_{cut}, R_{ac}, and R_g are aerodynamic resistance, laminar boundary layer resistance, stomata resistance, mesophyll resistance, cuticle resistance, in-canopy aerodynamic resistance and soil resistance, respectively, χ_{st} and χ_g are the stomata and ground compensation point, respectively. The stomata compensation point depends on ambient temperature and emission potential of the stomata. As for ground compensation point, it relies on soil temperature and emission potential of the ground. Both emission potentials of the stomata and ground are derived empirically from modeled and measured compensation points.

In my study, two models from Wang et al. (2014) and Wright and Zhang (2015) were chosen. Wang's model is based on the bidirectional exchange scheme from Bash (2010) and is updated with surface resistances from Zhang et al. (2002b, 2003). This surface resistances scheme is the same as Wright and Zhang (2015). Wang's model simulates pollutants exchange in air-terrestrial, air-stomata, air-cuticle, air-soil, and air-water. However, some parameters involving in physical and chemical processes, such as GOM concentration in soil, were assumed and needs further investigations. As for Wright and Zhang (2015), it was developed for site simulations. The physical and chemical processes in the model were simplified under assumptions. Thus, it is convenient for site simulating and the simulation results were reasonable by comparison with measurements (Wright and Zhang, 2015). However, Wright and Zhang's model does not simulate pollutants exchange between air and water. The exchange in air-stomata, air-cuticle, and air-soil were not considered.

CHAPTER 3 METHODOLOGY

3.1 The two models used

Wang's model (Wang et al., 2014) and Wright & Zhang's model (Wright and Zhang, 2015) were chosen in this study. Wang's model was developed based on Bash's model (Bash, 2010) with updated surface resistances. The simulated fluxes in United States by this model were comparable to measurements (Wang et al., 2014). The sensitivity of the simulated flux to physical and environmental parameters was examined (Wang et al., 2014). In Wright & Zhang's model, the GEM exchange flux was estimated for various land covers surrounding 24 sites in North America (Zhang et al., 2016b). The reliability and uncertainty of the model were discussed (Zhang et al., 2016b).

3.2 Land cover

In Wang's model, GEM exchange flux is estimated over canopy and water surfaces. Wright & Zhang's model was developed for canopy surfaces. Through ANOVA analysis, the effect of land cover is more significant on Wang's model than that on Wright & Zhang's model (11 vs. 2, Appendix F). However, the interaction between land cover and season is similar in the two models (13 vs. 10). In this study, the two models were run over canopies. Two out of 26 land cover categories in Zhang et al. (2003) were chosen, evergreen needleleaf forest and deciduous broadleaf forest. The two models produced different results (difference>45%) in all output, except aerodynamic resistance, quasi-laminar resistance, cuticle resistance, soil resistance, deposition velocity, and deposition flux, in the two land covers (Table E2).

3.3 Study site

The study site was chosen from National Atmospheric Deposition Program's Atmospheric Mercury Network sites. The detailed information of monitoring sites is in Zhang et al. (2016b). The study site was chosen under four considerations. (1) The site should locate in North America where meteorological data is available. (2) In order to reduce the effect of anthropogenic emission on ambient GEM concentration, the site should be located in rural areas or places without urban land cover. (3) The annual mercury emission of the site within 100km radius should be lower than 300 kg (Zhang et al., 2016b). Hence, the ambient GEM concentrations are closer to background concentration. (4) The site should have many land covers but without water because Wright & Zhang's model is only for canopies. Under all these four considerations, GA40 (33.9283^{o} N, 85.0456^{o} W) with evergreen needleleaf trees of 20.1%, deciduous broadleaf trees of 30.6%, and grass of 49.3% was chosen as the study site. GA40 site is at Rockmart, Georgia, United States and is 63km northwest of Atlanta, Georgia, United States (Fig. 3-1). The nearest airport is Paulding Northwest Atlanta Airport (33.9176^{o} N, 84.9407^{o} W) and is 9km east of GA40 site.

Figure 3-1. Location of GA40 site (base map adapted from Google Maps).

3.4 Seasons

Through ANOVA analysis, season is significant in the two models and its variability is larger than variability of land cover (Appendix F). In Wang's model, temperature is a factor in all output, except aerodynamic resistance, quasi-laminar resistance, cuticle resistance and in-canopy aerodynamic resistance. In Wright & Zhang's model, temperature is a factor in all output, except cuticle resistance and in-canopy aerodynamic resistance. Summer and winter were chosen because these two seasons have high LAI and low LAI, respectively. June-September and December-March were set as summer and winter, respectively, based on variation of LAI for evergreen needleleaf forest and deciduous broadleaf forest, as in Fig. 3-2. For both land covers, LAI is high during June-September and low during December-March. ANOVA analysis reveals that the two models provided different results (difference >45%) in all output, except aerodynamic resistance, quasi-laminar resistance, cuticle resistance, soil resistance, deposition velocity, and deposition flux, in the two seasons (Table E2).

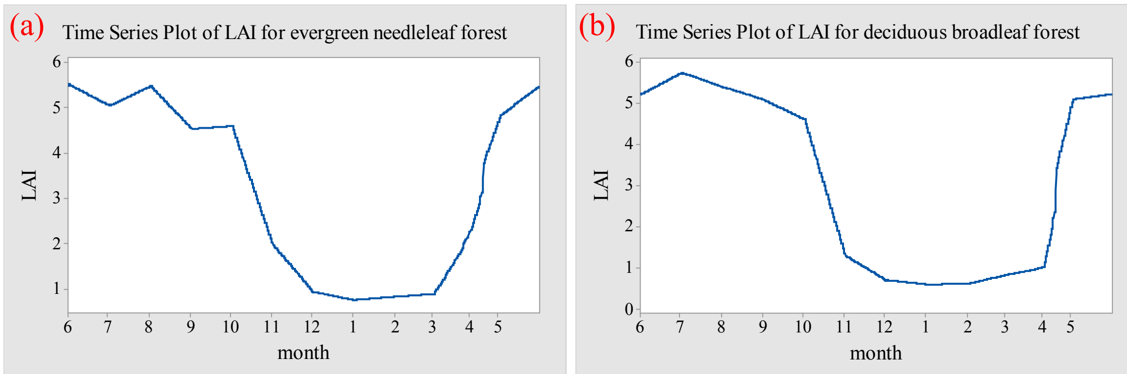

Figure 3-2. Variation of LAI for the two land covers, (a) evergreen needleleaf forest, (b) deciduous broadleaf forest.

3.5 Study period

There are six years hourly meteorological data and two-hour ambient GEM concentrations data in GA40—June 2009 to April 2014 (Zhang et al. 2016b). June 2010—September 2010 and December 2010—March 2011 were chosen, because of highest percentage of valid ambient GEM concentration data (88.7%), as in Table 3-1.

Table 3-1. GEM concentrations two-hour data points in 2009-2014.

Period	Missing hours	Data points	Total hours	Percentage of data points
Jun., Jul., Aug., Sep., Dec. in 2009 ,and Jan., Feb., Mar. in 2010	506	2410	2916	82.6%
Jun., Jul., Aug., Sep., Dec. in 2010 ,and Jan., Feb., Mar. in 2011	329	2587	2916	88.7%
Jun., Jul., Aug., Sep., Dec. in 2011 ,and Jan., Feb., Mar. in 2012	632	2296	2928	78.4%
Jun., Jul., Aug., Sep., Dec. in 2012 ,and Jan., Feb., Mar. in 2013	832	2084	2916	71.5%
Jun., Jul., Aug., Sep., Dec. in 2013 ,and Jan., Feb., Mar. in 2014	493	2423	2916	83.1%

3.6 Model settings

3.6.1 Reference height

GEM exchange between reference height and surface was simulated by the models. The reference height in Wang's model is fixed at 10m. The reference height in Wright & Zhang's model is flexible and decided by model user. Thus, the reference height in Wright & Zhang's model was set at 10m to enable comparison of the two models. However, 10m reference height may not be a suitable height to simulate GEM exchange for evergreen needleleaf forest and deciduous broadleaf forest. This is because trees as tall as 30m are not uncommon around latitude of 30 north degree.

3.6.2 GEM compensation point concentration on cuticle

Wang assumed that GOM on cuticle is reduced to GEM or fixed into leaves tissue. The GEM compensation point concentration on cuticle is calculated from the difference between reduced GOM and fixed GOM. However, when solar radiation is zero at night or is weak during daytime, calculated GEM compensation point concentration is negative, because reduced GOM is less than fixed GOM. Negative GEM compensation point concentration is unreasonable. Thus, GEM compensation point concentration on cuticle in Wang's model was set to be greater or equal to zero.

3.6.3 Meteorological conditions

Table 3-2 lists four parameters each with different settings in the two models. In order to run the two models under the same condition, each of the four parameters was set to be the same for the two models.

Table 3-2. Settings of four meteorological parameters in each of the two models, settings in Wright & Zhang's model were used.

Parameters	Wright & Zhang's model	Wang's model
occurrence of dew	surface air temperature) > 273.15K friction velocity < u_{min}	dew point temperature ≥surface air temperature
occurrence of rain	surface air temperature > 273.15K precipitation > 0.2mm/hour	precipitation > 0mm/hour
occurrence of snow	fraction of snow depth > 0.0001	snow depth > 0
how to get relative humidity	input from the meteorological data	calculated using surface air temperature and dew point temperature

(1) In Wright & Zhang's model, dew occurs on clear night with or without weak wind, and when temperature is above zero degree celsius. In Wang's model, dew occurs when dew point temperature is greater or equal to surface temperature. The approach in Wright & Zhang's model is used in both models because this approach gets closer to physical processes.

(2) In Wright & Zhang's model, precipitation occurs when surface temperature goes above zero degree celsius and precipitation is larger than 0.2 mm/hour. In Wang's model,

precipitation above 0 mm/hour is considered as rain. In monitor sites, both rain and snow are measured by means of liquid. Snow and rain play different roles in pollutants deposition because snow is ice crystal and rain is liquid. Only under the assumption that snow quickly melts to water as soon as snow falls on the surface, snow is seen as rain. However, when surface temperature is under zero degree celsius, it is difficult for snow to melt quickly unless there is enough solar radiation. Therefore, the approach in Wright & Zhang's model is closer to nature and used in both models.

(3) In Wright & Zhang's model, fraction of snow depth is the ratio of snow depth to maximum snow depth of 2 m for evergreen needleleaf forest and deciduous broadleaf forest. Snow occurs when fraction of snow depth is larger than 0.0001, namely snow depth above 0.02 cm. In Wang's model, snow happens when snow depth above zero. The judgements of occurrence of snow in the two models are similar. The approach in Wright & Zhang's model is used in both models.

(4) In Wang's model, relative humidity is calculated using surface air temperature and dew point temperature (the temperature that air becomes saturated with water vapor). This calculation is replaced by input, as in Wright & Zhang's model, because relative humidity is available in the meteorological dataset.

3.7 Data treatment

3.7.1 Input data

Input data for the two models is listed in Tables 3-3, 3-4, and 3-5. In Table 3-3, hourly meteorological data is for the study site (GA40) during June 2010—September

2010 and December 2010—March 2011. It is archived data produced by the Canadian weather forest model and is provided by Environment and Climate Change Canada. Two-hour ambient GEM concentration data is for the GA40 site during June 2010—September 2010 and December 2010—March 2011. It is the observation data in GA40 monitoring site and is provided by Environment and Climate Change Canada. In Table 3-4, constant input data that is not related with land cover is shown.

Table 3-3. Hourly input data in the two models.

Categories	Input data (unit)	In which models
without processing meteorological data	surface air temperature ($^{\circ}C$)	both
	ambient temperature ($^{\circ}C$)	Wright & Zhang
	relative humidity (fraction)	both
	barometric pressure (mbar)	both
	solar irradiance (W/m^2)	both
	soil volumetric water content (m^3/m^3)	Wang
	precipitation (mm/hour)	both
	snow depth (cm)	both
	fraction of cloud	both
without processing concentration data	ambient GEM concentration (ng/m^3)	both
preprocessing data	temperature at 10m ($^{\circ}C$)	Wright & Zhang
	wind speed (m/s)	both
	friction velocity (m/s)	both
	cosine value of zenith angle (dimensionless)	both
	LAI (dimensionless)	both

Table 3-4. Constant values in the two models.

Input parameter (unit)	Value	In which models
mesophyll resistance (s/m)	500	both
alpha	0	both
beta	0.1	both
GEM molar weight	200	Wright & Zhang
dair	17	Wright & Zhang
dh2o	13	Wright & Zhang
R_{st} for stomata closure (s/m)	99999.9	Wright & Zhang
k	0.41	Wang
kt (cm^2/s, air diffusivity)	0.22	Wang
dihg0 (cm^2/s, GEM diffusivity)	0.13	Wang
psea (kPa, sea level atmospheric pressure)	101.325	Wang
dh2o_dhg0 (water vapor diffusivity/GEM diffusivity)	1.82	Wang
cos_a (for visible solar radiation)	0.5	Wang
kla (GEM partitioning coefficient between air and leaf)	30000	Wang
foc (m^3/m^3, organic carbon content in soil)	0.025	Wang
cwash (fraction of GOM washed off from cuticle)	0.02	Wang
fdtgm (ng/m^3, total gaseous mercury depositing on leaves)	0.39	Wang
tl (m, leaf thickness)	0.000152	Wang
tdiff (s, time period)	3600	Wang
koc (GEM partitioning coefficient between organic carbon and water)	0.000052	Wang
krxn (s^{-1}, GOM reaction rate in soil)	$8*10^{-11}$	Wang
ccgs_hg2 (ng/m^3, GOM concentration in soil)	90	Wang

Table 3-5. Constant values associated with land cover in the two models.

Input parameter (unit)	Evergreen needleleaf forest	Deciduous broadleaf forest	In which models
roughness height (m)	0.9	0.4-1 (varying with LAI)	Wright & Zhang
emission potential of stomata	10	8	Wright & Zhang
emission potential of ground	10	10	Wright & Zhang
brs (constant for R_s)	44	43	both
bvpd (constant for R_s)	0.31	0.36	both
psi1 (constant for R_s)	-2	-1.9	both
psi2 (constant for R_s)	-2.5	-2.5	both
Rac1 (constant for R_{ac} in summer)	100	60	both
Rac2 (constant for R_{ac} in winter)	100	100	Wright & Zhang
	100	250	Wang
RcutdO (constant for R_{cut})	4000	6000	both
RcutwO (constant for R_{cut})	200	400	both
RcutdS (constant for R_{cut})	2000	2500	both
RgO (constant for R_g)	200	200	Wright & Zhang
RgS (constant for R_g)	200	200	both
rsmin (constant for R_{st})	250	150	both
maximum snow depth (cm)	200	200	both
tmax (constant for R_{st})	40	45	both
tmin (constant for R_{st})	-5	0	both
topt (constant for R_{st})	15	27	both

Table 3-5 lists constant input data associated with land cover. There are five input constants that are the same for the two land covers. Six input constants are similar for the two land covers. There are eight constants that are different for the two land covers, (1) roughness height has an effect on aerodynamic resistance, (2) constant for R_{ac} in summer (Rac1) has an influence on in-canopy aerodynamic resistance, (3) constant for R_{ac} in winter (Rac2) affects in-canopy aerodynamic resistance, (4) constant for R_{cut} (RcutdO) influences cuticle resistance, (5) constant for R_{cut} (RcutwO) has an effect on cuticle resistance, (6) constant for R_{cut} (RcutdS) has an influence on cuticle resistance, (7) constant for R_{st} (rsmin) affects stomata resistance, (8) constant for R_{st} (topt) influences stomata resistance. There is only one constant that is different in the two models—constant for R_{ac} in winter (Rac2), which has an influence on in-canopy aerodynamic resistance.

Although LAI for the two land covers are similar (Fig. 3-2), eight input constants are different for the two land covers and they have an effect on the output from the two models. The difference between the two models for the two land covers is analyzed in chapter 4.

3.7.2 Preprocessing

There are five hourly input variables need preprocessing—temperature at 10m, zenith angle, friction velocity (u_*, a measurement of the vertical flux of horizontal momentum in the surface layer), LAI, and wind speed at 10m (Table 3-3). Temperatures at the surface and at the first model-layer (typically at 40-50m) are available (Zhang et al. 2016b). The temperature at 10 m is calculated under the assumption that temperature varies linearly between these two heights.

Zenith angle, u_*, and LAI were calculated with the method in Wright & Zhang's model. Wind speed at 10m was calculated back from u_* with the method in Wright & Zhang's model. u_* is related with the roughness of underlying surfaces. u_* was calculated between roughness height and the first model-layer. It was also calculated between roughness height and 10m. The two calculated u_* are the same because the underlying surface is the same.

3.7.3 Interpolation of ambient GEM concentrations data

Two-hour ambient GEM concentration data from Zhang et al (2016b) were measured at even hours or odd hours. Here, all even hours were moved to odd hours by adding one to each even hour. Then, average of two data in one odd hour was processed. Linear Interpolation was made for 12 odd hours of each day to get hourly ambient GEM concentrations. If there was only one even hour absent between two closest odd hours, linear interpolation was made to get this even hour. Otherwise, interpolation was not made between two closest odd hours. The seasonal average diurnal cycles for ambient GEM concentration before and after interpolation are shown in Fig. 3-3. They have similar diurnal trends and the zigzag in original ambient GEM concentrations disappears in interpolated ambient GEM concentrations. After interpolation, hourly ambient GEM concentrations data and hourly meteorological data were merged.

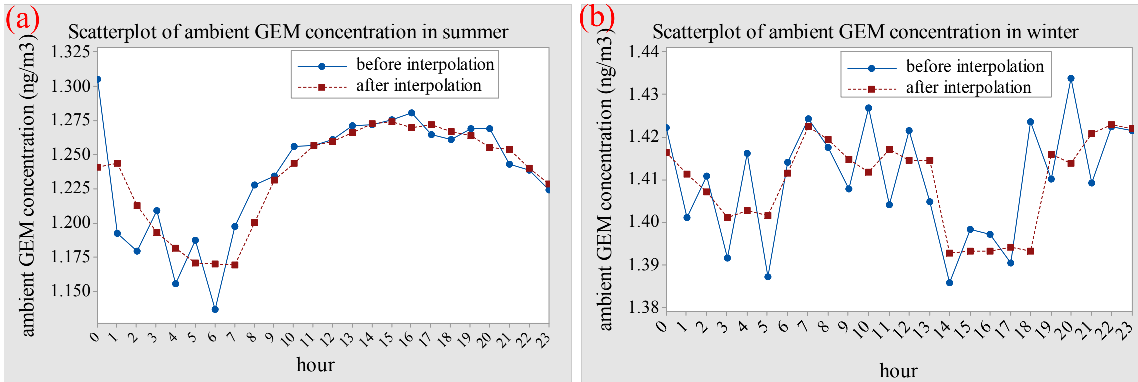

Figure 3-3. Seasonal average diurnal cycle for ambient GEM concentrations before and after interpolation, (a) in summer, (b) in winter.

3.7.4 Input data for each of the two models and conversion of units

Input data for two models are shown in Table 3-6. Four parameters have different units in the two models, (1) surface air temperature, conversion from degree celsius to Kelvin degree, (2) relative humidity, conversion from fraction to percentage, (3) barometric pressure, conversion from Milibar to Pascal, and (4) snow depth, conversion from centimetre to metre.

Table 3-6. Input data and units for the two models.

Category	Parameters	Units in Wright & Zhang's model	Units in Wang's model
The same units	wind speed	m/s	
	friction velocity	m/s	
	solar radiation	W/m^2	
	precipitation	mm/hour	
	fraction of cloud	fraction	
	cosine value of zenith angle	dimensionless	
	LAI	dimensionless	
	ambient GEM concentration	ng/m^3	
Different units	surface air temperature	°C	K
	relative humidity	fraction	%
	barometric pressure	mbar	Pa
	snow depth	cm	m
Input into only one model	ambient temperature	°C	--
	soil volumetric water content	--	m^3/m^3

There are two parameters that are only required by one of the two models. Ambient temperature in Wright & Zhang's model is used to calculate air diffusivity and GEM compensation point concentration in stomata. In Wang's model, air diffusivity was set as a constant of 0.22cm2/s and GEM compensation point concentration in stomata is dependent on LAI and solar radiation, not ambient temperature. Soil volumetric water content in Wang's model is used for wet soil and Wright & Zhang did not consider wet soil.

3.8 Hours of daytime

Hours for daytime were chosen based on the diurnal cycle of zenith angle. Seasonal average diurnal cycle for cosine value of zenith angle is shown in Fig. 3-4. Daytime was decided as 6:00-18:00 and 7:00-17:00 for summer and winter, respectively.

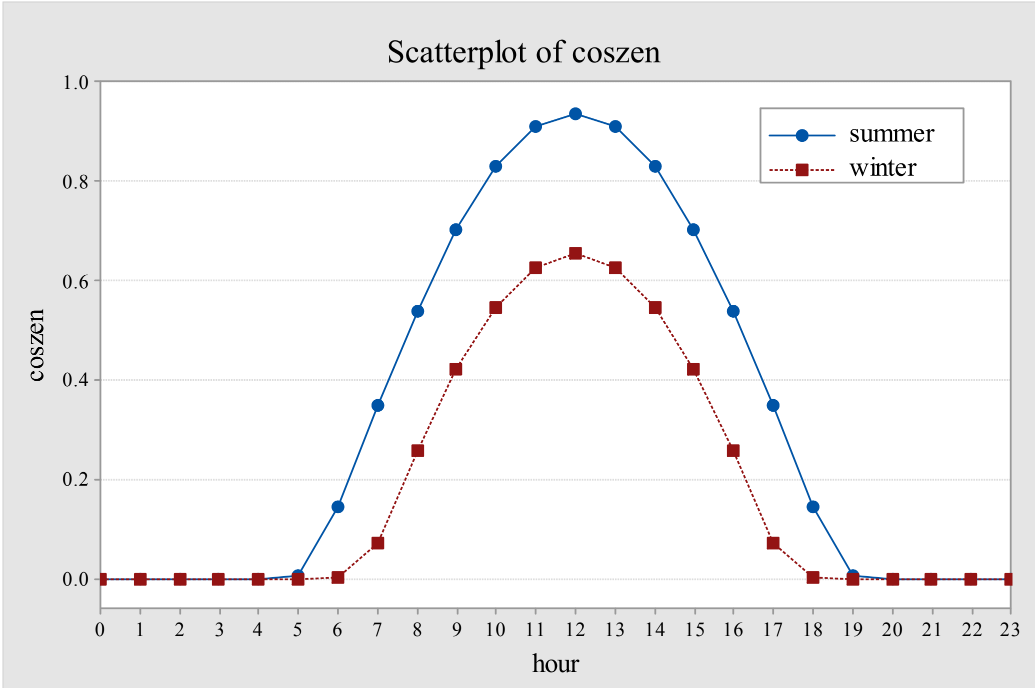

Figure 3-4. Seasonal average diurnal cycle for cosine of zenith angle in summer and winter.

3.9 Running the two models

The resistances and velocities were output from the two models with hourly meteorological data, because resistances and velocities only need meteorological data as input. The GEM compensation point concentrations and fluxes were output from the two models with merged hourly meteorological data and ambient GEM concentrations. Both meteorological data and ambient GEM concentrations are from 0:00 to 23:00. The general statistics of meteorological data before merge (Table D1) is similar to that after merge (Table D2).

3.10 Calculation of the percentage of difference between the two models

In the tables of chapter 4, all percentages of difference between the two models were calculated as equation 3-1.

$$\text{Percentage of difference} = \frac{\text{value from Wang's model} - \text{value from Wright \& Zhang's model}}{0.5*(\text{value from Wang's model} + \text{value from Wright \& Zhang's model})} * 100\% \quad (3\text{-}1)$$

3.11 Analysis of variance (ANOVA) of the difference between the two models

General Linear Model, one type of Analysis of Variance (ANOVA) in Minitab (version 18 developed by Minitab, Inc), was used to analyze the effect of land cover and season on difference within and between the two models. The difference between the two models is calculated as equation 3-1. When the p-value of land cover or season was less than 0.1, land cover or season was considered to be significant in the difference between the two models. Otherwise, land cover or season was considered to be insignificant in the difference between the two models. Main effect and interception figures were also plotted to analyze the effect of land cover and season on difference within and between the two models.

3.12 The tools

The two models were run on Matlab (developed by MathWorks). All data analysis and figures plotting were made on Minitab (version 18 developed by Minitab, Inc).

CHAPTER 4 RESULTS AND DISCUSSIONS

4.1 Resistances

4.1.1 Aerodynamic resistance (R_a)

Wright & Zhang considered the turbulence caused by wind (mechanical turbulence) and buoyancy (thermal turbulence). Wang only considered the turbulence caused by wind. Wright & Zhang assumed that the maximum R_a to be 1000s/m and Wang did not.

Evergreen needleleaf forest in summer

a) Compare the turbulence caused by wind in Wright & Zhang's model (without cap) with that in Wang's model

(1) R_a caused by wind in the two models

Table 4-1 shows values of R_a caused by wind in the two models. R_a caused by wind in the two models has similar diurnal trend with low values during daytime and high values during nighttime (Fig. 4-1 and Table E1). Aerodynamic resistance in Wang's model is always larger than that in Wright & Zhang's model (Fig. 4-2).

Table 4-1. Aerodynamic resistance (R_a, s/m) for the two models in the two seasons.

Season	Land cover	Model	Minimum	First quartile	Median	Third quartile	Maximum	Mean
summer	evergreen needleleaf forest	Wang (wind)	7	16	22	40	268020	1167
		Wright & Zhang (wind)	6	12	16	28	4504	65
		Wright & Zhang (buoyancy)	-12	-1	1	12	23761	226
		Wright & Zhang (wind+buoyancy)	6	12	16	36	28266	331
		Wright & Zhang (wind+buoyancy, with cap)	5	12	16	36	1000	123
	deciduous broadleaf forest	Wang (wind)	7	15	21	39	259817	1127
		Wright & Zhang (wind)	5	12	16	27	4339	63
		Wright & Zhang (buoyancy)	-12	-1	1	12	23430	262
		Wright & Zhang (wind+buoyancy)	5	11	16	35	27769	325
		Wright & Zhang (wind+buoyancy, with cap)	5	11	16	35	1000	122
winter	evergreen needleleaf forest	Wang (wind)	5	11	14	25	257065	561
		Wright & Zhang (wind)	4	8	11	17	4296	36
		Wright & Zhang (buoyancy)	-11	-0.1	0.3	4	22662	139
		Wright & Zhang (wind+buoyancy)	4	8	11	21	26957	174
		Wright & Zhang (wind+buoyancy, with cap)	4	8	11	21	1000	85
	deciduous broadleaf forest	Wang (wind)	8	17	23	40	390761	844
		Wright & Zhang (wind)	6	12	17	28	6965	58
		Wright & Zhang (buoyancy)	-14	-0.1	0.4	5	27485	169
		Wright & Zhang (wind+buoyancy)	6	12	17	32	34450	227
		Wright & Zhang (wind+buoyancy, with cap)	6	12	17	32	1000	102

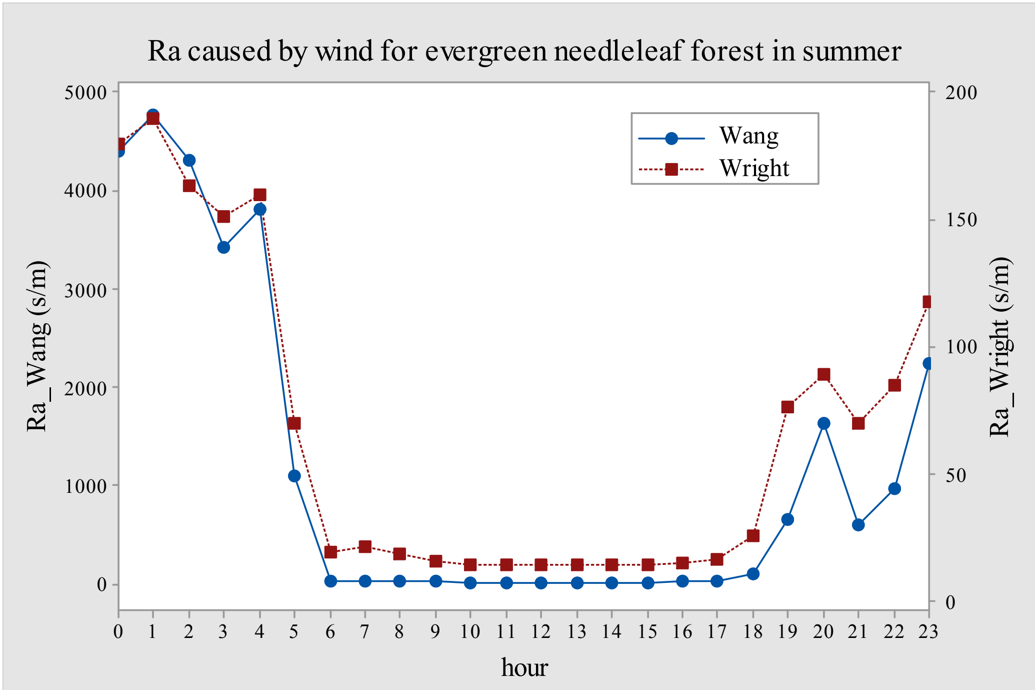

Figure 4-1. Diurnal trend for aerodynamic resistance caused by wind in the two models for evergreen needleleaf forest in summer.

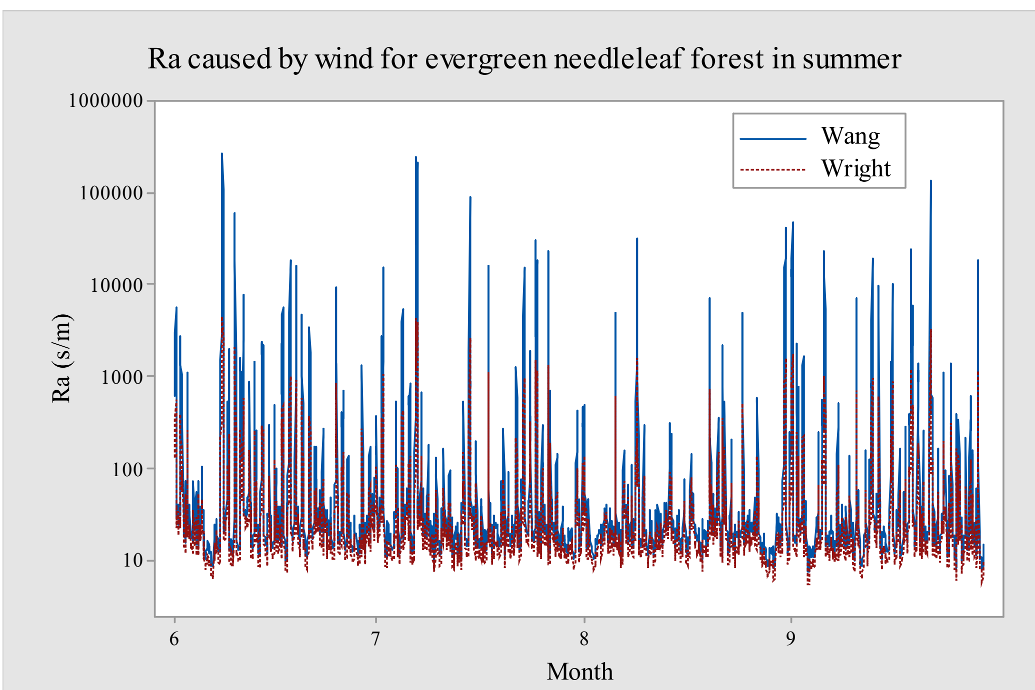

Figure 4-2. Time series for aerodynamic resistance caused by wind in the two models for evergreen needleleaf forest in summer.

(2) The difference between the two models and why

The two models have the same input for R_a caused by wind, but their equations are different. R_a in Wang's model was developed based on direct measurement of the turbulence (Hicks et al., 1987), and R_a in Wright & Zhang's model was developed based on micrometeorological approaches (Wesely and Hicks, 1977). As in Table 4-2, the difference between the two models is in the range of 11-193% (mean of 47%). The mean (47%) is greater than median (30%) because of the influence of large differences (>100%, 329 out of 2899) that are caused by low u_* and wind speed (Fig. 4-3). Large differences between the two models mostly happen during nighttime (Fig. 4-4) when u_* and wind speed are relatively low (Fig. 4-5). This is because low u_* and wind speed result in larger R_a in both models, but to a greater degree in Wang's model. Schwede et al. (2011) also found that large values of R_a are associated with low wind speed during nighttime. This is similar to R_a in Wang's model.

Table 4-2. Difference (%) in aerodynamic resistance for the two models in the two seasons.

Season	Land cover	Settings in Wright & Zhang's model	Minimum	First quartile	Median	Third quartile	Maximum	Mean of absolute difference
summer	evergreen needleleaf forest	wind	11	26	30	48	193	47
		wind+buoancy (without cap)	-129	12	28	34	162	32
		wind+buoancy (with cap)	-129	13	29	35	199	36
	deciduous broadleaf forest	wind	11	26	30	48	193	47
		wind+buoancy (without cap)	-131	11	28	34	161	33
		wind+buoancy (with cap)	-131	13	29	35	198	36
winter	evergreen needleleaf forest	wind	12	29	31	39	193	45
		wind+buoancy (without cap)	-129	20	28	31	162	30
		wind+buoancy (with cap)	-129	20	28	31	198	32
	deciduous broadleaf forest	wind	12	29	30	38	193	44
		wind+buoancy (without cap)	-116	22	29	30	168	30
		wind+buoancy (with cap)	-116	22	29	30	199	32

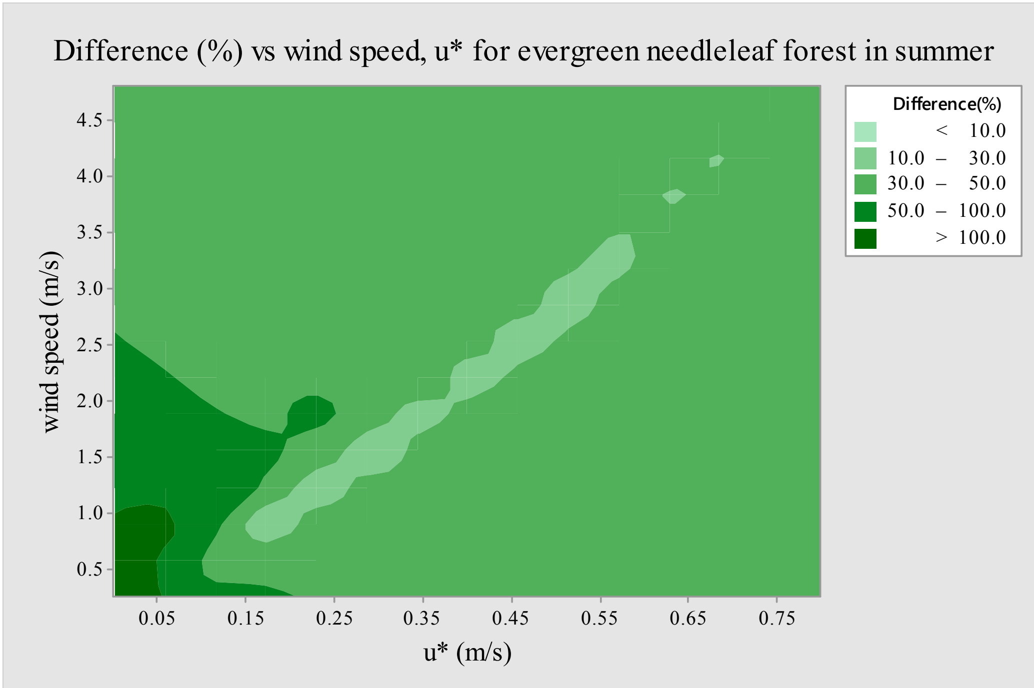

Figure 4-3. Contour plot for difference (%) versus wind speed and friction velocity for evergreen needleleaf forest in summer.

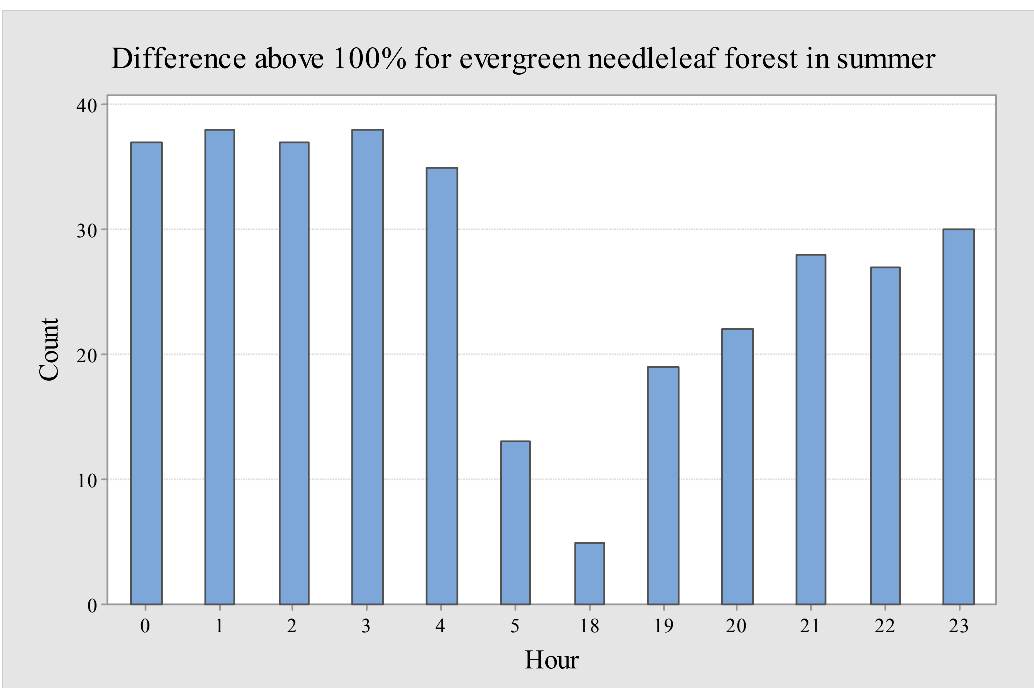

Figure 4-4. Hourly frequency of difference above 100% between the two models for evergreen needleleaf forest in summer.

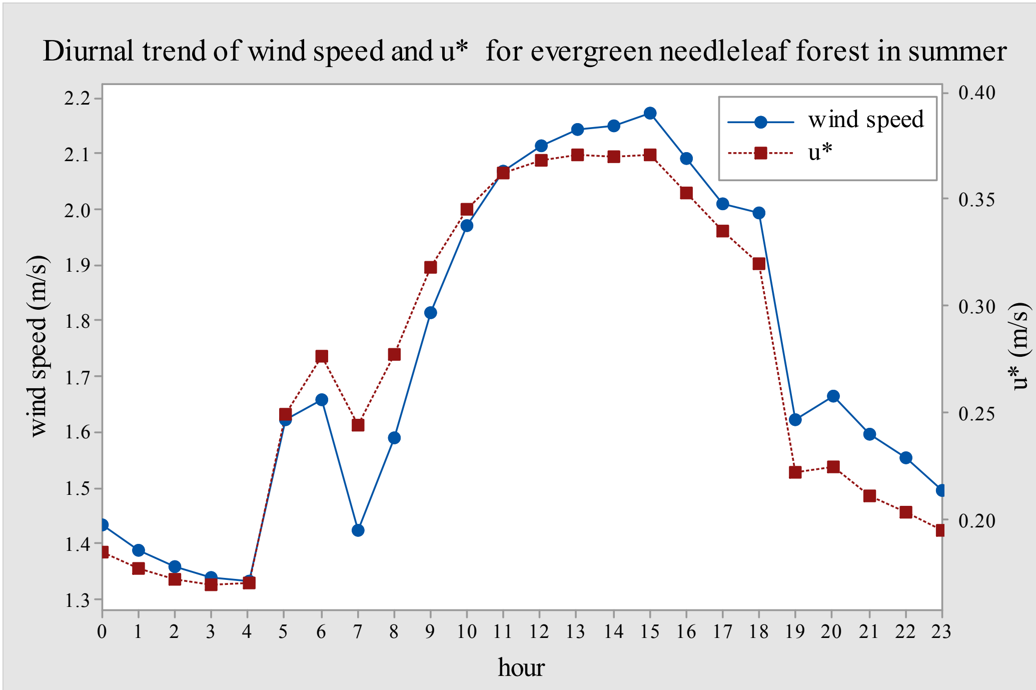

Figure 4-5. Diurnal trend for wind speed and friction velocity for evergreen needleleaf forest in summer.

(3) Which model is better

Aerodynamic resistance caused by wind in Wright & Zhang's model is more appropriate for representation of gaseous pollutants air-surface exchange, including GEM. This is because there are always some exchanges of gaseous pollutants between the atmosphere and the surface under weak wind conditions. Extreme large R_a leads to small velocity, as in Wang's model.

b) R_a caused by buoyancy in Wright & Zhang's model

As seen in Table 4-1, R_a caused by buoyancy in Wright & Zhang's model is in the range of -12s/m to 23761s/m and mean of absolute values is 266s/m. The value of R_a is positive during nighttime (Fig. 4-6) because thermal turbulence cause by buoyancy inhibits GEM air-surface exchange under stable atmosphere. Extreme large values above 4000s/m also happen during nighttime (Fig. 4-7). The value of R_a is negative during daytime (Fig. 4-6) because thermal turbulence accelerates GEM air-surface exchange under unstable atmosphere.

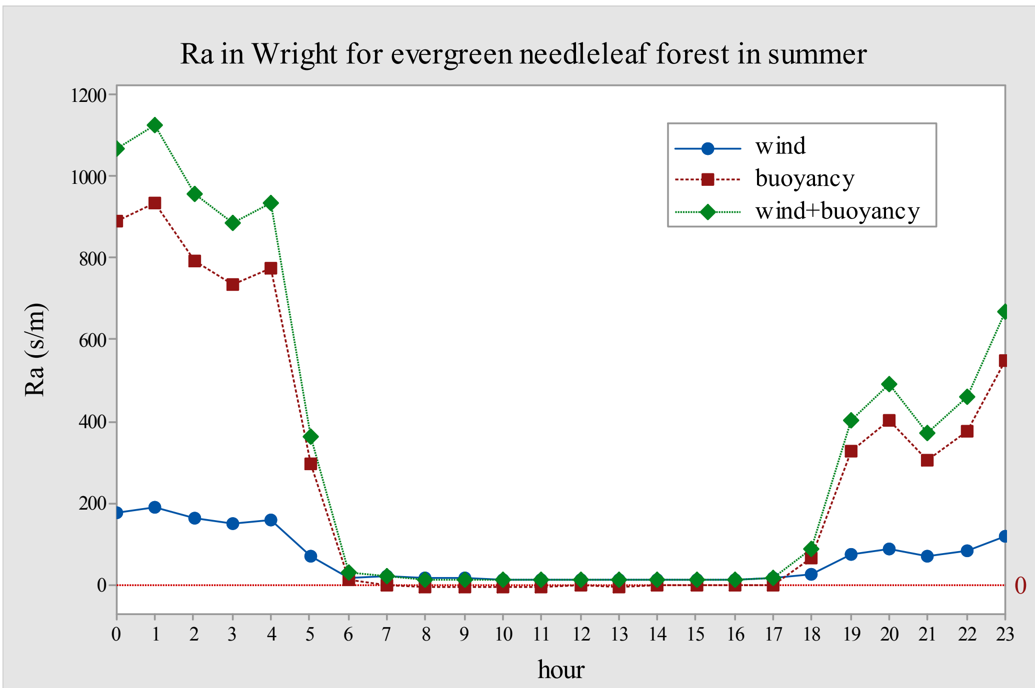

Figure 4-6. Diurnal trend for aerodynamic resistance caused by wind, buoyancy, and both wind and buoyancy in Wright & Zhang's model for evergreen needleleaf forest in summer.

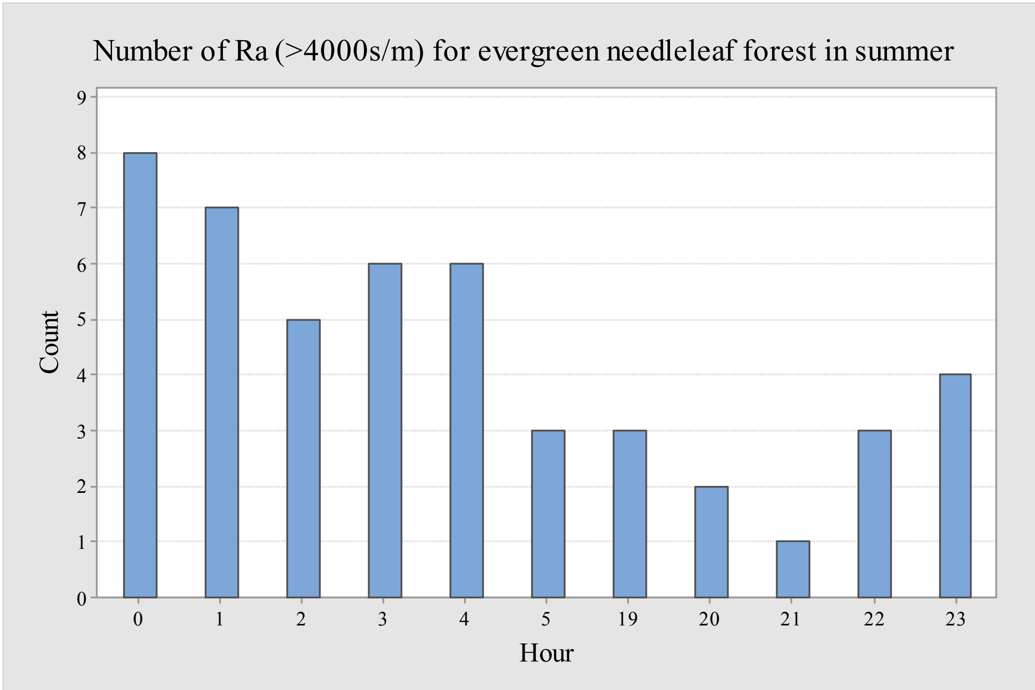

Figure 4-7. Hourly frequency of aerodynamic resistance above 4000s/m caused by buoyancy in Wright & Zhang's model for evergreen needleleaf forest in summer.

c) Compare the turbulence caused by wind and buoyancy in Wright & Zhang's model without cap with the turbulence caused by wind in Wang's model

(1) R_a caused by wind and buoyancy in Wright & Zhang's model

As seen in Table 4-1, R_a caused by wind and buoyancy in Wright & Zhang's model is in the range of 6-28266s/m (mean of 331s/m). Its value is always positive, because Wright & Zhang assumed that R_a caused by wind and buoyancy is 5s/m when R_a is smaller than 5s/m. R_a caused by wind and buoyancy is similar to that caused by wind during 6:00-17:00 (Fig. 4-6) due to small values of R_a caused by buoyancy. R_a caused by wind and buoyancy is much larger than that caused by wind during 0:00-5:00 and 18:00-23:00 (Fig. 4-6) owing to large values of R_a caused by buoyancy. R_a caused by wind and buoyancy in Wright & Zhang's model and R_a in Wang's model have similar diurnal trend with low values during daytime and high values during nighttime (Fig. 4-8).

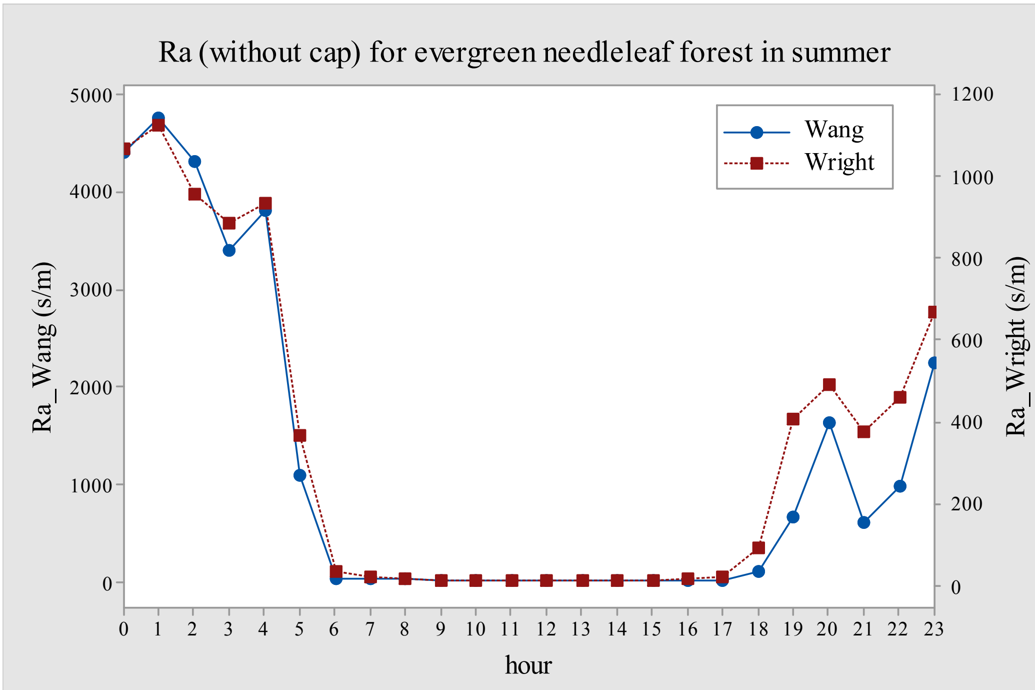

Figure 4-8. Diurnal trend for aerodynamic resistance in the two models without cap for evergreen needleleaf forest in summer.

(2) The difference between the two models and why

Table 4-2 shows the difference between the two models. Fig. 4-9 shows the time series of R_a in the two models and the difference between the two models is smaller compared with the difference in Fig. 4-2. This is because R_a caused by buoyancy results in larger R_a in Wright & Zhang's model. R_a in Wang's model smaller than that in Wright & Zhang's model mainly happens during nighttime (Fig. 4-10) because of large positive values in R_a caused by buoyancy (Fig. 4-7) in Wright & Zhang's.

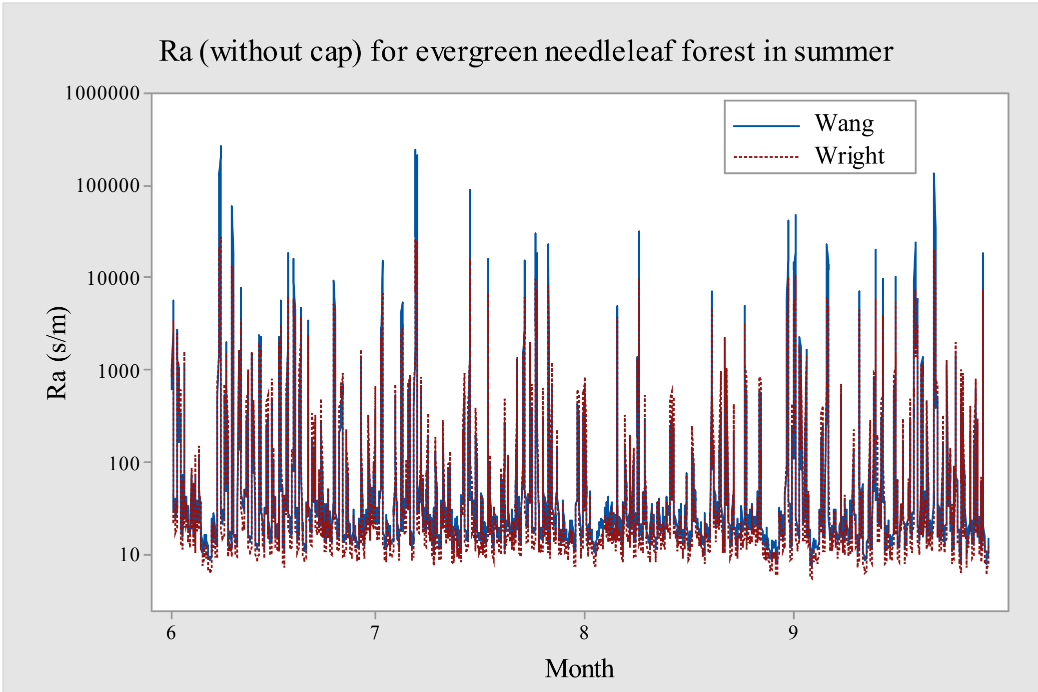

Figure 4-9. Time series for aerodynamic resistance in the two models without cap for evergreen needleleaf forest in summer.

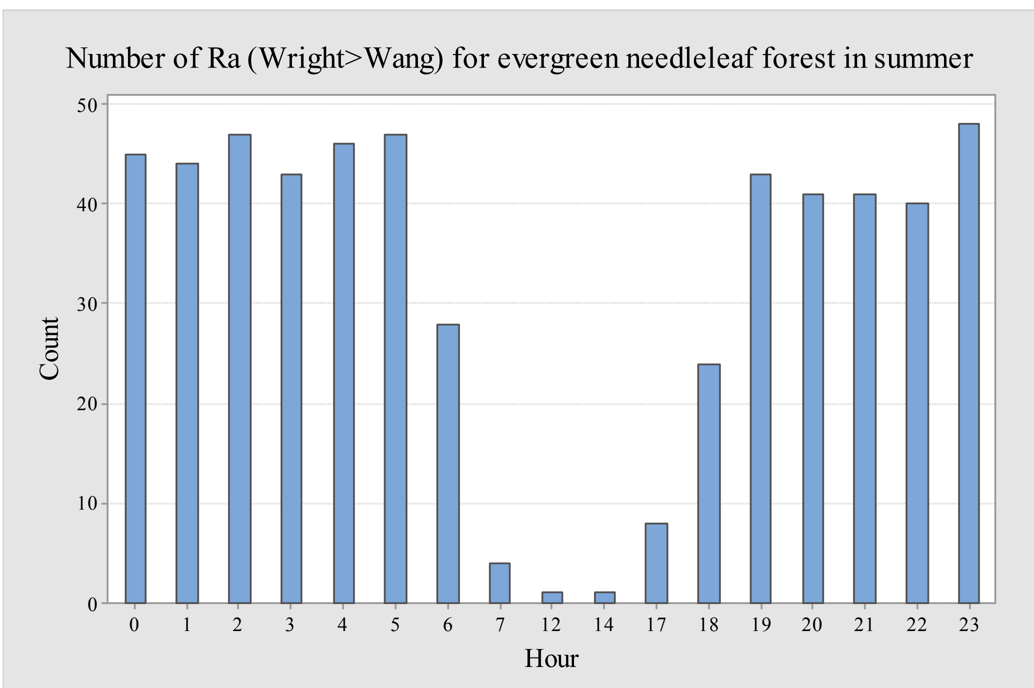

Figure 4-10. Hourly frequency of larger aerodynamic resistance in Wright & Zhang's model for evergreen needleleaf forest in summer.

(3) Which model is better

Aerodynamic resistance in Wright & Zhang's model is more appropriate for representation of GEM air-surface exchange. This is because Wright & Zhang considered the turbulence caused by wind and buoyancy. In nature, gaseous pollutants are transported from the atmosphere to the surface by both mechanical and thermal turbulence.

d) Compare the turbulence caused by wind and buoyancy in Wright & Zhang's model with cap with the turbulence caused by wind in Wang's model

(1) R_a caused by wind and buoyancy in Wright & Zhang's model with cap

6% of R_a in Wright & Zhang's model was capped and 99% of the capped R_a was at night. Table 4-11 shows capped R_a caused by wind and buoyancy in Wright & Zhang's model. R_a in the two models has similar diurnal trend with low values during daytime and high values during nighttime (Fig. 4-11). But trends at 2:00-4:00 and 19:00-22:00 are different in the two models because extreme large values of R_a in Wright & Zhang's model were capped. There is only one extreme large value (>10000s/m) at 3:00 and two extreme large values at 2:00 and 4:00 (Fig. 4-12). After R_a in Wright & Zhang's model was capped, R_a at 3:00 is relatively larger than that at 2:00 and 4:00. There is one extreme large value at 20:00 (Fig. 4-12). After R_a in Wright's model was capped, R_a at 20:00 is relatively smaller than that at 19:00 and 21:00.

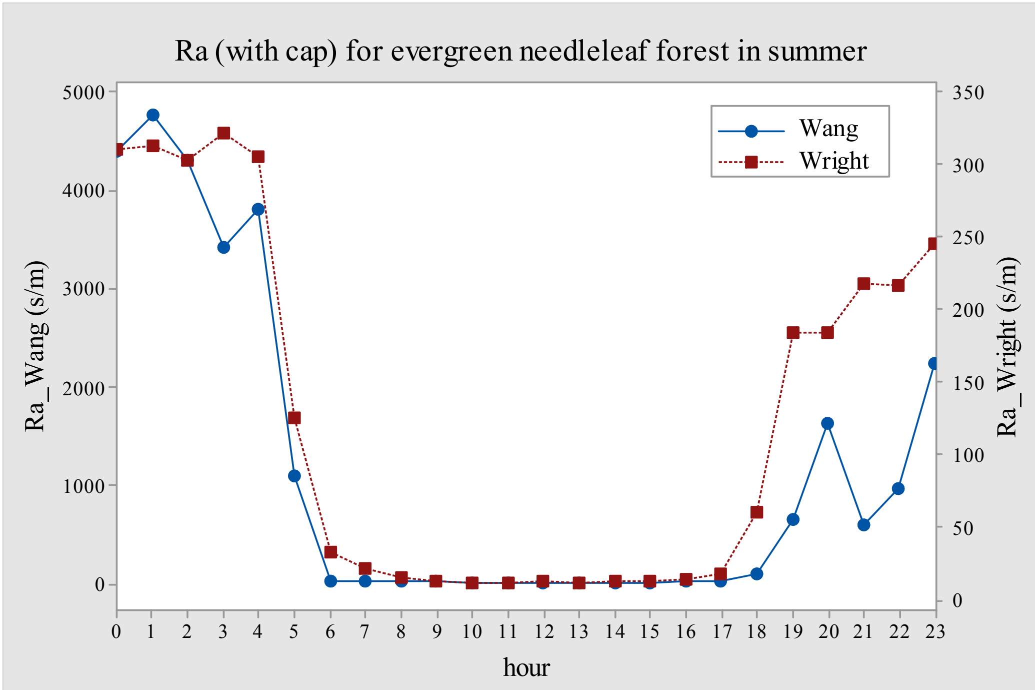

Figure 4-11. Diurnal trend for aerodynamic resistance in the two models with cap in Wright & Zhang's model for evergreen needleleaf forest in summer.

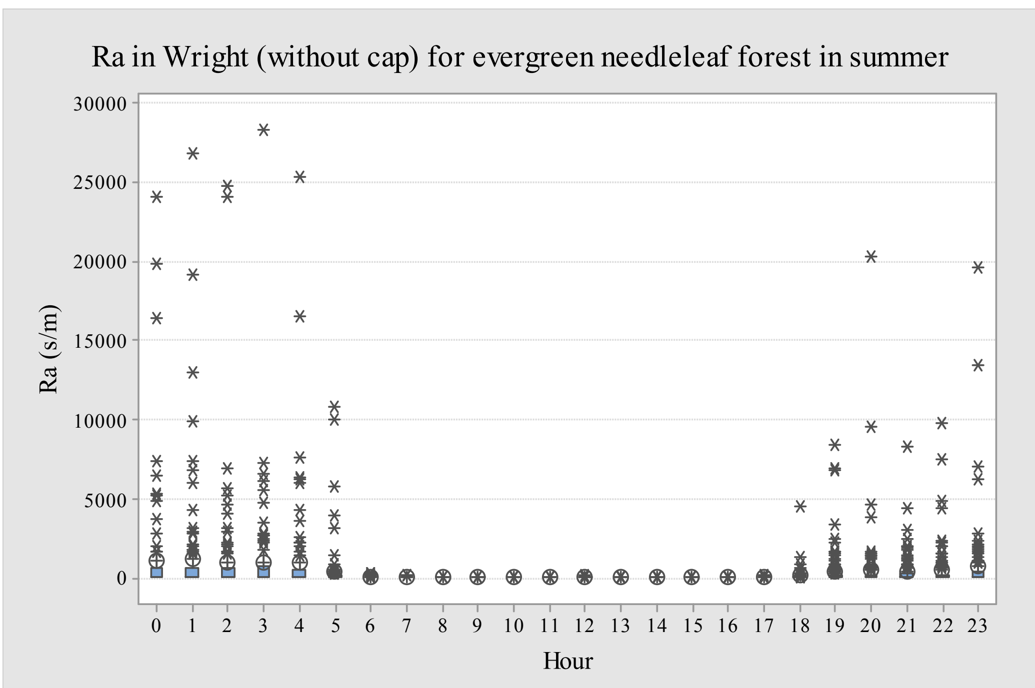

Figure 4-12. Boxplot for aerodynamic resistance caused by wind and buoyancy in Wright & Zhang's model without cap for evergreen needleleaf forest in summer.

(2) The difference between the two models and why

The difference between the two models is shown in Table 4-2. Fig. 4-13 shows the time series for R_a in the two models and the difference between the two models is larger compared with the difference in Fig. 4-9. This is because large R_a in Wright & Zhang's model was capped to 1000s/m.

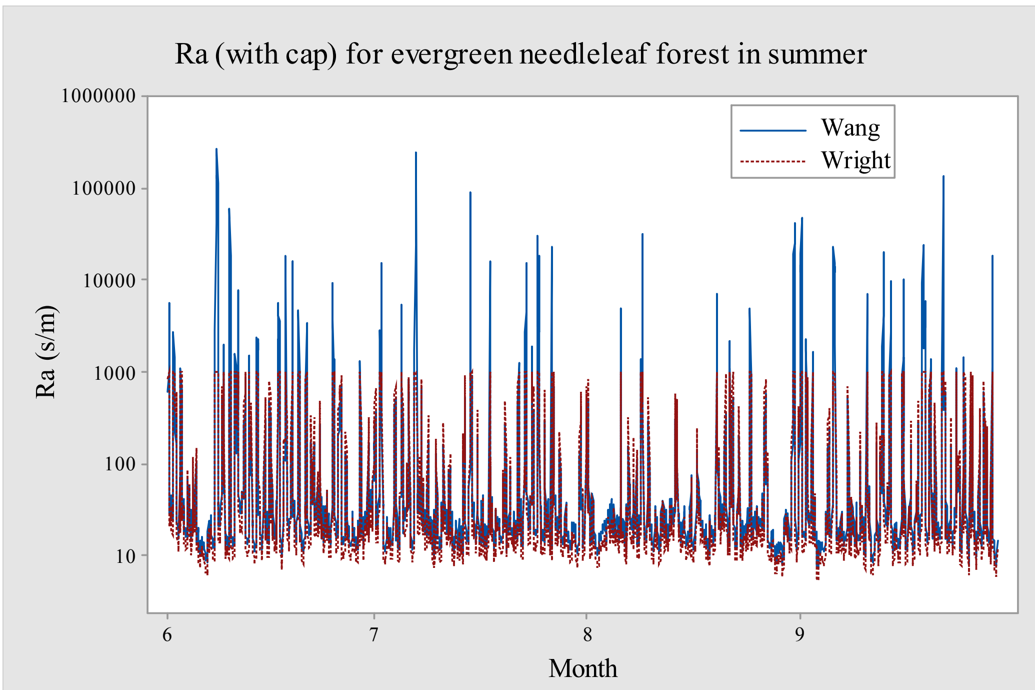

Figure 4-13. Time series for aerodynamic resistance in the two models with cap in Wright & Zhang's model for evergreen needleleaf forest in summer.

(3) Which model is better

Aerodynamic resistance in Wright & Zhang's model is more appropriate for representation of GEM air-surface exchange (Table E4). This is because Wright & Zhang considered the turbulence caused by wind and buoyancy. In nature, gaseous pollutants are transported from the atmosphere to the surface by both mechanical and thermal turbulence. In Wright & Zhang's model, the cap that prevents R_a to be extremely large reflects that there is always some exchange of gaseous pollutants between the atmosphere and the surface under weak wind conditions.

Deciduous broadleaf forest in summer

In R_a, only wind speed and roughness are related with land cover. In summer, wind speed for deciduous broadleaf forest is similar to that for evergreen needleleaf forest (Table D1). For evergreen needleleaf forest, roughness was assumed as a constant of 0.9m. For deciduous broadleaf forest, roughness is dependent on LAI. In summer, LAI ranges from 4.6 to 5.7 (mean of 5.3) and roughness is in the range of 0.87-1m (mean of 0.95m). Roughness for evergreen needleleaf forest (0.9m) is close to that for deciduous broadleaf forest (mean, 0.95m). Thus it is expected that the difference between the two models is similar for the two land covers in summer. As in Table 4-1, R_a in the same case is similar for the two land covers in summer. As seen in Table 4-2, the difference between the two models is also similar for the two covers in summer (36% vs. 36%), as expected.

Evergreen needleleaf forest in winter

As in Table 4-1, R_a caused by wind in Wang's model is larger than that caused by wind and buoyancy in Wright & Zhang's model (mean, 561m/s >85m/s). The reason is similar to that for evergreen needleleaf forest in summer. Higher wind speed in winter (Table D1) results in smaller R_a caused by wind in both models, but to a great degree in

Wang's model. Higher wind speed in winter also caused smaller R_a caused by buoyancy in Wright's model. Table 4-2 shows the difference between the two models is similar to that for evergreen needleleaf forest in summer (32% vs. 36%).

Deciduous broadleaf forest in winter

In R_a, only wind speed and roughness are related with land cover. In winter, wind speed for deciduous broadleaf forest is similar to that for evergreen needleleaf forest (Table D1). For evergreen needleleaf forest, roughness was assumed as a constant of 0.9m. For deciduous broadleaf forest, roughness is dependent on LAI. In winter, LAI ranges from 0.6 to 1 (mean of 0.72) and roughness is in the range of 0.4-0.44m (mean of 0.41m). Small roughness leads to large R_a in both models, to a greater degree in Wang's model. As in Table 4-1, R_a in Wang's model is larger than that in Wright & Zhang's model (mean, 844s/m>102s/m). As seen in Table 4-2, the difference between the two models is similar to that for evergreen needleleaf forest in winter (32% vs. 32%).

Summary

Regardless of season and land cover, R_a in Wang's model is larger than that in Wright & Zhang's model (mean, 927s/m>108s/m). For the same land cover and different seasons, the difference between the two models is similar (36% vs. 32% for evergreen needleleaf forest, 36% vs. 32% for deciduous broadleaf forest). Although higher wind speed in winter leads to smaller R_a in both models and to a greater degree in Wang's model, higher wind speed does not cause significant influence in the difference between the two models. As in Table 4-3, season is insignificant in the difference between the two models (p=0.926).

Table 4-3. Analysis of variance (ANOVA) of the difference in aerodynamic resistance between the two models.

Parameter	p-value
season	0.926
land cover	0.052
season*land cover	0.026

For different land covers and the same season, the difference between the two models is similar (36% vs. 36% in summer, 32% vs. 32% in winter). In summer, this is because of similar wind speed and roughness in the two land covers. In winter, although small roughness causes larger R_a in both models and to a great degree in Wang's model, small roughness does not cause significant effect on the difference between the two models. Wind speed in winter is similar for the two land covers. However, land cover is significant in the difference between the two models (p=0.052).

4.1.2 Quasi-laminar resistance (R_b)

For R_b, two parameters are different in the two models—air diffusivity (VI) and GEM diffusivity (DI), and other parameters are the same (Table C1). Wang assumed VI to be 0.22cm^2/s and DI to be 0.13cm^2/s. The ratio of VI to DI is 1.69. In Wright & Zhang's model, VI and DI are dependent on ambient temperature, and are not related with land cover.

Evergreen needleleaf forest in summer

a) R_b in the two models

Table 4-4 shows R_b in the two models. R_b in the two models has similar diurnal trend with low values during daytime and high values during nighttime (Fig. 4-14 and Table E1). R_b in Wang's model is always smaller than that in Wright & Zhang's (Fig. 4-15).

Table 4-4. Quasi-laminar resistance (R_b, s/m) for the two models in the two seasons.

Land cover	Season	Model	Minimum	First quartile	Median	Third quartile	Maximum	Mean
evergreen needleleaf forest	summer	Wang	9	19	25	43	7004	101
		Wright & Zhang	10	21	29	50	8302	118
	winter	Wang	6	12	16	27	6680	56
		Wright & Zhang	7	15	20	33	8257	69
deciduous broadleaf forest	summer	Wang	9	18	25	43	6907	99
		Wright & Zhang	10	21	29	49	8186	116
	winter	Wang	7	15	20	22	8102	68
		Wright & Zhang	8	18	24	39	10014	83

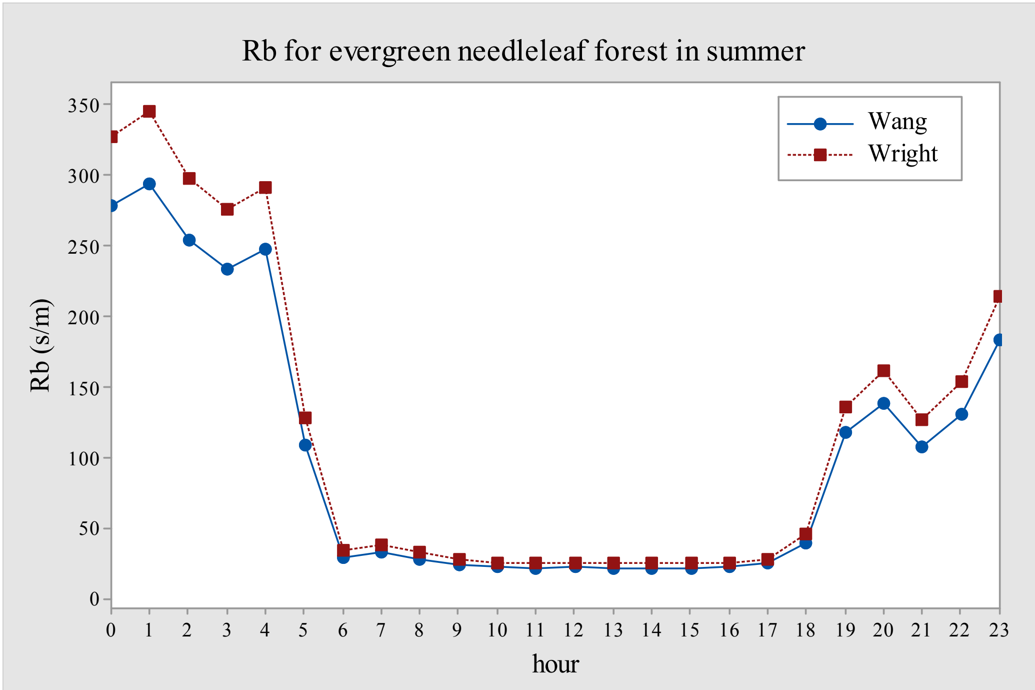

Figure 4-14. Diurnal trend for quasi-laminar resistance in the two models for evergreen needleleaf forest in summer.

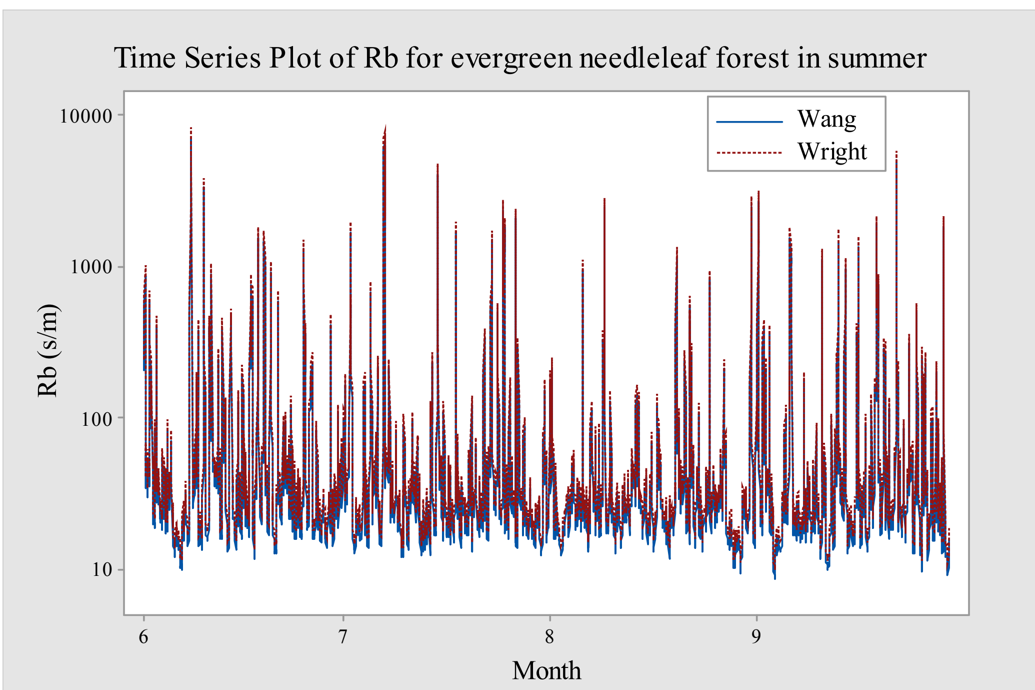

Figure 4-15. Time series for quasi-laminar resistance in the two models for evergreen needleleaf forest in summer.

b) The difference between the two models and why

The two models have the same equation for R_b, however their settings on VI and DI are different. Wang assumed that VI is 0.22cm^2/s and DI is 0.13cm^2/s. The ratio of VI to DI is 1.69. In Wright & Zhang's model, VI and DI are dependent on temperature. The difference between the two models is listed in Table 4-5. In summer, ambient temperature varies between 12.6°C and 35.5°C (mean of 26.9°C). In Wright & Zhang's model, the range of VI is 0.18-0.19cm^2/s (mean of 0.18cm^2/s) and VI is larger in Wang's model (0.22cm^2/s>0.18cm^2/s). The range of DI is 0.08-0.1cm^2/s (mean of 0.09cm^2/s) and DI is also larger in Wang's model (0.13cm^2/s>0.09cm^2/s). The ratio of VI to DI is in the range of 1.97-2.15 (mean of 2.04) and the ratio is smaller in Wang's model (1.69<2.04). Smaller ratio leads to smaller R_b in Wang's model.

Table 4-5. Difference (%) in quasi-laminar resistance for the two land covers in the two seasons.

Land cover	Season	Minimum	First quartile	Median	Third quartile	Maximum	Mean of absolute difference (%)
evergreen needleleaf forest	summer	-18	-15	-15	-14	-13	15
	winter	-23	-21	-19	-18	-15	19
deciduous broadleaf forest	summer	-18	-15	-15	-14	-13	15
	winter	-23	-21	-19	-18	-15	19

c) Which model is better

Quasi-laminar resistance in Wright & Zhang's model is more appropriate for GEM air-surface exchange (Table E4). This is because R_b in Wright & Zhang's model reflects the effect of ambient temperature on air diffusivity and GEM diffusivity. When the ratio of air diffusivity to GEM diffusivity is large, exchange of GEM is difficult.

Deciduous broadleaf forest in summer

The difference between the two models is only dependent on ambient temperature, and is not related with land cover. It is expected that the difference between the two models is the same for two land covers in summer. Table 4-4 shows that R_b in Wang's model is smaller than that in Wright & Zhang's model (mean, 99s/m<116s/m). As seen in Table 4-5, the difference between the two models is the same as that for evergreen needleleaf forest in summer, as expected (15% vs. 15%).

Evergreen needleleaf forest in winter

The difference between the two models is only dependent on ambient temperature, and ambient temperature is lower in winter (Table D1). In Wright & Zhang's model, VI in winter (mean, 0.17cm^2/s) is similar to that in summer (mean, 0.18cm^2/s). DI in winter (mean, 0.08cm^2/s) is also similar to that in summer (mean, 0.09cm^2/s). The ratio of VI to DI in winter (mean, 2.18) is similar to that in summer (mean, 2.04). In Wang's model, the ratio of VI to DI is a constant of 1.69. Thus, it is expected that the difference between the two models is similar in the two seasons. As seen in Table 4-4, R_b in Wang's model is smaller than that in Wright & Zhang's model (mean, 56s/m<69s/m). As in Table 4-5, the difference between the two models is similar to that for evergreen needleleaf forest in summer (19% vs. 15%), as expected.

Deciduous broadleaf forest in winter

The difference between the two models is only dependent on ambient temperature, and is not related with land cover. It is expected that the difference between the two models is the same for two land cover in winter. Table 4-4 shows that R_b in Wang's model is smaller than that in Wright & Zhang's model (mean, 68s/m<83s/m). As shown in Table 4-5, the difference between the two models is the same as that for evergreen needleleaf forest in winter, as expected (19% vs. 19%).

Summary

Regardless of season and land cover, R_b in Wang's model is smaller than that in Wright & Zhang's model (mean, 79s/m<94s/m). For the same land cover and different seasons, the difference between the two models is similar (15% vs. 19% for evergreen needleleaf forest, 15% vs. 19% for deciduous broadleaf forest) because of similar values of VI and DI as well as the ratio of VI to DI in Wright & Zhang's model. However, as in Table 4-6, season is significant in the difference between the two models (p=0.001).

Table 4-6. Analysis of variance (ANOVA) of the difference in quasi-laminar resistance between the two models.

Parameter	p-value
season	0.001
land cover	0.99
season*land cover	0.99

For the same season and different land cover, the difference between the two models is the same (15% vs. 15% in summer, 19% vs. 19% in winter). This is because VI and DI are not dependent on land cover. Table 4-6 shows that land cover has little effect on the difference between the two models (p=0.99).

4.1.3 Stomata resistance (R_{st})

For R_{st}, constant values for stomata closure, visible solar radiation, water vapor diffusivity (DV), GEM diffusivity (DI), and the range of correction factor for water vapor pressure deficit of air (f_D) are different in the two models, and other parameters are the same (Table C1). (1) Wang and Wright & Zhang set a constant value for R_{st} as 1820500s/m and 296120s/m, respectively, to represent stomata closure. (2) Parameterizations of visible solar radiation in the two models are different. Wang assumed that visible solar radiation is calculated from a constant solar radiation of 600W/m^2 at the top atmosphere. In Wright & Zhang's model, visible solar radiation is calculated from input solar radiation. Both Wang and Wright & Zhang assumed that barometric pressure has an effect on visible solar radiation. However Wang required input barometric pressure and Wright & Zhang assumed barometric pressure to be 101.3kPa. The difference in visible solar radiation between the two models is not related with land cover.

(3) In Wang's model, DV and DI were assumed to be 0.237cm^2/s and 0.13cm^2/s, respectively. The ratio of DV to DI is 1.82. In Wright & Zhang's model, DV and DI are dependent on ambient temperature. However the ratio of DV to DI is a constant of 2.96. The difference in ratio of DV to DI between the two models is not related with land cover and season. (4) f_D reflects the effect of water vapor pressure deficit on stomata.

Water vapor pressure deficit is the difference between actual air moisture and saturated air moisture. Water vapor pressure deficit is large when actual air moisture is much lower than saturated air moisture. f_D has different ranges in the two models. Wang assumed f_D to be in the range of 0-1.0, and Wright & Zhang set its range to be 0.1-1.0.

Evergreen needleleaf forest in summer

a) R_{st} in the two models

Table 4-7 shows R_{st} in the two models. R_{st} in Wright & Zhang's model always keeps small values during daytime, and that in Wang's model has large values during 11:00-16:00 (Fig. 4-16 and Table E1). Large values in Wang's model is caused by f_D smaller than 0.1 (Fig 4-17). Small f_D leads to large R_{st} in Wang's model. Assuming that f_D in Wang's model is greater or equal to 0.1, as in Wright & Zhang's model, R_{st} in Wang's model always keeps small values during daytime (Fig. 4-16). During daytime, 85% of R_{st} in Wright & Zhang's model is larger than that in Wang's model. However, R_{st} in Wang's model has extreme large values (>10^6s/m) (Fig. 4-18). Most of large values in Wang's model is due to f_D smaller than 0.1. Assuming that f_D in Wang's model is greater or equal to 0.1, large values in Wang's model are much fewer (Fig. 4-19). However, there are still large values in the two models in September. This is because daytime was set from 6:00 to 18:00 in summer. In September, sunrise occurs later and sundown occurs earlier. Solar radiation at 6:00 and 18:00 are weaker, and thus R_{st} in the two models are large. Overall, R_{st} in Wang's model is larger than that in Wright & Zhang's model (mean, 891108s/m>136953s/m).

Table 4-7. Stomata resistance (R_{st}, s/m) for the two models in the two seasons.

Season	Land cover	Model	Minimum	First quartile	Median	Third quartile	Maximum	Mean
summer	evergreen needleleaf forest	Wang	691	1410	17372	1820500	1820500	871108
		Wright & Zhang	936	2185	12900	296120	1123590	136953
	deciduous broadleaf forest	Wang	610	897	1820500	1820500	1820500	986362
		Wright & Zhang	731	1240	4078	296120	778415	135133
winter	evergreen needleleaf forest	Wang	807	1718	1820500	1820500	1820500	1070650
		Wright & Zhang	1072	3080	296120	296120	870393	178713
	deciduous broadleaf forest	Wang	953	2305	1820500	1820500	1820500	1152673
		Wright & Zhang	1391	4696	296120	296120	487310	192182

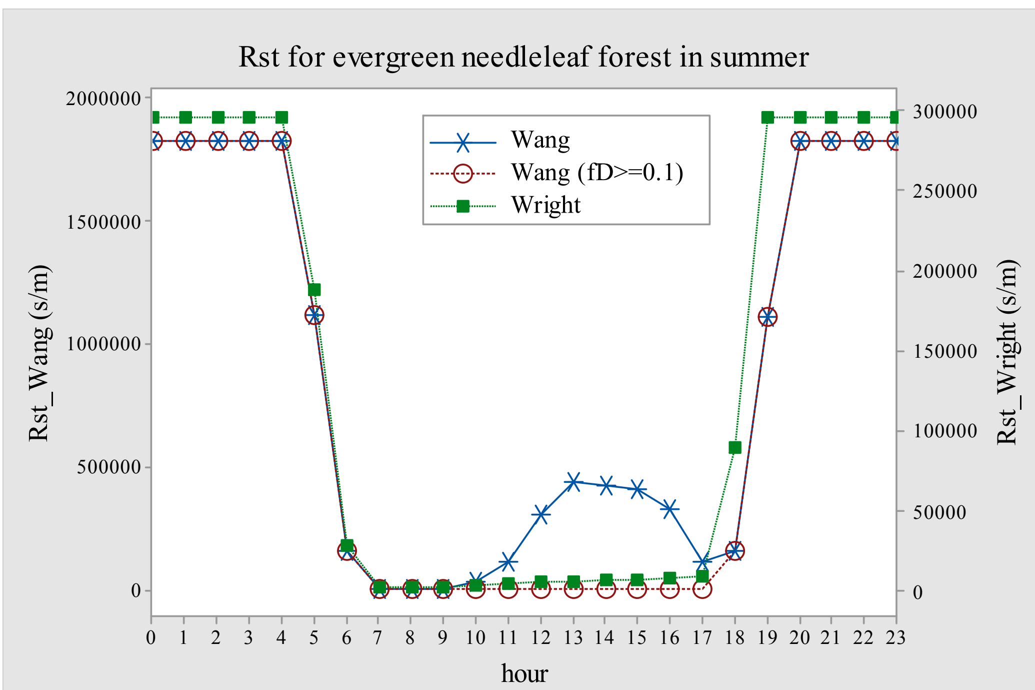

Figure 4-16. Diurnal trend for stomata resistance in the two models for evergreen needleleaf forest in summer.

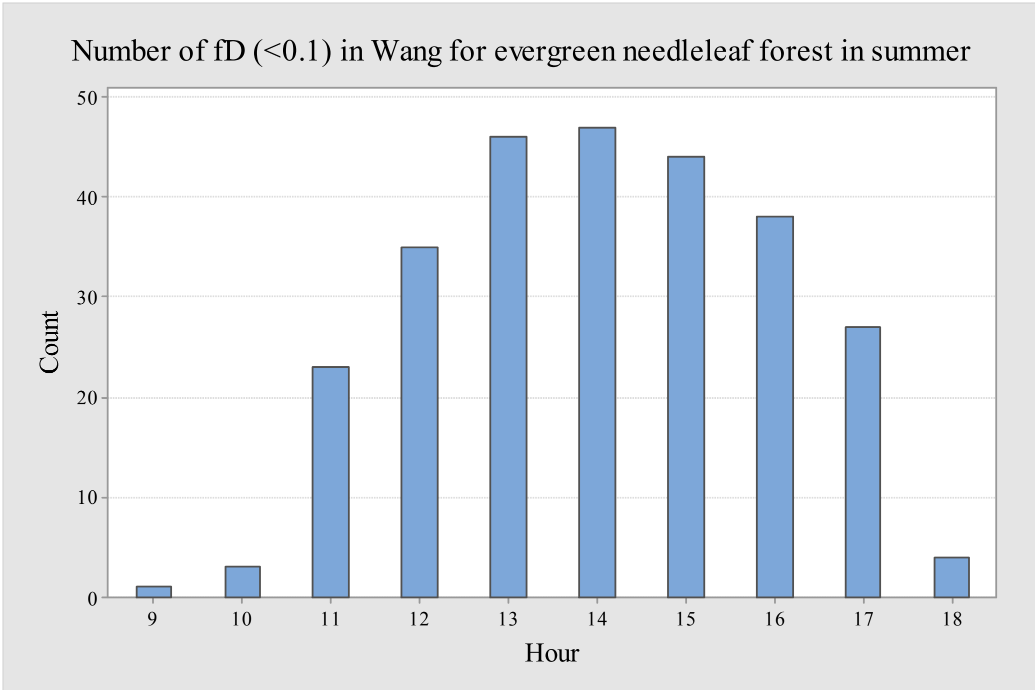

Figure 4-17. Hourly frequency of the correction factor for water vapor pressure deficit below 0.1 in Wang's model for evergreen needleleaf forest in summer.

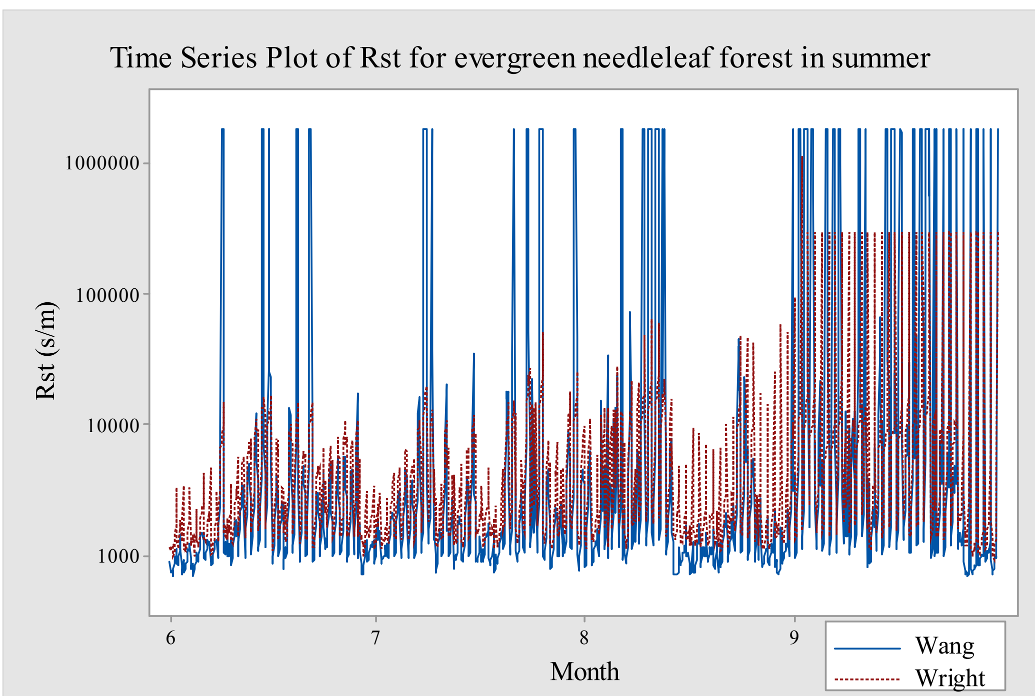

Figure 4-18. Time series for stomata resistance in the two models during daytime for evergreen needleleaf forest in summer.

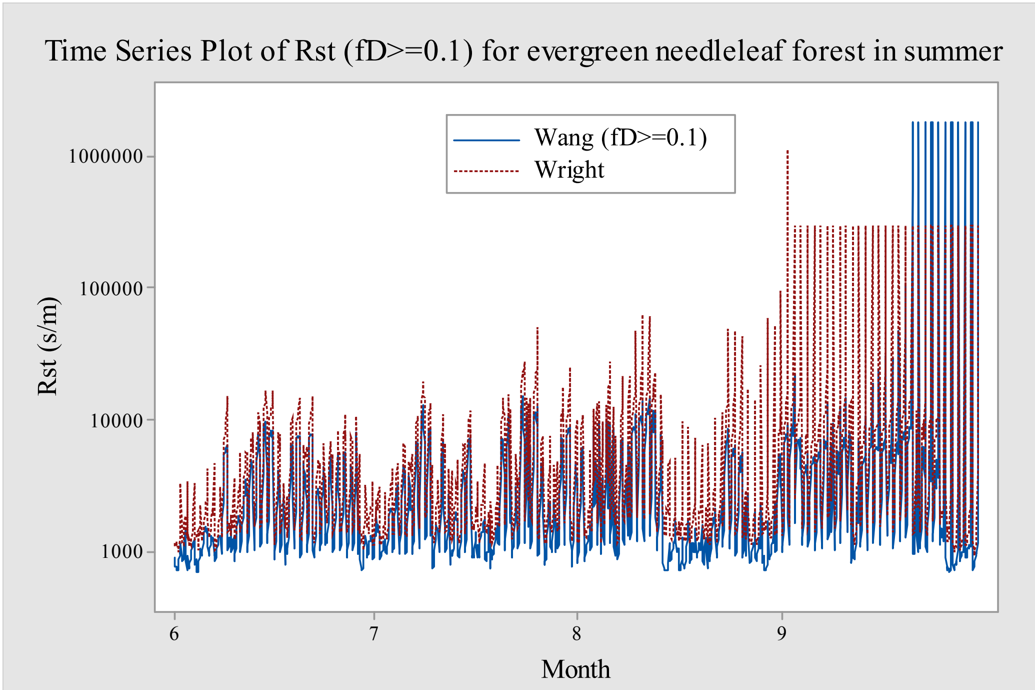

Figure 4-19. Time series for stomata resistance with correction factor for water vapor pressure deficit >=0.1 in Wang's model during daytime for evergreen needleleaf forest in summer.

b) The difference between the two models and why

(1) The difference between the two models

As seen in Table 4-8, the difference between the two models varies between -197% and 199%, and mean of absolute difference is 98%. The difference is mainly caused by f_D and constant values for stomata closure.

Table 4-8. Difference (%) in stomata resistance for the two models in the two seasons.

Season	Land cover	Settings in the two models	Minimum	First quartile	Median	Third quartile	Maximum	Mean of absolute difference (%)
summer	evergreen needleleaf forest	no change	-197	-36	11	144	199	98
		visible solar radiation in Wang's model (Wright & Zhang)	-195	-33	10	144	199	93
		DV/DI=1.82 (Wright & Zhang)	-195	-4	55	164	199	94
		$f_D \geq 0.1$ (Wang)	-197	-40	-26	144	144	91
	deciduous broadleaf forest	no change	-197	-24	144	144	199	104
winter	evergreen needleleaf forest	no change	-195	-42	144	144	144	108
	deciduous broadleaf forest	no change	-194	-42	144	144	144	113

(2) Effect of constant values for stomata closure

Stomata will close when there is no solar radiation during nighttime. Wang and Wright & Zhang assumed that R_{st} will be constants of 1820500s/m and 296120s/m for stomata closure, respectively. These two constant values are not affected by land cover and season.

(3) Effect of visible solar radiation

Both Wang and Wright & Zhang assumed that barometric pressure has an influence on visible solar radiation. Wang required input barometric pressure and Wright & Zhang assumed barometric pressure to be 101.3kPa. In summer, input barometric pressure is in the range of 97kPa and 99kPa (mean of 98kPa) and is close to 101.3kPa. Different treatments on barometric pressure have little effect on visible solar radiation.

Wang assumed that visible solar radiation is calculated from a constant solar radiation of 600W/m^2 at the top atmosphere. Visible solar radiation ranges from 0W/m^2 to 534W/m^2 (mean of 337W/m^2). Wright & Zhang assumed that visible solar radiation is calculated from input solar radiation. Visible solar radiation varies between 0W/m^2 and 403W/m^2 (mean of 179W/m^2). Large visible solar radiation leads to small R_{st} in Wang's model. Assuming that visible solar radiation in Wright & Zhang's model is the same as that in Wang's model, the difference between the two models is in the range of -195% to 199% and mean of absolute difference is 93% (Table 4-8). This difference is similar to 98%. Different parameterizations of visible solar radiation have little effect on the difference between the two models.

(4) Effect of ratio of DV to DI

In Wang's model, DV and DI were assumed to be 0.237cm^2/s and 0.13cm^2/s, respectively. The ratio of DV to DI is 1.82. In Wright & Zhang's model, DV and DI are dependent on temperature, and the ratio of DV to DI is a constant of 2.96. Small ratio of DV to DI results in small R_{st} in Wang's model. Assuming that the ratio of DV to DI is 1.82 in Wright & Zhang's model, the difference between the two models is in the range of -195% to 199% and mean of absolute difference is 94% (Table 4-8). This difference is similar to 98%. Different ratios of DV to DI have little effect on the difference between the two models.

(5) Effect of f_D

The range of f_D is different in the two models. Wang assumed f_D to be in the range of 0-1.0, and its range was 0.1-1.0 in Wright & Zhang's. When ambient water vapor pressure deficit is high, f_D is small because stomata will partially close to protect leaves from losing too much water. f_D below 0.1 leads to large R_{st} in Wang's model. f_D below 0.1 in Wang's model is only produced during daytime (Fig. 4-17). Assuming f_D in Wang's model is greater than or equal to 0.1, as in Wright & Zhang's model, the difference between the two models is in the range of -197% to 144% and mean of absolute difference is 91% (Table 4-8). This difference is smaller than 98%. Different ranges of f_D have an effect on the difference between the two models.

c) Which model is better

Wright & Zhang's model is more appropriate for representation of GEM air-surface exchange (Table E4). The parameterization of visible solar radiation in Wright & Zhang's model is more appropriate for the simulation of solar radiation received by leaves. This is because the calculation of visible solar radiation from input solar radiation reflects the effect of clouds. In Wright & Zhang's model, the dependence of DV and DI on ambient temperature is better. f_D above 0.1 is better because leaves in forest will close partially when ambient water vapor is deficient during daytime.

Deciduous broadleaf forest in summer

In R_{st}, only LAI and f_D are related with land cover. Larger LAI for deciduous broadleaf forest (Table D1) causes more visible solar radiation received by leaves and smaller R_{st} in both models. In f_D, water vapor pressure deficit (D) is not dependent on land cover, but empirical water vapour pressure deficit constant (b_{vpd}) is a constant for each land cover (Table C1). b_{vpd} was set as 0.31kPa^{-1} and 0.36kPa^{-1} for evergreen needleleaf forest and deciduous broadleaf forest, respectively. Larger b_{vpd} leads to smaller f_D and more f_D below 0.1 in Wang's model (Fig. 4-20) for deciduous broadleaf forest compared with Fig. 17. More f_D below 0.1 causes larger R_{st} in Wang's model. As in Table 4-7, R_{st} in Wang's model is larger than that for Wright & Zhang's model (mean, 986362s/m>135133s/m) and the reason is similar to that for evergreen needleleaf forest in summer. As seen in Table 4-8, there are more R_{st} in Wang's model larger than that in Wright & Zhang's model, compared with that for evergreen needleleaf forest in summer. However, the overall difference between the two models is similar to that for deciduous broadleaf forest in summer (104% vs. 98%).

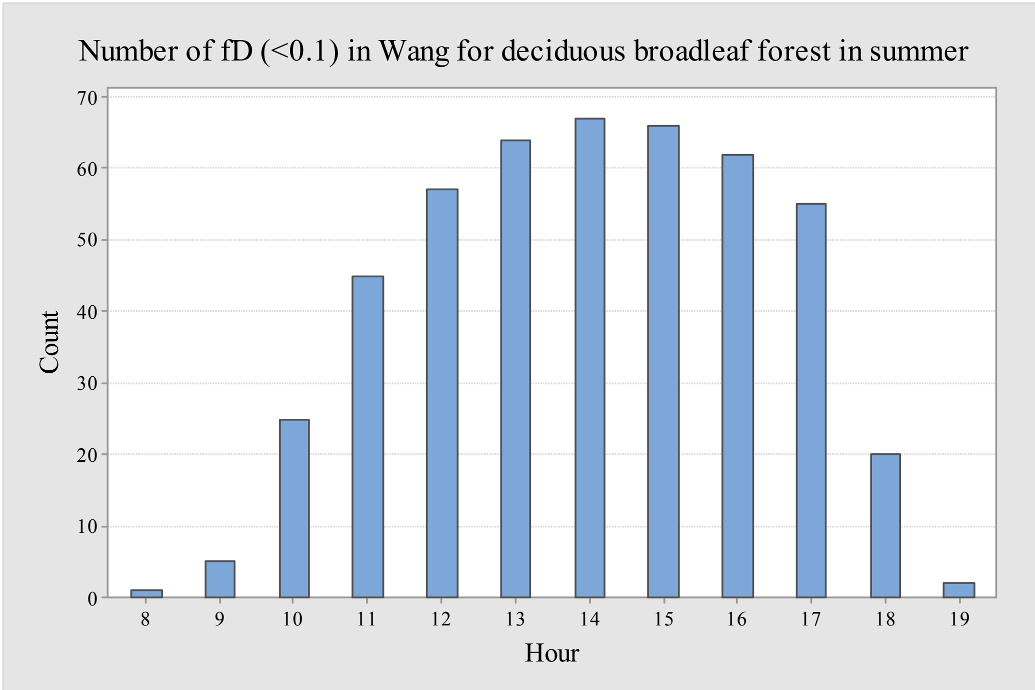

Figure 4-20. Hourly frequency of the correction factor for water vapor pressure deficit below 0.1 in Wang's model for deciduous broadleaf forest in summer.

Evergreen needleleaf forest in winter

In R_{st}, solar radiation, LAI, and f_D are related with season. Smaller solar radiation in winter (Table D1) leads to larger R_{st} for both models. Longer nighttime results in more stomata closure and more large values of R_{st} in the two models. Smaller LAI in winter (Table D1) also causes larger R_{st} in both models. f_D below 0.1 does not happen in winter because water vapor content in the air is high, which results in smaller R_{st} in Wang's model. As in Table 4-7, R_{st} in Wang's model is larger than that in Wright & Zhang's model (mean, 1070650s/m>178713s/m). As seen in Table 4-8, the difference between the two models is larger than that for evergreen needleleaf forest in summer (108% vs. 98%). For R_{st} that is smaller in Wang's model, the difference between the two models is larger because of f_D above 0.1. For R_{st} that is larger in Wang's model, the difference between the two models is also larger because of more stomata closure.

Deciduous broadleaf forest in winter

In R_{st}, only LAI and f_D are related with land cover. Smaller LAI for deciduous broadleaf forest (Table D1) causes fewer visible solar radiation received by leaves and larger R_{st} in both models. f_D is always larger than 0.1 in Wang's model. Table 4-7 shows that R_{st} in Wang's model is larger than that for Wright & Zhang's model (mean, 1152673s/m>192182s/m). As seen in Table 4-8, the difference between the two models is similar to that for evergreen needleleaf forest in winter (113% vs. 108%).

Summary

Regardless of season and land cover, R_{st} in Wang's model is larger than that in Wright & Zhang's model (mean, 1019048s/m>160435s/m). For the same land cover and different seasons, greater difference between the two models is in winter (98% vs. 108% for evergreen needleleaf forest, 104% vs. 113% for deciduous broadleaf forest) because of f_D above 0.1 and more stomata closure under longer nighttime. For R_{st} that is smaller in Wang's model, the difference between the two models is larger because of f_D above 0.1. For R_{st} that is larger in Wang's model, the difference is also larger because of more stomata closure. As in Table 4-9, season is significant in the difference between the two models (p=0.001).

Table 4-9. Analysis of variance (ANOVA) of the difference in stomata resistance between the two models.

Parameter	p-value
season	0.001
land cover	0.001
season*land cover	0.002

For different land cover in summer, although smaller b_{vpd} leads to more f_D below 0.1 and larger R_{st} in Wang's model for deciduous broadleaf forest, the difference between the two models is similar (98% vs. 104%). For different land cover in winter, the difference between the two models is similar (108% vs. 113%) due to f_D above 0.1 in Wang's model in winter. However, Table 4-9 shows that land cover is significant in the difference between the two models (p=0.001).

4.1.4 Cuticle resistance (R_{cut})

R_{cut} is the same in the two models, and thus there is no difference between the two models regardless of season and land cover.

4.1.5 In-canopy aerodynamic resistance (R_{ac})

For evergreen needleleaf forest, regardless of season, there is no difference between the two models because R_{ac} is the same in the two models. For deciduous broadleaf forest, only one parameter is different in the two models—reference value of R_{ac} (R_{ac0}), and other parameters are the same (Table C1). Wang assumed R_{ac0} to be a constant of 250s/m for deciduous broadleaf forest. In Wright & Zhang's model, R_{ac0} is dependent on LAI.

Deciduous broadleaf forest in summer

a) R_{ac} in the two models

Table 4-10 shows R_{ac} in the two models. R_{ac} in the two models has similar diurnal trend with low values during daytime and high values during nighttime (Fig. 4-21 and Table E1). R_{ac} in Wang's model is always larger than that in Wright & Zhang's model (Fig. 4-22).

Table 4-10. In-canopy aerodynamic resistance (R_{ac}, s/m) in the two models for deciduous broadleaf forest in the two seasons.

Land cover	Season	Model	Minimum	First quartile	Median	Third quartile	Maximum	Mean
deciduous broadleaf forest	summer	Wang	581	2651	4862	14460	$3.8*10^8$	1431131
		Wright & Zhang	220	1022	1877	5657	$1.5*10^8$	556848
	winter	Wang	240	1009	1865	5100	$3*10^8$	485466
		Wright & Zhang	59	246	455	1242	$7*10^7$	117880

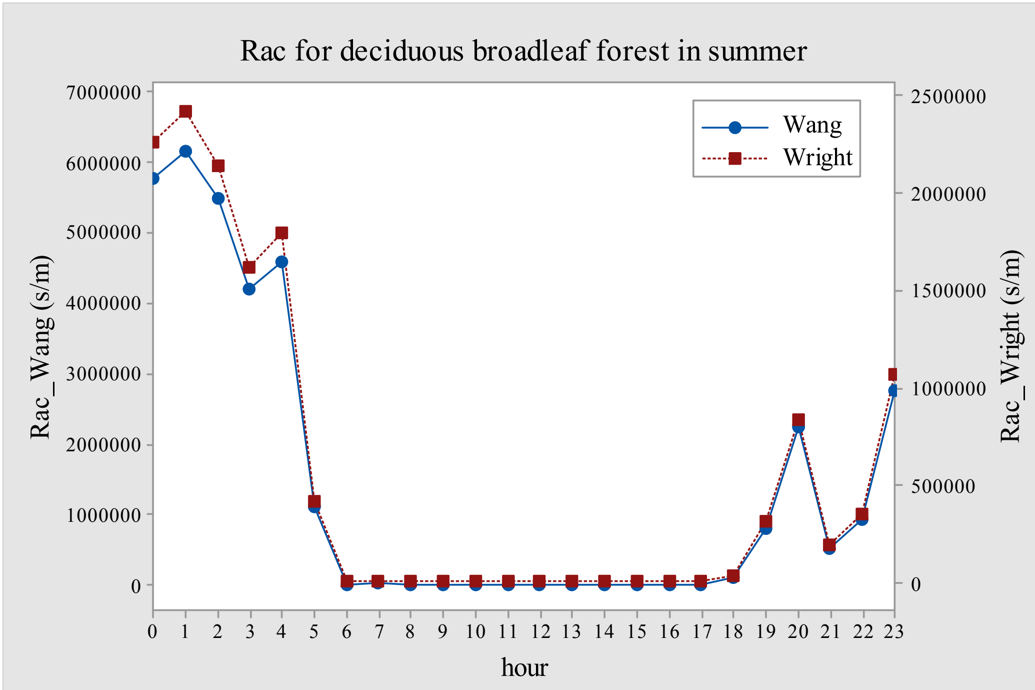

Figure 4-21. Diurnal trend for in-canopy aerodynamic resistance in the two models for deciduous broadleaf forest in summer.

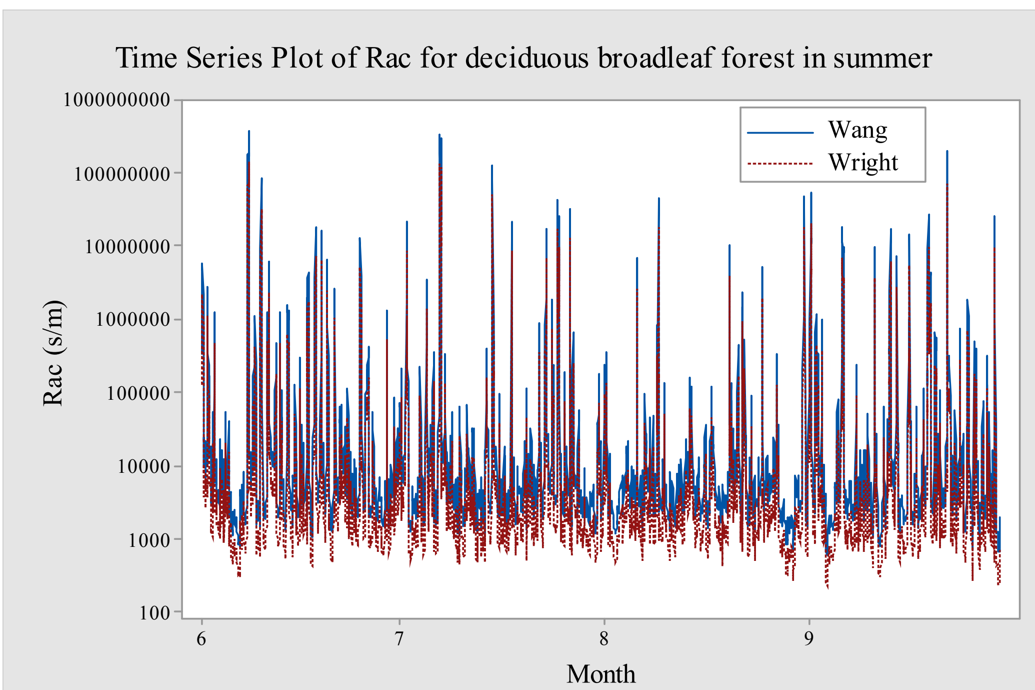

Figure 4-22. Time series for in-canopy aerodynamic resistance in the two models for deciduous broadleaf forest in summer.

b) The difference between the two models and why

The two models have the same equation for R_{ac}, but their settings on R_{ac0} are different. Wang assumed R_{ac0} to be a constant of 250s/m for deciduous broadleaf forest. In Wright & Zhang's model, R_{ac0} is related with LAI. As in Table 4-11, the difference between the two models is in the range of 86-93% (mean of 89%). For deciduous broadleaf forest in summer, LAI ranges from 4.64-5.75 (mean of 5.3) and R_{ac0} in Wright & Zhang's model is in the range of 91-100s/m (mean of 96s/m). Larger R_{ac0} results in larger R_{ac} in Wang's model.

Table 4-11. Difference (%) in In-canopy aerodynamic resistance for deciduous broadleaf forest in the two seasons.

Season	Minimum	First quartile	Median	Third quartile	Maximum	Mean
summer	86	87	88	90	93	89
winter	119	121	122	123	123	122

c) Which model is better

R_{ac} in Wright & Zhang's model is more appropriate for representation of GEM air-surface exchange (Table E4). This is because R_{ac0} in Wright & Zhang's model reflects the effect of canopy growth on GEM exchange through canopies. When LAI is large, it is difficult for GEM to be transported through canopies.

Deciduous broadleaf forest in winter

The difference between the two models for deciduous broadleaf forest is only dependent on LAI. For deciduous broadleaf forest, LAI in summer ranges between 4.64 and 5.75 (mean of 5.3) and that in winter is in the range of 0.6-1 (mean of 0.72). In Fig. 4-23, R_{ac0} in summer and winter is plotted with daily data from Wright & Zhang's model. Smaller LAI in winter (mean, 0.72<5.3) leads to smaller R_{ac0} and smaller R_{ac} in Wright & Zhang's model. In Wang's model, R_{ac0} is a constant of 250s/m. Therefore, it is expected that greater difference between the two models for deciduous broadleaf forest is in winter. As seen in Table 4-10, R_{ac} in Wang's model is larger than that in Wright & Zhang's model (mean, 485466s/m>117880s/m). Table 4-11 shows the difference between the two models is greater in winter (89% vs. 122%), as expected.

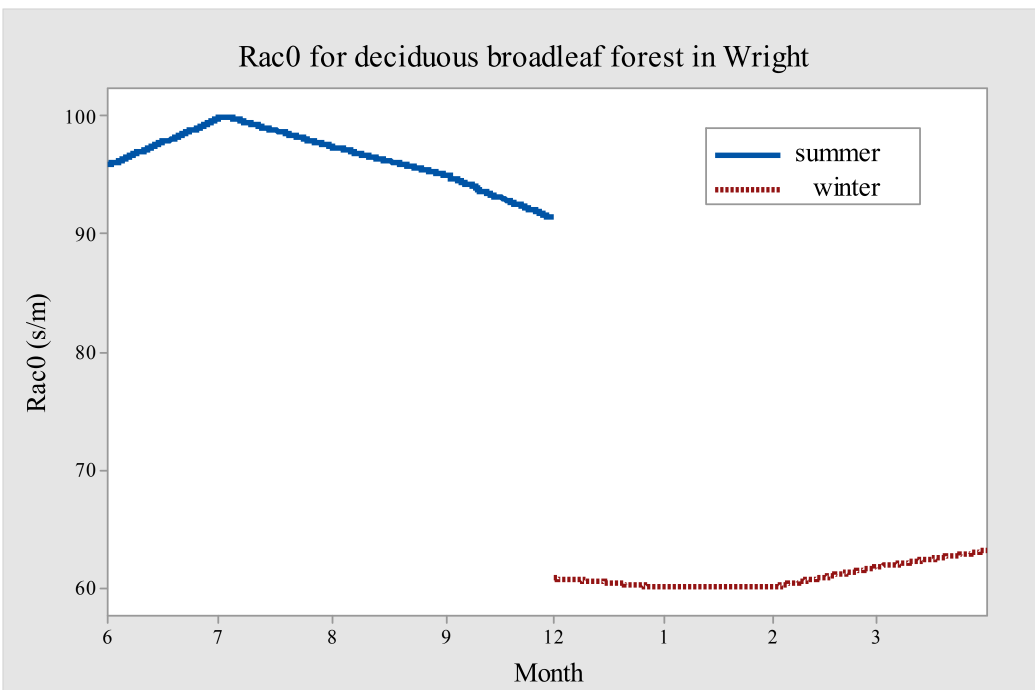

Figure 4-23. Time series of reference value for in-canopy aerodynamic resistance for deciduous broadleaf forest in Wright & Zhang's model.

Summary

Regardless of season, R_{ac} for evergreen needleleaf forest is the same in the two models. For deciduous broadleaf forest, R_{ac} in Wang's model is larger than that in Wright & Zhang's model (mean, 964244s/m>340124s/m). This is because larger R_{ac0} leads to larger R_{ac} in Wang's model. For deciduous broadleaf forest and different seasons, greater difference between the two models is in winter (89% vs. 122%). This is caused by smaller LAI (mean, 0.72<5.3), smaller R_{ac0} (mean, 61s/m<96s/m), smaller R_{ac} in Wright & Zhang's model. As in Table 4-12, both season and land cover are significant in the difference between the two models (p=0.001).

Table 4-12. Analysis of variance (ANOVA) of the difference in in-canopy aerodynamic resistance between the two models.

Parameter	p-value
season	0.001
land cover	0.001
season*land cover	0.001

4.1.6 Soil resistance (R_g)

Soil resistance is not related with land cover in both models, thus the difference between the two models is not related with land cover. For R_g, Wang considered both dry and wet soil, and Wright & Zhang only considered dry soil. Wang assumed that R_g for dry and wet soil are 2000s/m and 5000s/m, respectively. Wet soil will occur when soil volumetric water content is greater than or equal to $0.2m^3/m^3$. Wright & Zhang assumed R_g to be 2000s/m, regardless of dry and wet soil. Wright & Zhang considered surface temperature below -1°C in winter and Wang did not. In Wright & Zhang's model, R_g increases by as much as two times when surface temperature is below -1°C (Zhang et al., 2003).

Evergreen needleleaf forest in summer

a) R_g in the two models

Table 4-13 shows R_g in the two models. R_g in Wright & Zhang's model has no diurnal variation and that in Wang's model has an obvious diurnal trend with low values during daytime and high values during nighttime (Fig. 4-24 and Table E1). The diurnal trend in Wang's model corresponds to the diurnal trend for wet soil (Fig. 4-25). Wet soil results in larger R_g in Wang's model. R_g in Wang's model is always greater than or equal to that in Wright & Zhang's model (Fig. 4-26).

Table 4-13. Soil resistance (R_g, s/m) in the two models for evergreen needleleaf forest in the two seasons.

Season	Model	Minimum	First quartile	Median	Third quartile	Maximum	Mean
summer	Wang	2000	2000	2000	5000	5000	2979
	Wright & Zhang	2000	2000	2000	2000	2000	2000
winter	Wang	2000	2000	2000	5000	5040	2950
	Wright & Zhang	2000	2000	2000	2036	4450	2315

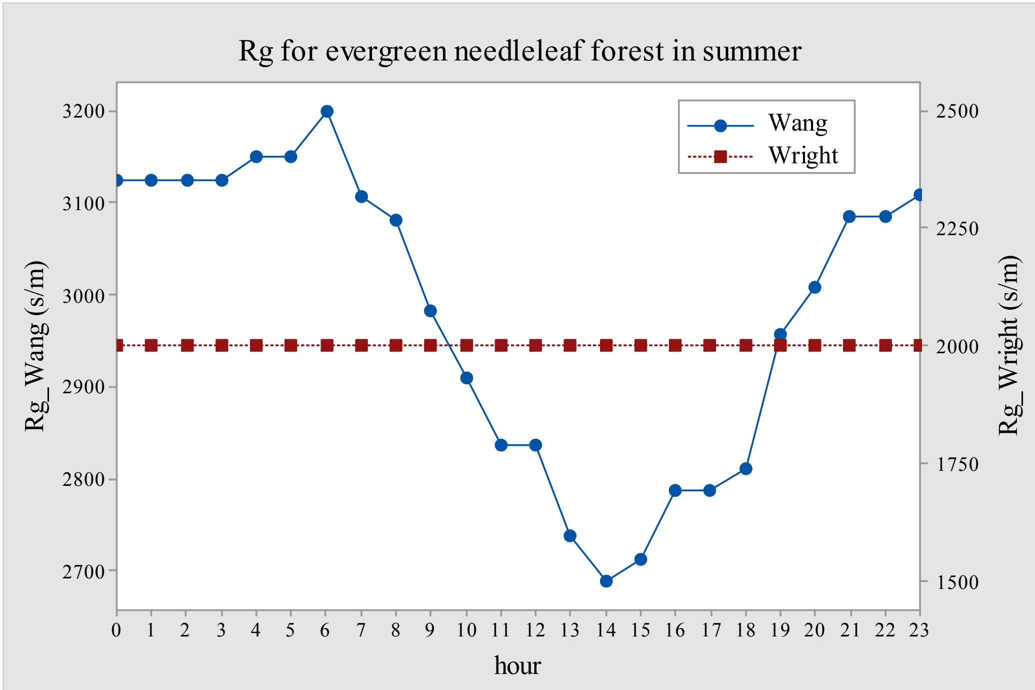

Figure 4-24. Diurnal trend for soil resistance in the two models for evergreen needleleaf forest in summer.

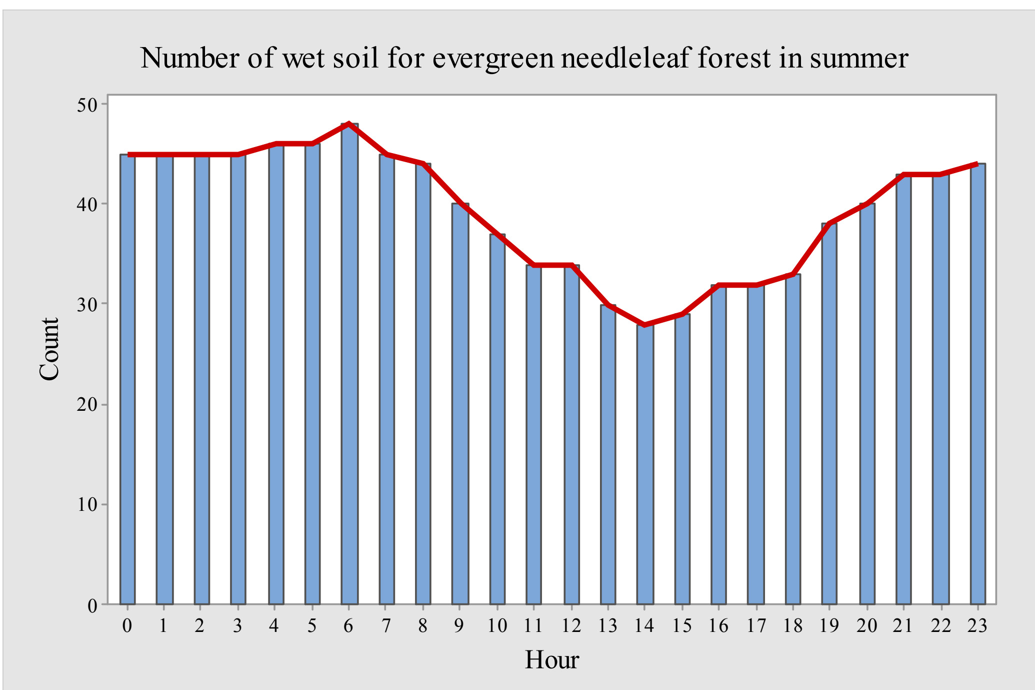

Figure 4-25. Diurnal trend for wet soil for evergreen needleleaf forest in summer.

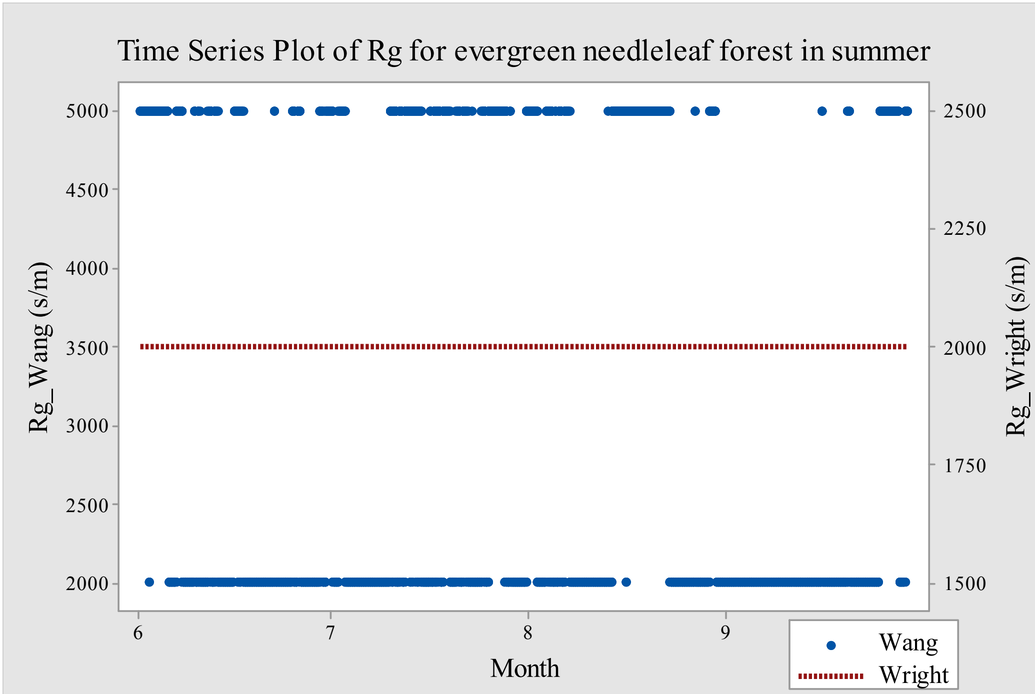

Figure 4-26. Time series for soil resistance in the two models for evergreen needleleaf forest in summer.

b) The difference between the two models and why

For dry soil, R_g in the two models is the same (2000s/m). For wet soil, R_g is 2000s/m and 5000s/m in Wright & Zhang's model and Wang's model, respectively. As in Table 4-14, the difference between the two models is in the range of 0-86% (mean of 28%). Wet soil leads to larger R_g in Wang's model. Wesely and Hicks (2000) introduced that wet soil leads to small surface deposition velocity for ozone (with low solubility). This proves that wet soil causes large soil resistance.

Table 4-14. Difference (%) in soil resistance for evergreen needleleaf forest in summer.

Season	Minimum	First quartile	Median	Third quartile	Maximum	Mean of absolute difference (%)
summer	0	0	0	86	86	28
winter	-67	0	0	86	86	32

c) Which model is better

R_g in Wang's model is more appropriate for representation of gaseous pollutants air-surface exchange, including GEM. This is because Wang considered the effect of wet soil on exchange of gaseous pollutants through soil. When there is more water in the soil, it is difficult for gaseous pollutants to be transported through soil.

Evergreen needleleaf forest in winter

a) R_g in the two models

R_g in the two models is shown in Table 4-13. Diurnal trend of R_g in the two models is different (Fig. 4-27). The diurnal trend in Wang's model corresponds to the diurnal trend for wet soil (Fig. 4-28). Wet soil results in larger R_g in Wang's model. The diurnal trend in Wright & Zhang's model corresponds to the diurnal trend for surface temperature below -1°C (Fig. 4-29). Surface temperature below -1°C leads to larger R_g in Wright & Zhang's model. Overall, R_g in Wang's model is larger than that in Wright & Zhang's model (mean, 2950s/m>2315s/m).

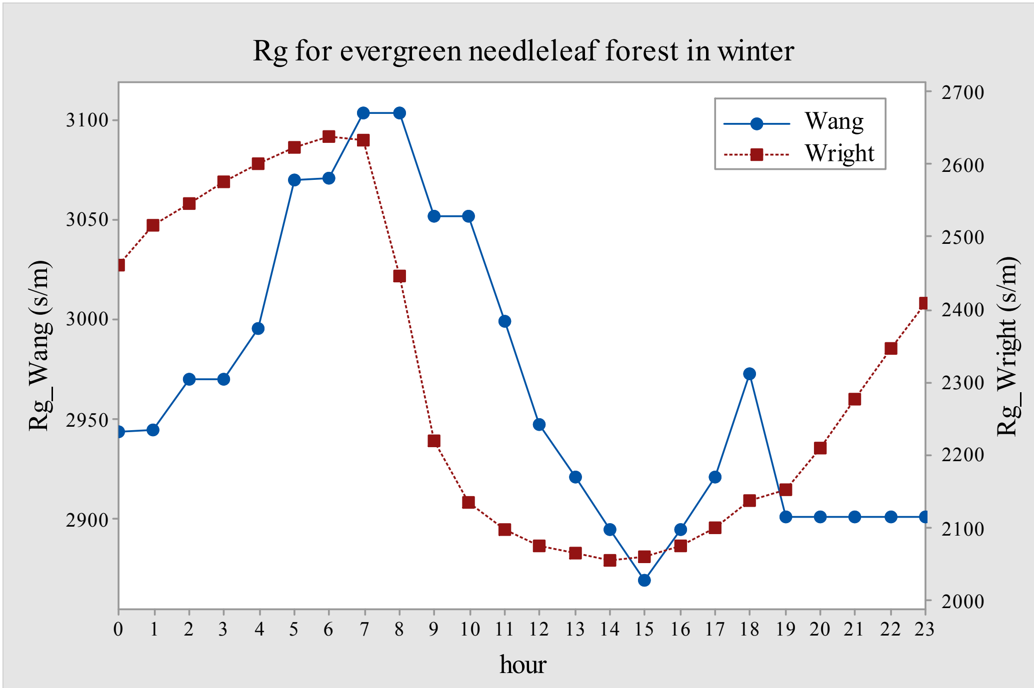

Figure 4-27. Diurnal trend for soil resistance in the two models for evergreen needleleaf forest in winter.

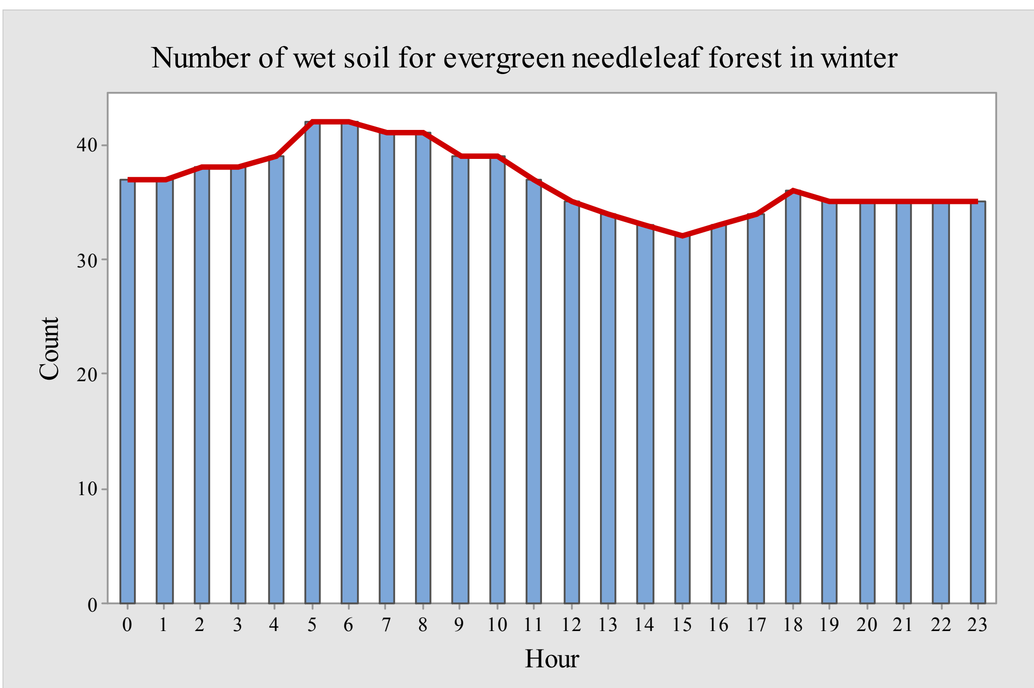

Figure 4-28. Diurnal trend for wet soil for evergreen needleleaf forest in winter.

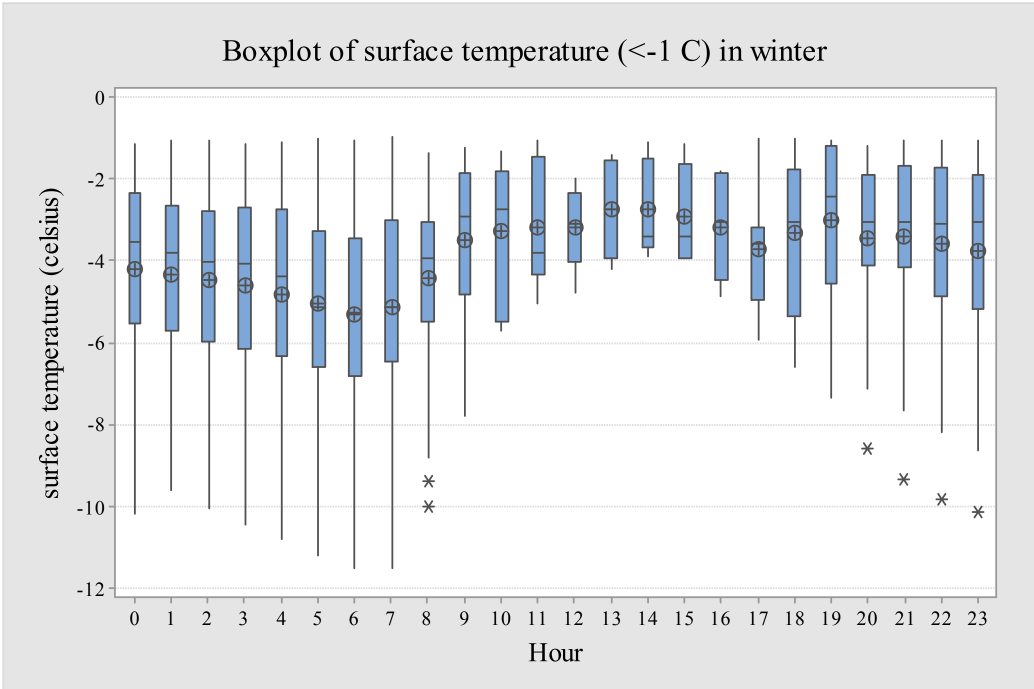

Figure 4-29. Diurnal trend for surface temperature below -1°C in winter.

b) The difference between the two models and why

Both wet soil and surface temperature below -1°C have an influence in the difference between the two models. For dry soil, R_g in the two models is the same (2000s/m). For wet soil, R_g is 2000s/m and 5000s/m in Wright & Zhang's model and Wang's model, respectively. Wet soil leads to larger R_g in Wang's model. With surface temperature below -1°C, R_g in Wright & Zhang's model is larger and at most 4450s/m. As in Table 4-14, the difference between the two models is in the range of -67% to 86% and mean of absolute difference is 32%. Surface temperature below -1°C during December-February causes small difference between the two models, and surface temperature above -1°C during February -March leads to large difference between the two models (Fig. 4-30).

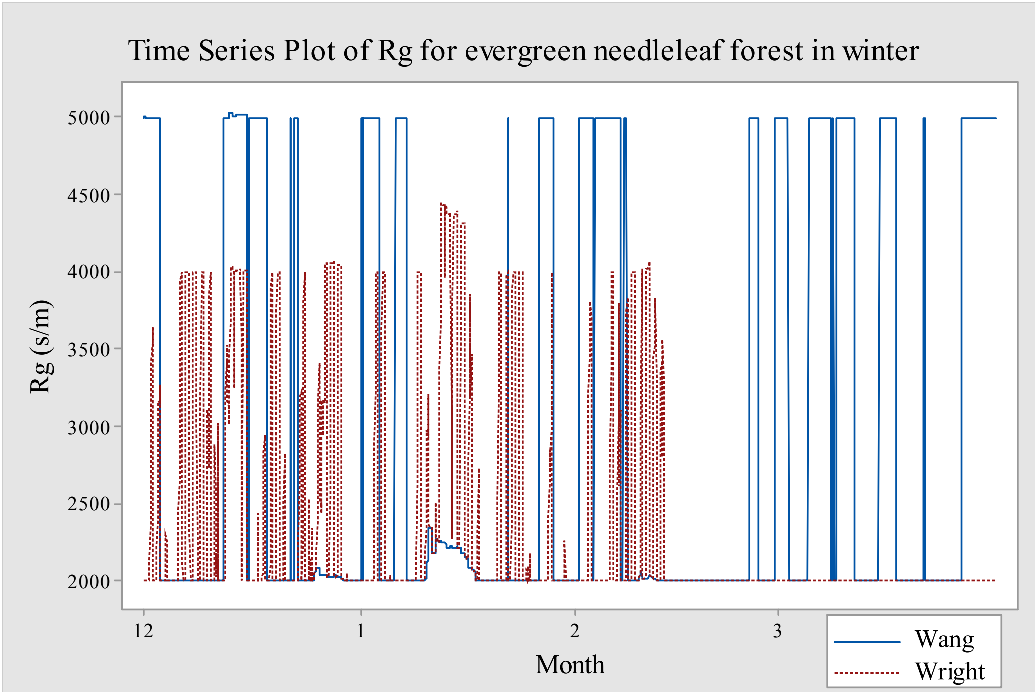

Figure 4-30. Time series for soil resistance in the two models for evergreen needleleaf forest in winter.

c) Which model is better

Each model has its own strength for representation of gaseous pollutants air-surface exchange (Table E4). Wang considered the effect of wet soil on exchange of gaseous pollutants through soil. When there is more water in the soil, it is difficult for gaseous pollutants to be transported through soil. Wright & Zhang considered the effect of surface temperature on exchange of gaseous pollutants. When the water in the soil is frozen, it is difficult for gaseous pollutants to move through soil. If Wright & Zhang consider the effect of wet soil, their model will be more appropriate.

Summary

Regardless of season and land cover, R_g in Wang's model is larger than that in Wright & Zhang's model (mean, 2965s/m>2155s/m) because wet soil leads to larger R_g in Wang's model. For different land cover and the same season, the difference between the two models is the same because R_g is not dependent on land cover. For the same land cover and different seasons, the difference is similar in the two seasons (28% vs. 32%), however the reason is different. In summer, wet soil results in larger R_g in Wang's model. In winter, surface temperature below -1°C leads to larger R_g in Wright & Zhang's model, and wet soil results in larger R_g in Wang's model. As seen in Table 4-15, season is significant in the difference between the two models (p=0.001).

Table 4-15. Analysis of variance (ANOVA) of the difference in soil resistance between the two models.

Parameter	p-value
season	0.001
land cover	0.99
season*land cover	0.99

4.2 Velocities

4.2.1 Stomata emission velocity (V_{st})

The parameterization of V_{st} is the same in the two models (Table C2).

Evergreen needleleaf forest in summer

a) V_{st} in the two models

Table 4-16 shows V_{st} in the two models. V_{st} in the two models has similar diurnal trend with high values during daytime and low values during nighttime (Fig. 4-31 and

Table E1). V_{st} is calculated from all six resistances, (1) R_a is larger in Wang's model (section 4.1.1), (2) R_b is smaller in Wang's model (section 4.1.2), (3) R_{st} is larger in Wang's model (section 4.1.3), (4) R_{cut} is the same in the two models (section 4.1.4), (5) R_{ac} is the same in the two models (section 4.1.5), and (6) R_g is larger in Wang's model (section 4.1.6).

Table 4-16. Stomata emission velocity (V_{st}, µm/s), $1/R_{st}$ (µm/s), and $R_t/(R_a+R_b)$ for the two models in the two seasons.

Season	Land cover	Model	V_{st},$1/R_{st}$, or $R_t/(R_a+R_b)$	Minimum	First quartile	Median	Third quartile	Maximum	Mean
summer	evergreen needleleaf forest	Wang	V_{st}	0	1	56	591	1355	293
			$1/R_{st}$	0	1	57	616	1448	310
			$R_t/(R_a+R_b)$	0.32	0.96	0.97	0.98	0.99	0.96
		Wright & Zhang	V_{st}	1	3	74	386	934	199
			$1/R_{st}$	1	3	76	400	983	207
			$R_t/(R_a+R_b)$	0.76	0.96	0.97	0.98	0.99	0.97
	deciduous broadleaf forest	Wang	V_{st}	0	1	1	927	1560	401
			$1/R_{st}$	0	1	1	974	1640	426
			$R_t/(R_a+R_b)$	0.2	0.96	0.98	0.99	1	0.97
		Wright & Zhang	V_{st}	1	3	224	656	1197	335
			$1/R_{st}$	1	3	230	686	1271	352
			$R_t/(R_a+R_b)$	0.7	0.96	0.97	0.98	0.99	0.97
winter	evergreen needleleaf forest	Wang	V_{st}	0	1	1	543	1176	237
			$1/R_{st}$	1	1	1	560	1238	245
			$R_t/(R_a+R_b)$	0.83	0.97	0.98	0.99	1	0.98
		Wright & Zhang	V_{st}	1	3	3	302	899	143
			$1/R_{st}$	1	3	3	309	933	147
			$R_t/(R_a+R_b)$	0.79	0.97	0.98	0.99	1	0.98
	deciduous broadleaf forest	Wang	V_{st}	0	1	1	398	990	187
			$1/R_{st}$	1	1	1	409	1049	194
			$R_t/(R_a+R_b)$	0.79	0.97	0.99	0.99	1	0.98
		Wright & Zhang	V_{st}	2	3	3	194	688	111
			$1/R_{st}$	2	3	3	199	719	115
			$R_t/(R_a+R_b)$	0.83	0.97	0.98	0.98	0.99	0.98

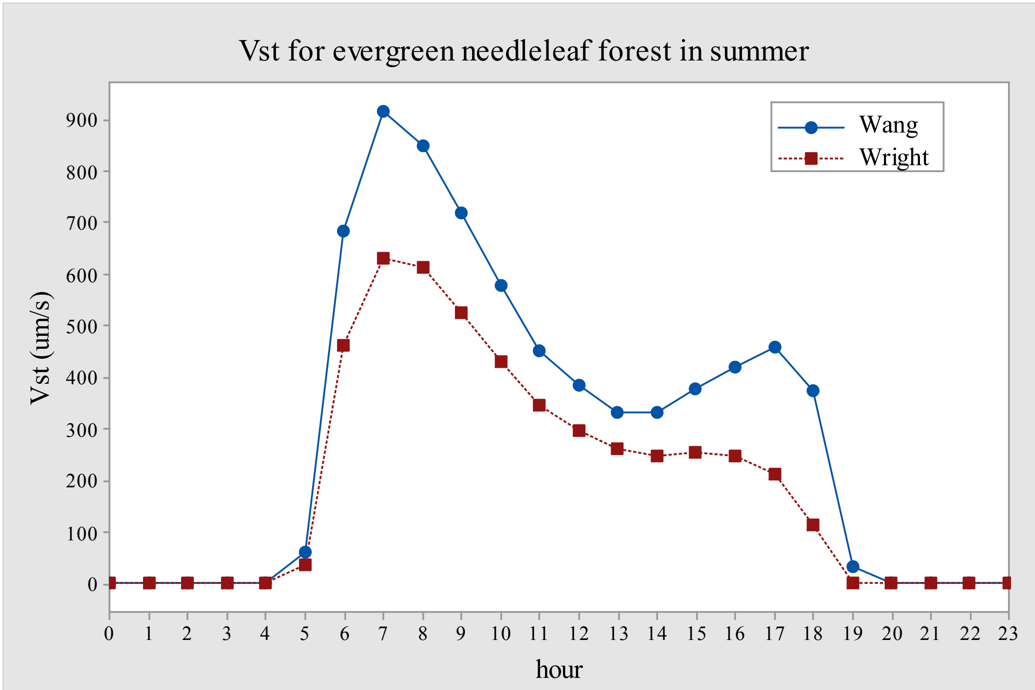

Figure 4-31. Diurnal trend for stomata emission velocity in the two models for evergreen needleleaf forest in summer.

V_{st} in each of the two models is mainly controlled by $1/R_{st}$ because $R_t/(R_a+R_b)$ is close to one (Fig 4-32). $1/R_{st}$ is close to V_{st} in each model (Table 4-16). In R_{st}, the constant value for stomata closure and f_D below 0.1 cause large difference in large values of R_{st} between the two models (section 4.1.3). However these two parameters cause little difference in V_{st} between the two models because large R_{st} corresponds to small V_{st}. For high values, V_{st} in Wang's model is larger than that in Wright & Zhang's model (Fig. 4-33). This is because larger visible solar radiation and smaller ratio of DV to DI lead to smaller R_{st}, larger $1/R_{st}$, and larger V_{st} in Wang's model. Overall, V_{st} for Wang's model is larger than that for Wright & Zhang's model (mean, 293µm/s>199µm/s) due to larger visible solar radiation and smaller ratio of DV to DI in Wang's model.

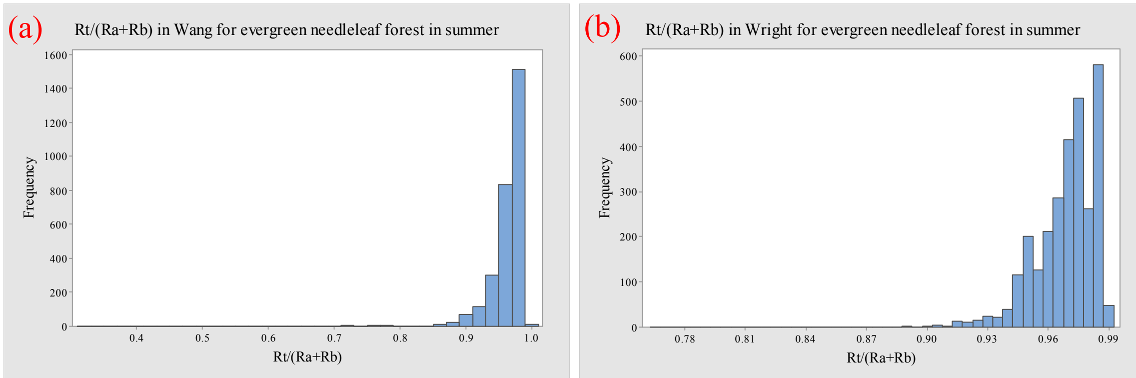

Figure 4-32. Distribution of $R_t/(R_a+R_b)$ in the two models for evergreen needleleaf forest in summer, (a) in Wang's model, (a) in Wright & Zhang's model.

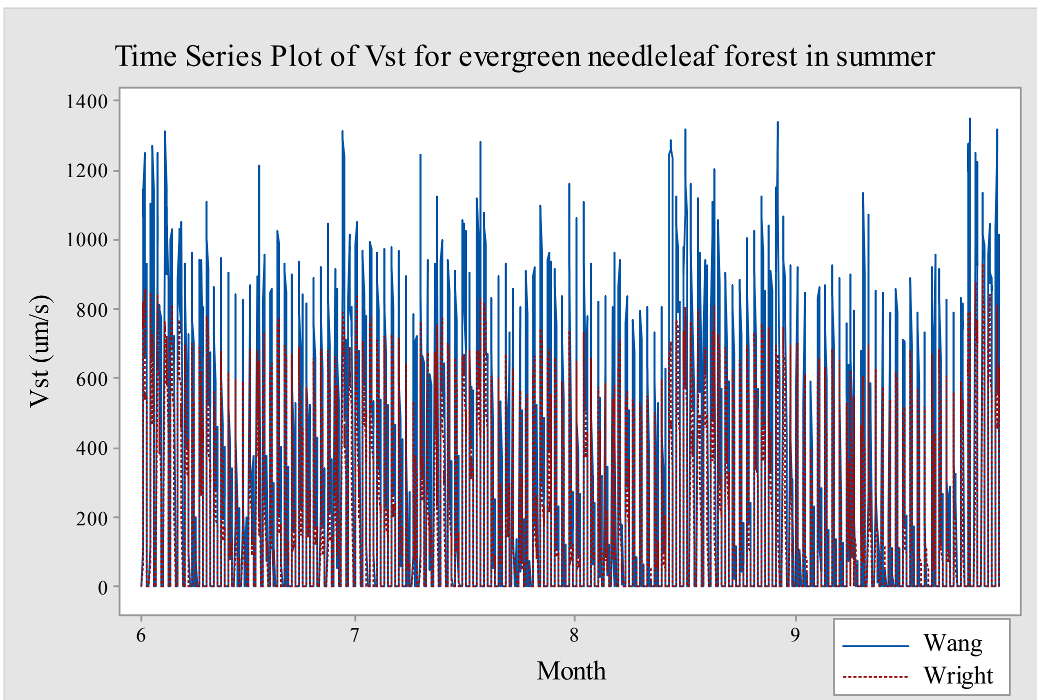

Figure 4-33. Time series for V_{st} in the two models for evergreen needleleaf forest in summer.

b) The difference between the two models and why

As seen in Table 4-17, the difference in V_{st} between the two models is in the range of -199% to 197% and mean of absolute difference is 98%. Larger visible solar radiation and smaller ratio of DV to DI lead to smaller R_{st}, larger $1/R_{st}$, and larger V_{st} in Wang's model. Larger constant value for stomata closure and f_D below 0.1 result in larger R_{st}, smaller $1/R_{st}$, and smaller V_{st} in Wang's model.

Table 4-17. Difference (%) in stomata emission velocity for the two models in the two seasons.

Season	Land cover	Minimum	First quartile	Median	Third quartile	Maximum	Mean of absolute difference (%)
summer	evergreen needleleaf forest	-199	-144	-11	34	197	98
	deciduous broadleaf forest	-199	-144	-143	23	196	104
winter	evergreen needleleaf forest	-151	-144	-144	41	195	108
	deciduous broadleaf forest	-153	-144	-143	42	194	113

Deciduous broadleaf forest in summer

Table 4-16 shows that V_{st} in Wang's model is larger than that in Wright & Zhang's model (mean, 401μm/s>335μm/s) and the reason is similar to that for evergreen needleleaf forest in summer. V_{st} is mainly controlled by $1/R_{st}$. In R_{st}, only LAI and f_D are related with land cover. Larger LAI for deciduous broadleaf forest (Table D1) results in more visible solar radiation received by leaves, smaller R_{st}, and larger V_{st} for both models. In f_D, larger b_{vpd} for deciduous broadleaf forest leads to smaller f_D and more f_D below 0.1 in Wang's model (section 4.1.3). More f_D below 0.1 results in larger R_{st} and smaller V_{st} in Wang's model. Thus, the negative values of difference between the two models are smaller (Table 4-17). However, the mean of absolute difference between the two models is still similar to that for evergreen needleleaf forest in summer (Table 4-17, 98% vs. 104%).

Evergreen needleleaf forest in winter

Table 4-16 shows that V_{st} in Wang's model is larger than that in Wright & Zhang's model (mean, 237μm/s>143μm/s) and the reason is similar to that for evergreen needleleaf forest in summer. V_{st} is mainly controlled by $1/R_{st}$. In R_{st}, solar radiation, LAI, and f_D are related with season. Smaller solar radiation in winter (Table D1) leads to larger R_{st} and smaller V_{st} in both models. Smaller LAI in winter (Table D1) also causes larger R_{st} and smaller V_{st} in both models. f_D above 0.1 in winter results in smaller R_{st} and larger V_{st} in Wang's model. The negative values of difference between the two models are smaller than that for evergreen needleleaf forest in summer (Table 4-17). This is because longer nighttime in winter causes more constant values of R_{st} for stomata closure, larger R_{st}, and smaller V_{st} in Wang's model. The mean of absolute difference between the two models is larger than that for evergreen needleleaf forest in summer (Table 4-17, 98% vs. 108%).

Deciduous broadleaf forest in winter

As shown in Table 4-16, V_{st} in Wang's model is larger than that in Wright & Zhang's model (mean, 187μm/s>111μm/s) and the reason is similar to that for evergreen needleleaf forest in summer. In R_{st}, only LAI and f_D are related with land cover. Smaller LAI for deciduous broadleaf forest (Table D1) causes fewer visible solar radiation received by leaves, larger R_{st}, and smaller V_{st} in both models. f_D is always above 0.1 in Wang's model in winter, which is the same as that for evergreen needleleaf forest in winter. As in Table 4-17, the difference between the two models is similar to that for evergreen needleleaf forest in winter (108% vs. 113%).

Summary

Regardless of season and land cover, V_{st} in Wang's model is larger than that in Wright & Zhang's model (mean, 280μm/s >198μm/s). The difference in V_{st} between the two models is mainly caused by the visible solar radiation, the range of f_D, and water vapor diffusivity and GEM diffusivity.

For the same land cover and different seasons, greater difference between the two models is in winter (98% vs. 108% for evergreen needleleaf forest, 104% vs. 113% for deciduous broadleaf forest) because longer nighttime in winter causes more constant value of R_{st} for stomata closure, larger R_{st}, and smaller V_{st} in Wang's model. As in Table 4-18, season is significant in the difference between the two models (p=0.001). For different land cover and the same season, the difference between the two models is similar (98% vs. 104% in summer, 108% vs. 113% in winter). However, Table 4-18 shows that land cover is significant in the difference between the two models (p=0.001).

Table 4-18. Analysis of variance (ANOVA) of the difference in stomata emission velocity between the two models.

Parameter	p-value
season	0.001
land cover	0.001
season*land cover	0.002

4.2.2 Soil emission velocity (V_g)

The parameterization of V_g is the same in the two models (Table C2).

Evergreen needleleaf forest in summer

a) V_g in the two models

Table 4-19 shows V_g in the two models. V_g in the two models has similar diurnal trend with high values during daytime and low values during nighttime (Fig. 4-34 and Table E1). V_g is calculated from all six resistances, (1) R_a is larger in Wang's model (section 4.1.1), (2) R_b is smaller in Wang's model (section 4.1.2), (3) R_{st} is larger in Wang's model (section 4.1.3), (4) R_{cut} is the same in the two models (section 4.1.4), (5) R_{ac} is the same in the two models (section 4.1.5), and (6) R_g is larger in Wang's model (section 4.1.6).

Table 4-19. Soil emission velocity (V_g, μm/s), $1/(R_{ac}+R_g)$ (μm/s), and $R_t/(R_a+R_b)$ for the two models in the two seasons.

Season	Land cover	Model	V_g, $1/(R_{ac}+R_g)$, or $R_t/(R_a+R_b)$	Minimum	First quartile	Median	Third quartile	Maximum	Mean
summer	evergreen needleleaf forest	Wang	V_g	0	105	166	293	445	188
			$1/(R_{ac}+R_g)$	0	109	172	301	449	194
			$R_t/(R_a+R_b)$	0.32	0.96	0.97	0.98	0.99	0.96
		Wright & Zhang	V_g	0	122	244	317	445	219
			$1/(R_{ac}+R_g)$	0	127	252	325	449	225
			$R_t/(R_a+R_b)$	0.76	0.96	0.97	0.98	0.99	0.97
	deciduous broadleaf forest	Wang	V_g	0	55	118	185	384	124
			$1/(R_{ac}+R_g)$	0	58	123	189	388	128
			$R_t/(R_a+R_b)$	0.2	0.96	0.98	0.99	1	0.97
		Wright & Zhang	V_g	0	124	249	322	446	223
			$1/(R_{ac}+R_g)$	0	131	258	331	451	229
			$R_t/(R_a+R_b)$	0.7	0.96	0.97	0.98	0.99	0.97
winter	evergreen needleleaf forest	Wang	V_g	0	173	281	401	478	271
			$1/(R_{ac}+R_g)$	0	177	286	408	483	274
			$R_t/(R_a+R_b)$	0.83	0.97	0.98	0.99	1	0.98
		Wright & Zhang	V_g	0	226	355	419	477	310
			$1/(R_{ac}+R_g)$	0	229	363	427	483	316
			$R_t/(R_a+R_b)$	0.79	0.97	0.98	0.99	1	0.98
	deciduous broadleaf forest	Wang	V_g	0	115	177	285	442	192
			$1/(R_{ac}+R_g)$	0	118	180	290	446	196
			$R_t/(R_a+R_b)$	0.79	0.97	0.99	0.99	1	0.98
		Wright & Zhang	V_g	0	237	371	429	481	322
			$1/(R_{ac}+R_g)$	0	242	381	438	486	329
			$R_t/(R_a+R_b)$	0.83	0.97	0.98	0.98	0.99	0.98

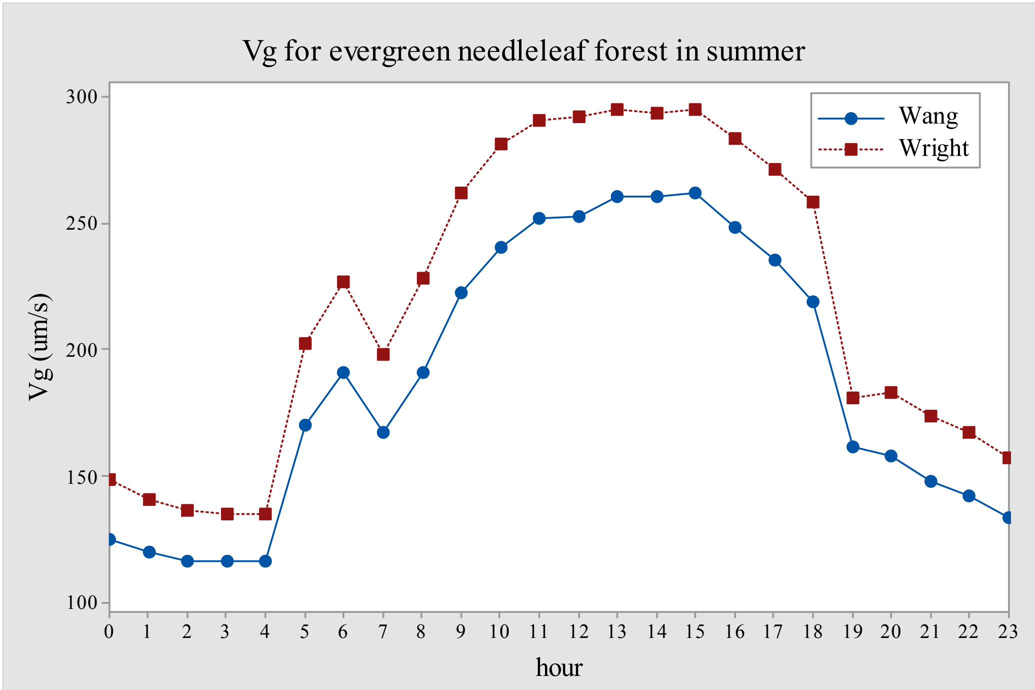

Figure 4-34. Diurnal trend for V_g in the two models for evergreen needleleaf forest in summer.

V_g in each of the two models is mainly controlled by $1/(R_{ac}+R_g)$ because $R_t/(R_a+R_b)$ is close to one (Fig 4-32). $1/(R_{ac}+R_g)$ is close to V_g in each model (Table 4-19). Most of V_g in Wang's model is smaller than that in Wright & Zhang's model (Fig. 4-35). This is because R_{ac} is the same in the two models and wet soil results in larger R_g, smaller $1/(R_{ac}+R_g)$, and smaller V_g in Wang's model. Overall, V_g in Wang's model is smaller than that in Wright & Zhang's model (mean, 188µm/s<219µm/s) due to wet soil.

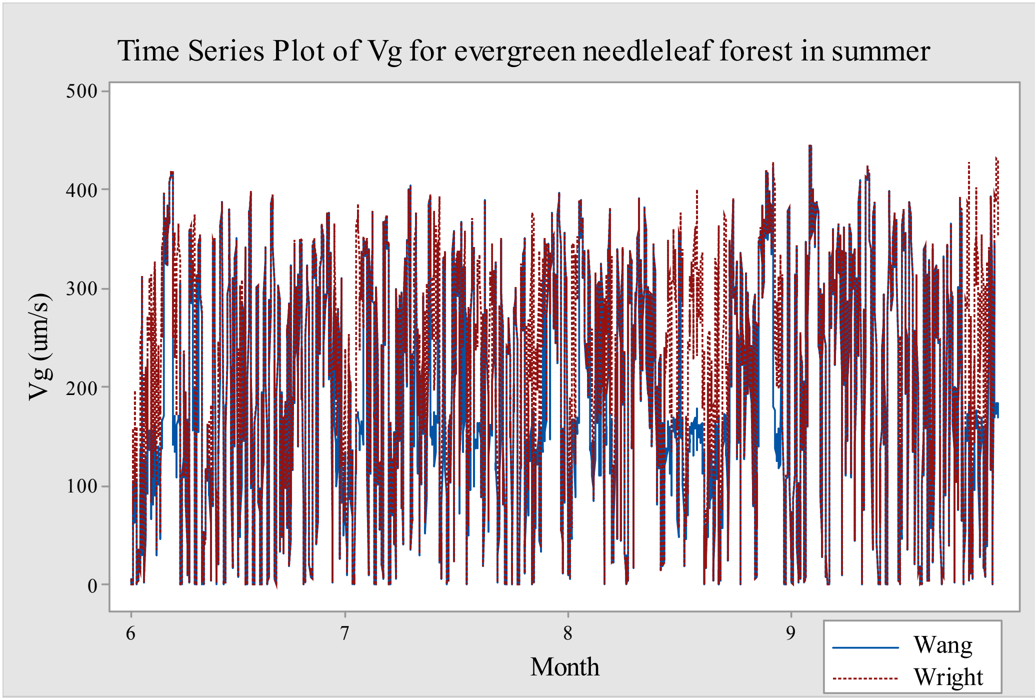

Figure 4-35. Time series for V_g in the two models for evergreen needleleaf forest in summer.

b) The difference between the two models and why

As seen in Table 4-20, the difference in V_g between the two models is in the range of -102% to 12% and mean of absolute difference is 16%. V_g is mainly controlled by $1/(R_{ac}+R_g)$. R_{ac} is the same in the two models. Wet soil results in larger R_g, smaller $1/(R_{ac}+R_g)$, and smaller V_g in Wang's model. Larger V_g in Wang's model is caused by larger $R_t/(R_a+R_b)$.

Table 4-20. Difference (%) in soil emission velocity for the two models in the two seasons.

Seasons	Land cover	Minimum	First quartile	Median	Third quartile	Maximum	Mean of absolute difference (%)
summer	evergreen needleleaf forest	-102	-27	-1	-0.01	12	16
	deciduous broadleaf forest	-171	-87	-72	-47	-15	67
winter	evergreen needleleaf forest	-84	-39	-1	0.1	61	24
	deciduous broadleaf forest	-134	-94	-62	-32	43	64

Deciduous broadleaf forest in summer

V_g is mainly controlled by $1/(R_{ac}+R_g)$. R_g is not related with land cover. For deciduous broadleaf forest, larger R_{ac0} results in larger R_{ac}, smaller $1/(R_{ac}+R_g)$, and smaller V_g in Wang's model. V_g in Wang's model is much smaller, thus it is expected that the difference between the two models is greater for deciduous broadleaf forest in summer. Table 4-19 shows that V_g in Wang's model is smaller than that in Wright & Zhang's model (mean, 124μm/s<223μm/s). As in Table 4-20, the difference between the two models is larger than that for evergreen needleleaf forest in summer (16% vs. 67%), as expected.

Evergreen needleleaf forest in winter

As shown in Table 4-19, V_g in Wang's model is smaller than that in Wright & Zhang's model (mean, 271μm/s<310μm/s) because wet soil results in larger R_g, smaller

$1/(R_{ac}+R_g)$, and smaller V_g in Wang's model. V_g is mainly controlled by $1/(R_{ac}+R_g)$. R_{ac} is the same in the two models. In R_g, soil volumetric water content and surface temperature are related with season. Soil volumetric water content is similar in the two seasons (Table D1). Surface temperature is much lower in winter (Table D1). Surface temperature below -1°C causes smaller R_g, larger $1/(R_{ac}+R_g)$, and larger V_g in Wang's model. However, as seen in Table 4-20, the difference between the two models is similar to that for evergreen needleleaf forest in summer (16% vs. 24%).

Deciduous broadleaf forest in winter

V_g is mainly controlled by $1/(R_{ac}+R_g)$. R_g is not related with land cover. In R_{ac}, LAI is related with season. Smaller LAI in winter (Table D1) results in larger R_{ac0}, smaller $1/(R_{ac}+R_g)$, and smaller V_g in Wang's model. V_g in Wang's model is much smaller, thus it is expected that the difference between the two models is greater for evergreen needleleaf forest in winter. As seen in Table 4-19, V_g in Wang's model is smaller than that in Wright & Zhang's model (mean, 192μm/s<322μm/s), because larger R_{ac0} and wet soil lead to smaller $1/(R_{ac}+R_g)$ and smaller V_g in Wang's model. As in Table 4-20, the difference between the two models is larger than that for evergreen needleleaf forest in winter (24% vs. 64%), as expected. However, the difference is similar to that for deciduous broadleaf forest in summer (67% vs. 64%).

Summary

Regardless of season and land cover, V_g in Wang's model is smaller than that in

Wright & Zhang's model (mean, 193μm/s<268μm/s). The difference in V_g between the two models is mainly due to wet soil, surface temperature below -1°C, and R_{ac0}. For the same land cover and different seasons, the difference between the two models is similar (16% vs. 24% for evergreen needleleaf forest, 67% vs. 64% for deciduous broadleaf forest) and the reason is different. For evergreen needleleaf forest, it is because R_{ac} is the same in the two models and surface temperature below -1°C in winter causes little effect on the difference between the two models. For deciduous broadleaf forest, this is because R_{ac0} and surface temperature below -1°C have little effect on the difference between the two models. However, season is significant in the difference between the two model (p=0.001), as in Table 4-21.

Table 4-21. Analysis of variance (ANOVA) of the difference in soil emission velocity between the two models.

Parameter	p-value
season	0.001
land cover	0.001
season*land cover	0.001

For different land cover and the same season, greater difference between the two models is for deciduous broadleaf forest (16% vs. 67% in summer, 24% vs. 64% in winter). R_g is not related with land cover. For deciduous broadleaf forest, larger R_{ac0} results in smaller V_g in Wang's model. Table 4-21 shows that land cover is significant in the difference between the two models (p=0.001).

4.2.3 Deposition velocity (V_d)

The parameterization of V_d is the same in the two models (Table C2).

Evergreen needleleaf forest in summer

a) V_d in the two models

Table 4-22 shows V_d in the two models. Negative sign represents that deposition velocity is downward. V_d in the two models has similar diurnal trend with high values during daytime and low values during nighttime (Fig. 4-36 and Table E1). V_d is calculated from all six resistances, (1) R_a is larger in Wang's model (section 4.1.1), (2) R_b is smaller in Wang's model (section 4.1.2), (3) R_{st} is larger in Wang's model (section 4.1.3), (4) R_{cut} is the same in the two models (section 4.1.4), (5) R_{ac} is the same in the two models (section 4.1.5), and (6) R_g is larger in Wang's model (section 4.1.6).

Table 4-22. Deposition velocity (V_d, μm/s) for the two models in the two seasons.

Season	Land cover	Model	Minimum	First quartile	Median	Third quartile	Maximum	Mean
summer	evergreen needleleaf forest	Wang	-2491	-995	-519	-284	-1	-640
		Wright & Zhang	-1809	-832	-526	-295	-4	-576
	deciduous broadleaf forest	Wang	-2309	-1178	-331	-159	-1	-613
		Wright & Zhang	-1801	-1034	-566	-278	-4	-646
winter	evergreen needleleaf forest	Wang	-1744	-945	-519	-335	-1	-617
		Wright & Zhang	-1511	-795	-543	-316	-4	-562
	deciduous broadleaf forest	Wang	1463	-639	-319	-187	-1	-424
		Wright & Zhang	-1184	-638	-464	-284	-3	-478

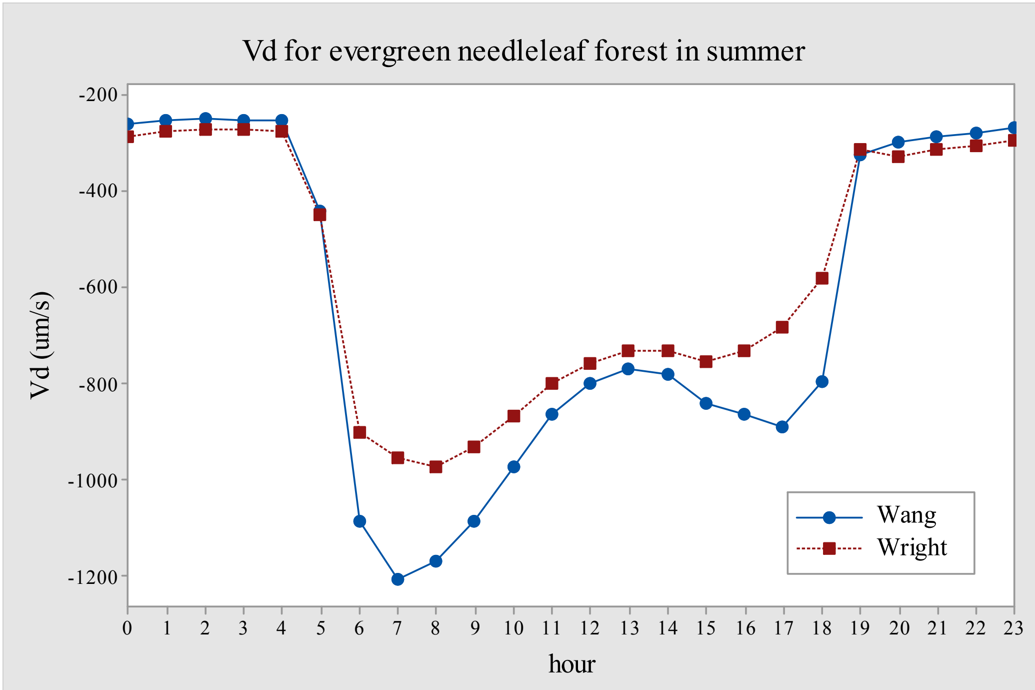

Figure 4-36. Diurnal trend for deposition velocity in the two models for evergreen needleleaf forest in summer.

For high values of V_d (>900µm/s), 91% of V_d (784 out of 859) is larger in Wang's model (Fig. 4-37). 99.7% of these larger V_d (782 out of 784) in Wang's model happens during daytime. This is because smaller R_b and smaller R_{st} lead to larger V_d in Wang's model. The low values of V_d in the two models are similar (Fig. 4-37). Overall, V_d in Wang's model is larger than that in Wright & Zhang's model (mean, 640µm/s>576µm/s).

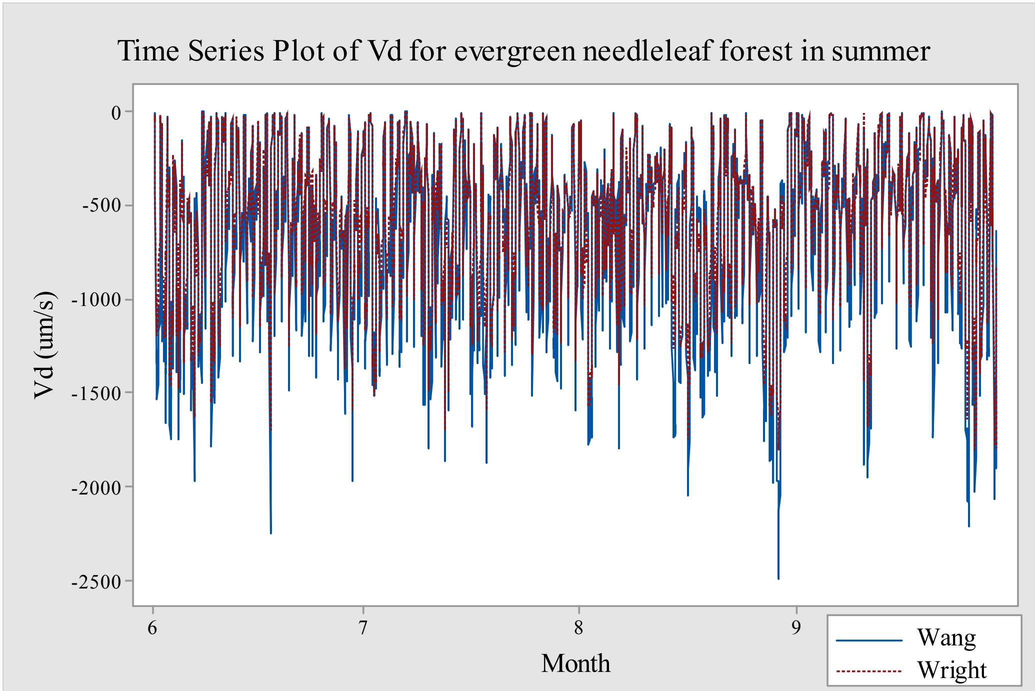

Figure 4-37. Time series for deposition velocity in the two models for evergreen needleleaf forest in summer.

b) The difference between the two models and why

As seen in Table 4-23, the difference in V_d between the two models is in the range of -116% to 168% and mean of absolute difference is 15%. The difference between the two models is dependent on joint effect of R_a, R_b, R_{st}, and R_g because R_{ac} and R_{cut} are the same in the two models. Larger R_a and R_g lead to smaller V_d in Wang's model. Smaller R_b and R_{st} result in larger V_d in Wang's model. Wu et al. (2018b) found that the difference in R_a and R_b among dry deposition models caused little effect on modeled deposition velocity.

Table 4-23. Difference (%) in deposition velocity for the two models in the two seasons.

Season	Land cover	Minimum	First quartile	Median	Third quartile	Maximum	Mean of absolute difference (%)
summer	evergreen needleleaf forest	-116	-6	-0.5	17	168	15
	deciduous broadleaf forest	-161	-45	-29	7	175	37
winter	evergreen needleleaf forest	-137	-6	-0.3	21	82	20
	deciduous broadleaf forest	-146	-69	-28	5	71	40

Deciduous broadleaf forest in summer

As in Table 4-22, V_d in Wang's model is smaller than that in Wright & Zhang's model (mean, 613μm/s<646μm/s) because larger R_a, R_{ac}, and R_g leads to smaller V_d in Wang's. As shown in Table 4-23, the difference between the two models is larger than that for evergreen needleleaf forest in summer (15% vs. 37%). This is because smaller ratio of air diffusivity to GEM diffusivity leads to smaller R_b and larger V_d in Wang's model.

Evergreen needleleaf forest in winter

As seen in Table 4-22, V_d in Wang's model is larger than that in Wright & Zhang's model (mean, 617μm/s>562μm/s) and the reason is similar to that for evergreen needleleaf forest in summer. As in Table 4-23, the difference between the two models is also similar to that for evergreen needleleaf forest in summer (15% vs. 20%).

Deciduous broadleaf forest in winter

As in Table 4-22, V_d in Wang's model is smaller than that in Wright & Zhang's model (mean, 613µm/s<646µm/s) the reason is similar to that for evergreen needleleaf forest in winter. As in Table 4-23, the difference between the two models is larger than that for evergreen needleleaf forest in winter (20% vs. 40%). This is because smaller ratio of air diffusivity to GEM diffusivity leads to smaller R_b and larger V_d in Wang's model. However, the difference between the two models is similar to that for deciduous broadleaf forest in summer (37% vs. 40%).

Summary

Regardless of season, for evergreen needleleaf forest, V_d in Wang's model is larger than that in Wright & Zhang's model (mean, 629µm/s>569µm/s) due to smaller R_b and smaller R_{st} in Wang's. For deciduous broadleaf forest, V_d in Wang's model is smaller than that in Wright & Zhang's model (mean, 520µm/s<563µm/s) as a result of larger R_a, R_{ac}, and R_g in Wang's. The difference in V_d between the two models is mainly owing to air diffusivity and GEM diffusivity.

For the same land cover and different seasons, the difference between the two models is similar (15% vs. 20% for evergreen needleleaf forest, 37% vs. 40% for deciduous broadleaf forest). However, as in Table 4-24, season is significant in the difference between the two models (p=0.001). For different land cover and the same season, greater difference between the two models is for deciduous broadleaf forest (15% vs. 37% in summer, 20% vs. 40% in winter). This is because smaller ratio of air diffusivity to GEM diffusivity leads to smaller R_b and larger V_d in Wang's model. Land cover is significant in the difference between the two models (p=0.001), as in Table 4-

24.

Table 4-24. Analysis of variance (ANOVA) of the difference in deposition velocity between the two models.

Parameter	p-value
season	0.001
land cover	0.001
season*land cover	0.001

4.3 GEM compensation point concentrations

4.3.1 Compensation point concentration in stomata (χ_{st})

The parameterization of χ_{st} is different in the two models (Table C3). Wang assumed that deposited GEM in stomata is the difference between dry deposited total gaseous mercury (TGM) on leaves and dry deposited gaseous oxidized mercury (GOM) on cuticle. Deposited GEM in stomata is emitted back to the atmosphere or fixed in stomata, and the fraction of emitted GEM is dependent on LAI. χ_{st} in Wright & Zhang's model is assumed as the concentration at which there is equilibrium between the different phases (Wright and Zhang, 2015). It is derived from the Clausius-Clapeyron equation and is only related with ambient temperature. Mercury pool in stomata is infinite in both models.

Evergreen needleleaf forest in summer

a) χ_{st} in the two models

Table 4-25 shows χ_{st} in the two models. The diurnal trend of χ_{st} in the two models is different (Fig. 4-38 and Table E1). In Wang's model, low values happen during daytime due to high values of GOM concentration on cuticle (Fig. 4-39). Wang assumed that dry deposited TGM on leaves is a constant of 2566 ng m^{-3}, as a summation of GOM concentration on cuticle and GEM concentration in stomata. Larger GOM concentration on cuticle leads to smaller GEM concentration in stomata. In Wright & Zhang's model, high values occur during daytime owing to relatively high ambient temperature (Fig. 4-40). χ_{st} in Wang's model is always smaller than that in Wright & Zhang's (Fig. 4-41). van Hove et al. (2002) found that the diurnal trend of ammonia compensation point concentration in stomata has high values during 8:00-16:00. Ammonia is a substance that tends to emit back to the atmosphere, like GEM. It is expected that GEM also has a tendency to emit to air and has a high compensation point concentration in stomata during daytime.

Table 4-25. Compensation point concentration in stomata (χ_{st}, ng m^{-3}) for the two models in the two seasons.

Season	Land cover	Model	Minimum	First quartile	Median	Third quartile	Maximum	Mean
summer	evergreen needleleaf forest	Wang	0.02	0.02	0.06	0.06	0.06	0.04
		Wright & Zhang	0.04	1.5	1.8	2.5	4.6	2
	deciduous broadleaf forest	Wang	0.02	0.02	0.06	0.06	0.06	0.04
		Wright & Zhang	0.03	1.2	1.5	2	3.7	1.6
winter	evergreen needleleaf forest	Wang	0.02	0.05	0.07	0.07	0.07	0.06
		Wright & Zhang	0.04	0.13	0.23	0.45	1.7	0.34
	deciduous broadleaf forest	Wang	0.04	0.06	0.07	0.07	0.07	0.06
		Wright & Zhang	0.03	0.1	0.18	0.36	1.3	0.27

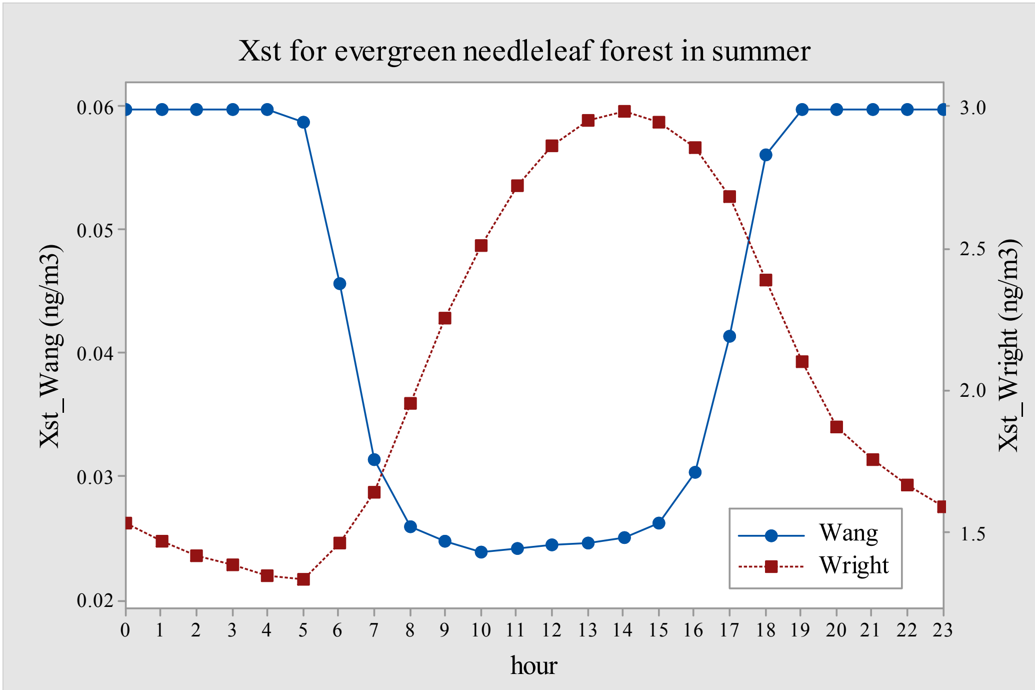

Figure 4-38. Diurnal trend for GEM compensation point concentration in stomata in the two models for evergreen needleleaf forest in summer.

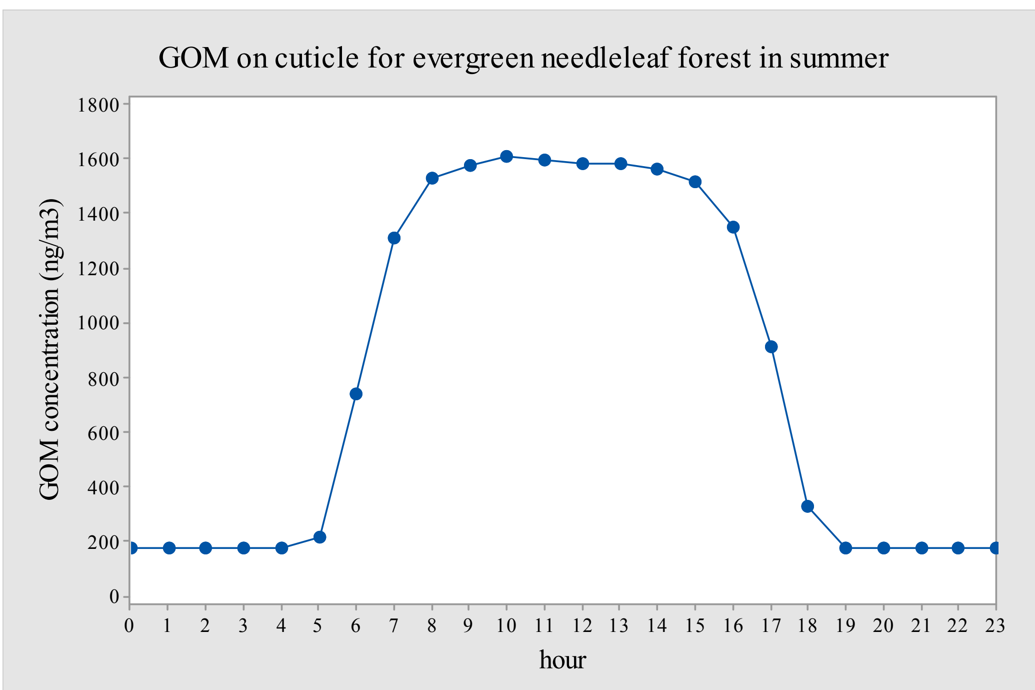

Figure 4-39. Diurnal trend for GOM concentration on cuticle in Wang's model for evergreen needleleaf forest in summer.

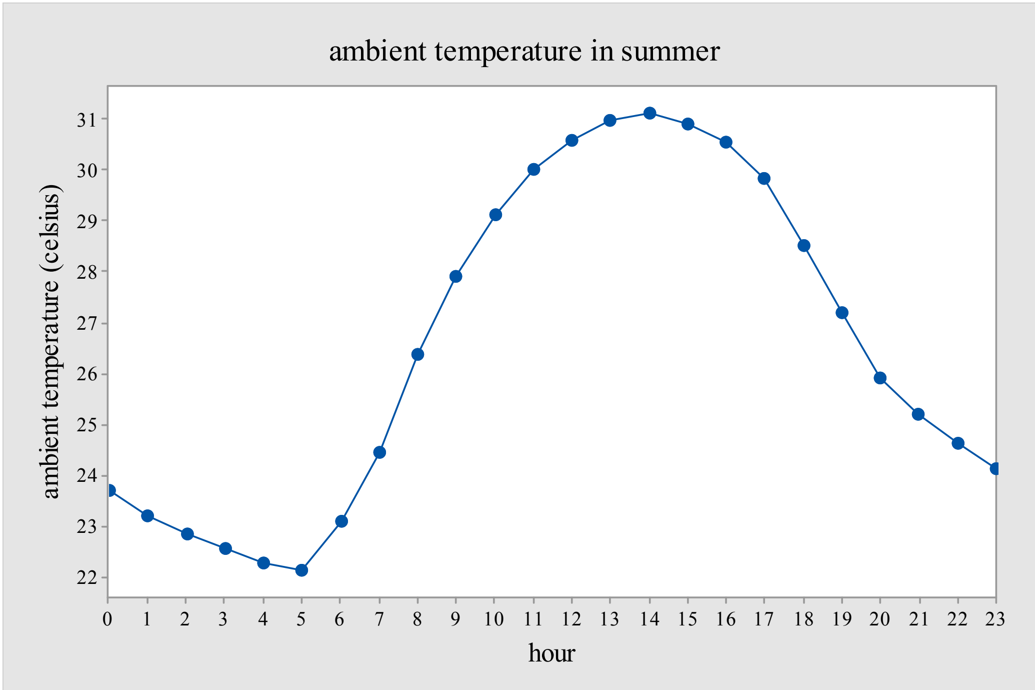

Figure 4-40. Diurnal trend for ambient temperature in summer.

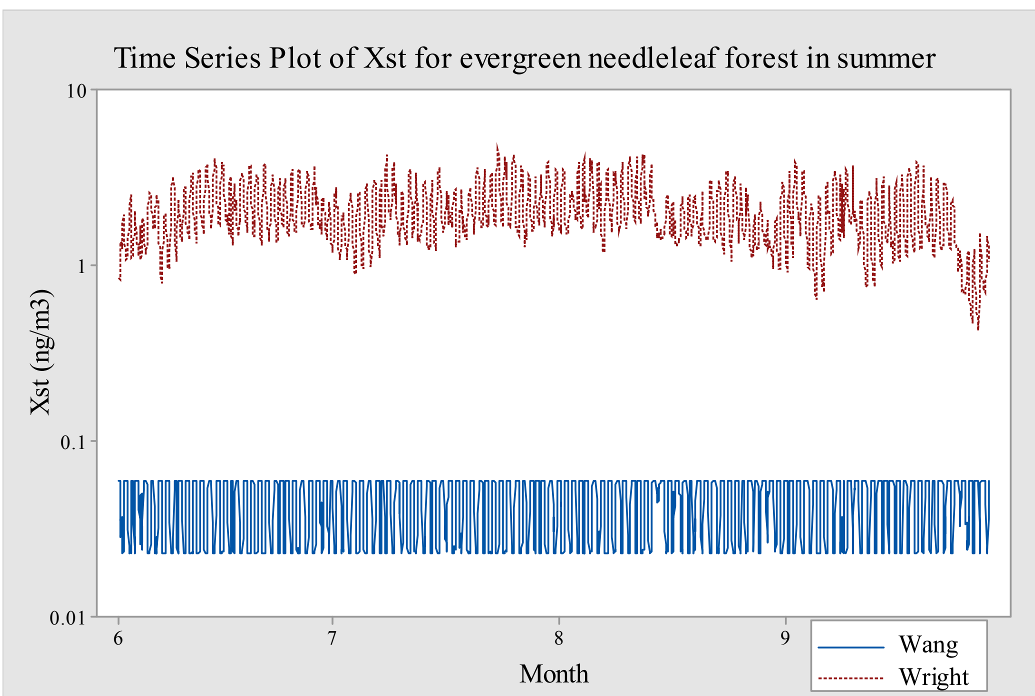

Figure 4-41. Time series for GEM compensation point concentration in stomata in the two models for evergreen needleleaf forest in summer.

b) The difference between the two models and why

As shown in Table 4-26, the difference between the two models ranges from -198% to -152% and mean of absolute difference is 189%. Wright & Zhang considered that χ_{st} is dependent on ambient temperature. In Wang's model, χ_{st} is dependent on GOM concentration on cuticle and GOM concentration on cuticle is related with solar radiation and LAI.

Table 4-26. Difference (%) in GEM compensation point concentration in stomata for the two models in the two seasons.

Season	Land cover	Minimum	First quartile	Median	Third quartile	Maximum	Mean of absolute difference (%)
summer	evergreen needleleaf forest	-198	-196	-189	-185	-152	189
	deciduous broadleaf forest	-198	-195	-187	-181	-142	187
winter	evergreen needleleaf forest	-195	-155	-117	-70	53	110
	deciduous broadleaf forest	-187	-141	-96	-43	78	93

c) Which model is better

Wright & Zhang's model is more appropriate for GEM compensation point concentration in stomata (Table E4). This is because the diurnal trend of χ_{st} in Wright & Zhang's is reasonable. When solar radiation is strong during daytime, more GOM is chemically reduced to GEM. GEM in stomata also trends to emit from stomata to the air under high ambient temperature. Thus, the χ_{st} is expected to have high values during daytime.

Deciduous broadleaf forest in summer

In Wang's model, only LAI is related with land cover. LAI for the two land cover in summer is similar (Table D2). In Wright & Zhang's model, only emission potential of stomata (Γ_{st}, Table C3) is dependent on land cover. Γ_{st} for evergreen needleleaf forest (10) and deciduous broadleaf forest (8) are similar. Thus, it is expected that the difference between the two models is similar for the two land cover in summer. As shown in Table 4-25, χ_{st} in Wang's model is smaller than that in Wright & Zhang's (mean, 0.04 ng m^{-3}<1.6 ng m^{-3}). As seen in Table 4-26, the difference is similar to that for evergreen needleleaf forest in summer (189% vs. 187%), as expected.

Evergreen needleleaf forest in winter

In Wang's model, LAI and solar radiation is related with season. Smaller LAI and solar radiation in winter (Table D2) lead to smaller GOM concentration on cuticle, larger GEM concentration stored in stomata, and larger χ_{st}. In Wright & Zhang's model, lower ambient temperature in winter (Table D2) causes smaller χ_{st}. Thus, it is expected that the difference between the two models is smaller for evergreen needleleaf forest in winter. As in Table 4-25, χ_{st} in Wang's model is smaller than that in Wright & Zhang's model (mean, 0.06 ng m^{-3}<0.34 ng m^{-3}). The difference between the two models is smaller than that for evergreen needleleaf forest in summer (Table 4-26, 189% vs. 110%), as expected.

Deciduous broadleaf forest in winter

In Wang's model, only LAI is related with land cover. LAI in winter is smaller for deciduous broadleaf forest (Table D2). Smaller LAI leads to smaller GOM concentration on cuticle, larger GEM concentration stored in stomata, and larger χ_{st}. In Wright & Zhang's model, Γ_{st} for evergreen needleleaf forest (10) and deciduous broadleaf forest (8) are similar. Thus, it is expected that the difference between the two models is smaller for deciduous broadleaf forest in winter. As shown in Table 4-25, χ_{st} in Wang's model is smaller than that in Wright & Zhang's (mean, 0.06 ng m^{-3}<0.27 ng m^{-3}). The difference between the two models is smaller than that for evergreen needleleaf forest in winter (Table 4-26, 110% vs. 93%), as expected.

Summary

Regardless of season and land cover, χ_{st} in Wang's model is smaller than that in Wright & Zhang's model (mean, 0.05 ng m^{-3}<1.1 ng m^{-3}). For the same land cover and different seasons, greater difference between the two models is in summer (189% vs. 110% for evergreen needleleaf forest, 187% vs. 93% for deciduous broadleaf forest). This is because large LAI and solar radiation lead to small χ_{st} in Wang's model, and high ambient temperature results in large χ_{st} in Wright & Zhang's model. Table 4-27 shows that season is significant in the difference between the two models (p=0.001).

Table 4-27. Analysis of variance (ANOVA) of the difference in GEM compensation point concentration in stomata between the two models.

Parameter	p-value
Season	0.001
Land cover	0.001
Season*land cover	0.001

For different land cover in summer, the difference between the two models is similar (189% vs. 187%) owing to similar LAI and Γst for the two land cover. For different land cover in winter, greater difference between the two models is for evergreen needleleaf forest (110% vs. 93%) because larger LAI leads to larger GOM concentration on cuticle, smaller GEM concentration stored in stomata, and smaller χst in Wang's model. As seen in Table 4-27, land cover is significant in the difference between the two models ($p=0.001$).

4.3.2 Soil compensation point concentration (χ_g)

The parameterization of χ_g is different in the two models (Table C3). Wang assumed that GOM stored in soil is chemically reduced to be GEM. The GOM concentration in soil and GOM chemically reduction rate were assumed to be 90ng/g and $8*10^{-11}$ s^{-1}, respectively. In Wright & Zhang's model, χ_g is similar to χ_{st} (section 4.3.1). It is also derived from the Clausius-Clapeyron equation and is only related with surface air temperature. Wright assumed that χ_g will be zero when snow covers the soil. Both χ_g in Wang's model and Wright & Zhang's model is not related with land cover. Mercury pool in soil is infinite in both models.

Evergreen needleleaf forest in summer

a) χ_g in the two models

Table 4-28 shows χ_g in the two models. The diurnal trend of χ_g in the two models is similar with high values during daytime and low values during nighttime (Fig. 4-42 and

Table E1). χ_g in Wang's model is always larger than that in Wright & Zhang's (Fig. 4-43).

Table 4-28. Compensation point concentration in soil (χ_g, ng m^{-3}) for the two models in the two seasons.

Season	Land cover	Model	Minimum	First quartile	Median	Third quartile	Maximum	Mean
summer	evergreen needleleaf forest	Wang	4.2	6	6.5	7.2	8.7	6.6
		Wright & Zhang	0.4	1.4	1.8	2.6	4.7	2
	deciduous broadleaf forest	Wang	4.2	6	6.5	7.2	8.7	6.6
		Wright & Zhang	0.4	1.4	1.8	2.6	4.7	2
winter	evergreen needleleaf forest	Wang	2.1	2.9	3.5	4.3	6.4	3.7
		Wright & Zhang	0	0.1	0.2	0.4	1.7	0.3
	deciduous broadleaf forest	Wang	2.1	2.9	3.5	4.3	6.4	3.7
		Wright & Zhang	0	0.1	0.2	0.4	1.7	0.3

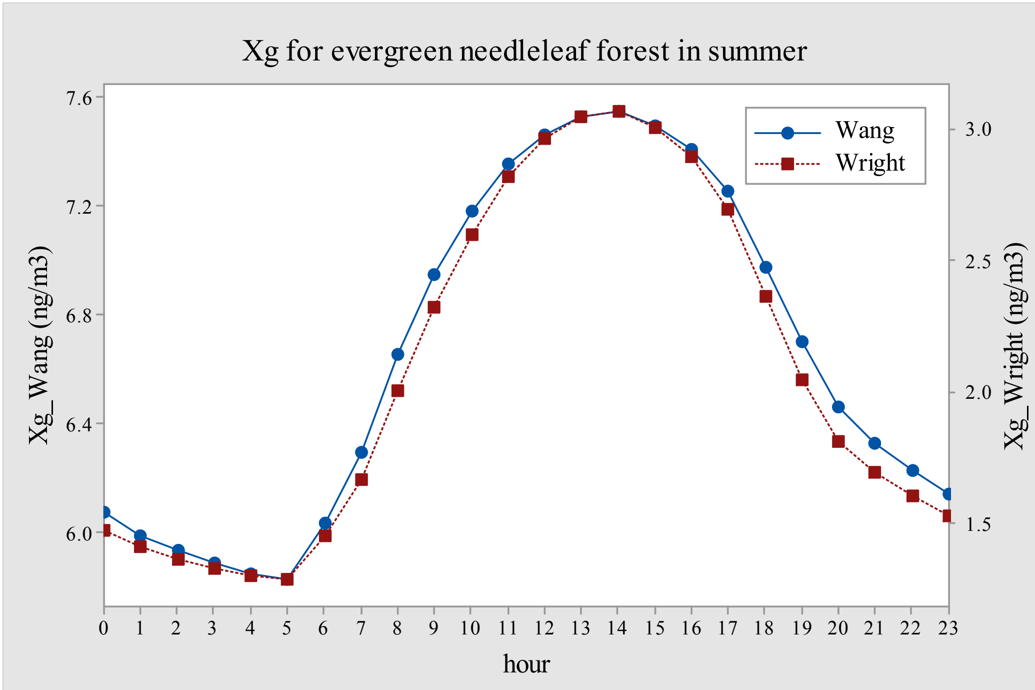

Figure 4-42. Diurnal trend for GEM compensation point concentration in soil in the two models for evergreen needleleaf forest in summer.

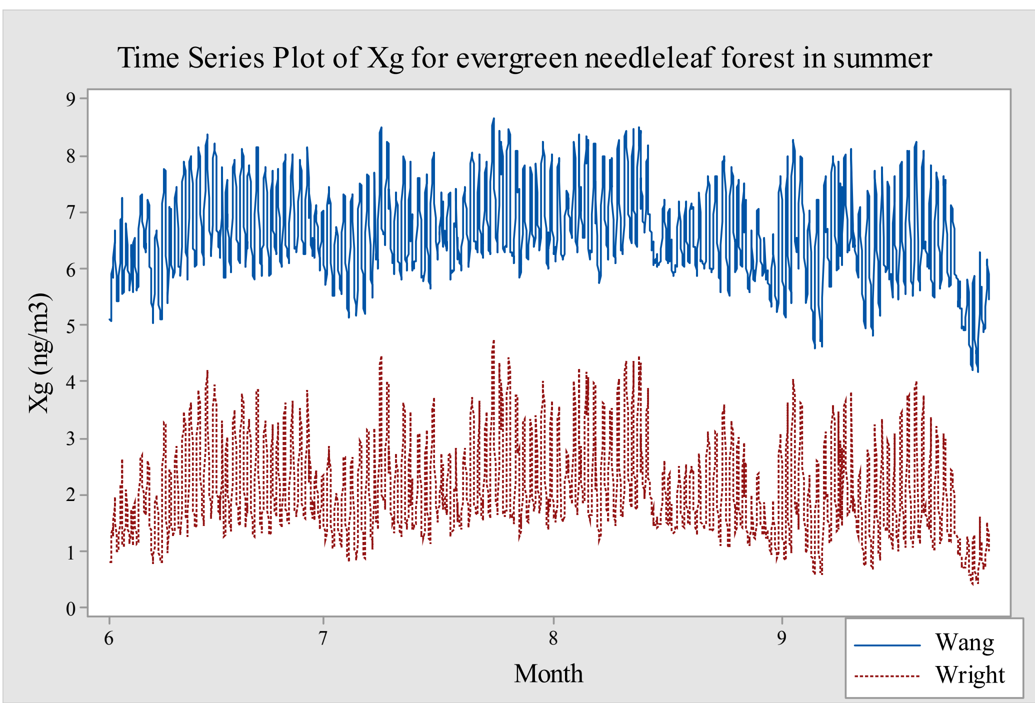

Figure 4-43. Time series for GEM compensation point concentration in soil in the two models for evergreen needleleaf forest in summer.

b) The difference between the two models and why

As shown in Table 4-29, the difference between the two models ranges from 58% to 165% (mean of 110). Wright & Zhang assumed that χ_g is dependent on surface air temperature. In Wang's model, GEM in soil is chemically reduced from GOM. Wang assumed that GOM content in soil is a constant of 90 ng/g and chemically reduction rate of GOM is also a constant of $8*10^{-11}$ s^{-1}. χ_g is calculated with Henry's law constant between soil and air, thus χ_g is related with ambient temperature. The mercury in soil is infinite in both models.

Table 4-29. Difference (%) in GEM compensation point concentration in soil for the two models in the two seasons.

Season	Land cover	Minimum	First quartile	Median	Third quartile	Maximum	Mean
summer	evergreen needleleaf forest	58	95	113	124	165	110
	deciduous broadleaf forest	58	95	113	124	165	110
winter	evergreen needleleaf forest	115	162	177	186	200	174
	deciduous broadleaf forest	115	162	177	186	200	174

c) Which model is better

Wang's model is more appropriate for representation of GEM compensation point concentration in soil (Table E4). In Wang's model, GEM in soil is reduced from GOM and χ_g is related with organic carbon content in soil and Henry's law constant.

Deciduous broadleaf forest in summer

Both χ_g in the two models are not related with land cover. Thus the difference between the two models is the same as that for evergreen needleleaf forest in summer (Table 4-29, 110% vs. 110%).

Evergreen needleleaf forest in winter

As in Table 4-28, χ_g in Wang's model is larger than that in Wright & Zhang's (mean, 3.7 ng m^{-3}>0.3 ng m^{-3}). In Wang's model, lower ambient temperature in winter (Table D2) results in fewer GEM emitting into air and smaller χ_g. In Wright & Zhang's model, lower surface air temperature in winter (Table D2) leads to fewer GEM in soil and smaller χ_g. However, the difference between the two models is greater than that for evergreen needleleaf forest in summer (Table 4-29, 110% vs. 174%).

Deciduous broadleaf forest in winter

Both χ_g in the two models are not related with land cover. Thus the difference between the two models is the same as that for evergreen needleleaf forest in winter (Table 4-29, 174% vs. 174%).

Summary

Regardless of season and land cover, χ_g in Wang's model is larger than that in Wright & Zhang's model (mean, 5.2 ng m^{-3}>1.2 ng m^{-3}). For different land cover and the same season, the difference between the two models is the same (110% vs. 110% in summer, 174% vs. 174% in winter) because χ_g in both models is not related with season. Table 4-30 shows that land cover is insignificant in the difference between the two models (p=0.99). For the same land cover and different seasons, greater difference between the two models is in winter (110% vs. 174% for evergreen needleleaf forest, 110% vs. 174% for deciduous broadleaf forest). In Wright & Zhang's model, lower surface air temperature leads to smaller χ_g. In Wang's model, lower ambient temperature results in smaller χ_g. As in Table 4-30, season is significant in the difference between the two models (p=0.001).

Table 4-30. Analysis of variance (ANOVA) of the difference in GEM compensation point concentration in soil between the two models.

Parameter	p-value
season	0.001
land cover	0.99
season*land cover	0.99

4.4 GEM emission and deposition fluxes

4.4.1 Stomata emission flux (F_{st})

In both models, F_{st} is a product of V_{st} and χ_{st}.

Evergreen needleleaf forest in summer

a) F_{st} in the two models

Table 4-31 shows F_{st} in the two models. F_{st} in the two models has a similar diurnal cycle with high values during daytime and low values during nighttime (Fig. 4-44 and Table E1). But F_{st} for Wang's model has a peak at 18:00 due to more visible solar radiation, smaller R_{st}, and large V_{st} in Wang's (Fig. 4-31). V_{st} in Wang's model is larger than that in Wright's model (mean, 293μm/s>199μm/s). χ_{st} in Wang's model is smaller than that in Wright's model (mean, 0.04 ng m^{-3}<2 ng m^{-3}). Overall, F_{st} in Wang's model is smaller than that in Wright & Zhang's model (Fig. 4-45), reflecting that F_{st} in the two models is mainly controlled by χ_{st}.

Table 4-31. Stomata emission flux (F_{st}, pg m^{-2} s^{-1}) for the two models in the two seasons.

Season	Land cover	Model	Minimum	First quartile	Median	Third quartile	Maximum	Mean
summer	evergreen needleleaf forest	Wang	0	0	0	0.02	0.08	0.01
		Wright & Zhang	0	0.01	0.18	0.85	1.71	0.41
	deciduous broadleaf forest	Wang	0	0	0	0.02	0.09	0.01
		Wright & Zhang	0	0	0.28	1.12	2.19	0.59
winter	evergreen needleleaf forest	Wang	0	0	0	0.02	0.05	0.01
		Wright & Zhang	0	0	0	0.06	0.86	0.06
	deciduous broadleaf forest	Wang	0	0	0	0.02	0.06	0.01
		Wright & Zhang	0	0	0	0.03	0.68	0.05

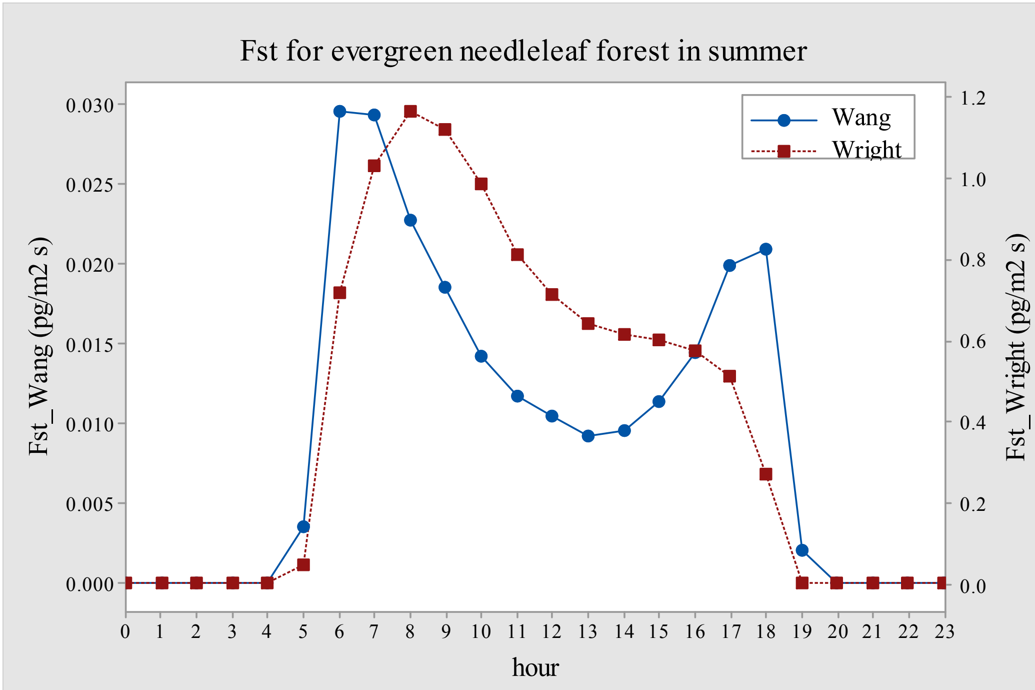

Figure 4-44. Diurnal trend for stomata emission flux in the two models for evergreen needleleaf forest in summer.

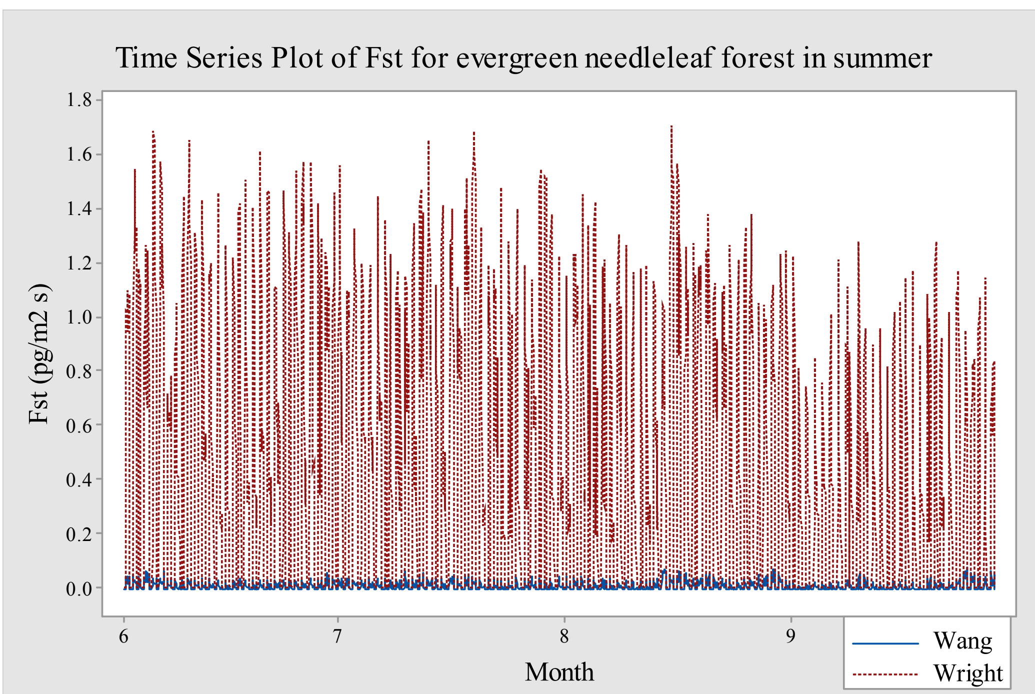

Figure 4-45. Time series for stomata emission flux in the two models for evergreen needleleaf forest in summer.

b) The difference between the two models and why

As in Table 4-32, the difference between the two models ranges from -200% to 65% and mean of absolute difference is 190%. V_{st} in Wang's model is larger than that in Wright & Zhang's model (section 4.2.1). χ_{st} in Wang's model is smaller than that in Wright's model (section 4.3.1). The difference in F_{st} is dominant by different parameterizations of χ_{st}. For χ_{st}, Wang assumed that dry deposited GEM in stomata is the difference between dry deposited TGM on leaves and dry deposited GOM on cuticle. Dry deposited GEM in stomata is emitted back to the atmosphere or fixed in stomata, and the fraction of emitted GEM is dependent on LAI. χ_{st} in Wright & Zhang's model is assumed as the concentration at which there is equilibrium between the different phases (Wright and Zhang, 2015). It is derived from the Clausius-Clapeyron equation and is only related with ambient temperature.

Table 4-32. Difference (%) in stomata emission flux for the two models in the two seasons.

Season	Land cover	Minimum	First quartile	Median	Third quartile	Maximum	Mean of absolute difference (%)
summer	evergreen needleleaf forest	-200	-198	-196	-193	65	190
	deciduous broadleaf forest	-200	-197	-196	-192	125	190
winter	evergreen needleleaf forest	-197	-184	-166	-128	145	148
	deciduous broadleaf forest	-196	-177	-159	-123	147	142

Deciduous broadleaf forest in summer

As seen in Table 4-31, F_{st} in Wang's model is smaller than that in Wright & Zhang's model (mean, 0.01 pg m^{-2} s^{-1}<0.59 pg m^{-2} s^{-1}), and the reason is similar to that for evergreen needleleaf forest in summer. The difference between the two models is also similar to that for evergreen needleleaf forest in summer (Table 4-32, 190% vs. 190%).

Evergreen needleleaf forest in winter

As in Table 4-31, F_{st} in Wang's model is smaller than that in Wright & Zhang's model (mean, 0.01 pg m^{-2} s^{-1}<0.06 pg m^{-2} s^{-1}), and the reason is similar to that for evergreen needleleaf forest in summer. Smaller solar radiation in winter (Table D1) leads to larger R_{st} and smaller V_{st} in both models. Smaller LAI and solar radiation in winter (Table D2) result in smaller GOM concentration on cuticle, larger GEM concentration stored in stomata, and larger χ_{st} in Wang's model. Lower surface air temperature in winter (Table D2) causes smaller χ_{st} in Wright & Zhang's model. The difference in F_{st} is dominant by χ_{st}. Larger χ_{st} in Wang's model and smaller χ_{st} in Wright & Zhang's model lead to smaller difference in F_{st} between the two models (Table 4-32, 190% vs. 148%).

Deciduous broadleaf forest in winter

Table 4-31 shows that F_{st} in Wang's model is smaller than that in Wright & Zhang's model (mean, 0.01 pg m^{-2} s^{-1}<0.05 pg m^{-2} s^{-1}), and the reason is similar to that for evergreen needleleaf forest in winter. The difference between the two models is also similar to that for evergreen needleleaf forest in winter (Table 4-32, 148% vs. 142%).

Summary

Regardless of season and land cover, F_{st} in Wang's model is smaller than that in Wright & Zhang's model (mean, 0.01 pg m^{-2} s^{-1}<0.29 pg m^{-2} s^{-1}). The difference between the two models is mainly controlled by χ_{st}. For different land cover and the same season, the difference between the two models is similar (190% vs. 190% in summer, 148% vs. 142% in winter). This is because, regardless of season, χ_{st} in each model is similar between the two land cover. In summer, larger LAI for deciduous broadleaf forest results in smaller R_{st} and larger V_{st} in both models. In winters, smaller LAI for deciduous broadleaf forest causes smaller V_{st} in both models. Table 4-33 shows that land cover is significant in the difference between the two models (p=0.001).

Table 4-33. Analysis of variance (ANOVA) of the difference in stomata emission flux between the two models.

Parameter	p-value
Season	0.001
Land cover	0.001
Season*land cover	0.097

For the same land cover and different seasons, smaller difference between the two models is in winter (190% vs. 148% for evergreen needleleaf forest, 190% vs. 142% for deciduous broadleaf forest). This is because smaller LAI and solar radiation result in larger χ_{st} in Wang's model, and lower surface air temperature causes smaller χ_{st} in Wright & Zhang's model. Smaller solar radiation and smaller LAI in winter lead to smaller V_{st} in both models. As seen in Table 4-33, season is significant in the difference between the two models (p=0.001).

4.4.2 Soil emission flux (F_g)

In both models, F_g is a product of V_g and χ_g.

Evergreen needleleaf forest in summer

a) F_g in the two models

Table 4-34 shows F_g in the two models. F_g in the two models has similar diurnal trends with high values during daytime and low values during nighttime (Fig. 4-46 and Table E1). V_g in Wang's model is smaller than that in Wright & Zhang's (mean, 188μm/s<219μm/s). χ_g in Wang's model is larger than that in Wright & Zhang's (mean, 6.6 ng m^{-3}>2 ng m^{-3}). Overall, F_g in Wang's model is larger than that in Wright & Zhang's (Fig. 4-47), reflecting that F_g in the two models is mainly controlled by χ_g.

Table 4-34. Soil emission flux (F_g, pg m^{-2} s^{-1}) for the two models in the two seasons.

Season	Land cover	Model	Minimum	First quartile	Median	Third quartile	Maximum	Mean
summer	evergreen needleleaf forest	Wang	0	0.6	1.07	1.96	3.54	1.27
		Wright & Zhang	0	0.19	0.42	0.7	1.66	0.47
	deciduous broadleaf forest	Wang	0	0.33	0.75	1.23	3.05	0.83
		Wright & Zhang	0	0.19	0.43	0.71	1.67	0.48
winter	evergreen needleleaf forest	Wang	0	0.56	0.95	1.47	2.95	1.04
		Wright & Zhang	0	0.01	0.07	0.16	0.74	0.11
	deciduous broadleaf forest	Wang	0	0.39	0.66	1.05	2.71	0.74
		Wright & Zhang	0	0.01	0.07	0.17	0.74	0.12

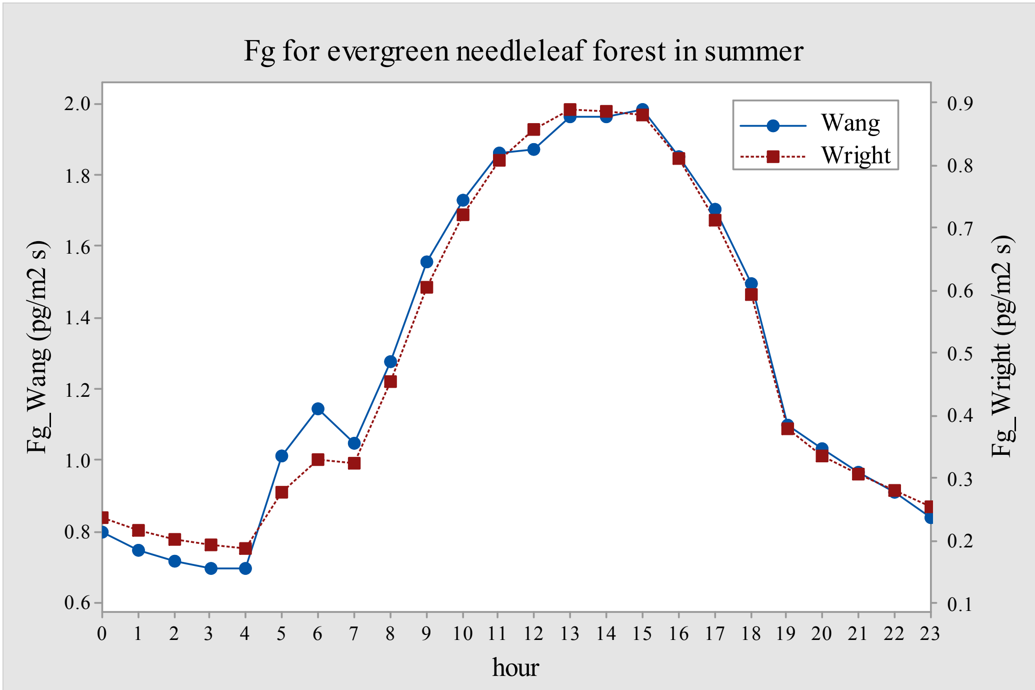

Figure 4-46. Diurnal trend for soil emission flux in the two models for evergreen needleleaf forest in summer.

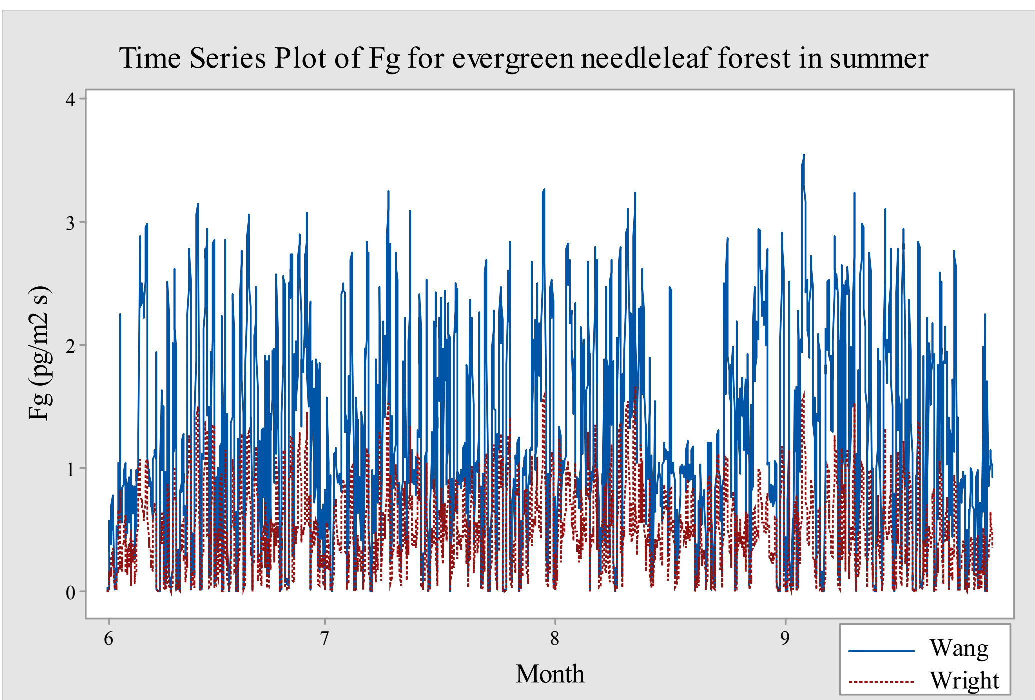

Figure 4-47. Time series for soil emission flux in the two models for evergreen needleleaf forest in summer.

b) The difference between the two models and why

As seen in Table 4-35, the difference between the two models varies between 8% and 161% (mean of 98%). V_g in Wang's model is smaller than that in Wright & Zhang's (section 4.2.2). χ_g in Wang's model is larger than that in Wright & Zhang's (section 4.3.2). Larger F_g in Wang's model is owing to larger χ_g. The difference in F_g is dominant by different parameterizations of χ_g. Wang assumed that GOM stored in soil is reduced to be GEM and χ_g is only dependent on ambient temperature. In Wright & Zhang's model, χ_g is derived from the Clausius-Clapeyron equation and is only related with surface air temperature.

Table 4-35. Difference (%) in soil emission flux for the two models in the two seasons.

Season	Land cover	Minimum	First quartile	Median	Third quartile	Maximum	Mean of absolute difference (%)
summer	evergreen needleleaf forest	8	80	100	117	161	98
	deciduous broadleaf forest	-111	36	51	70	132	53
winter	evergreen needleleaf forest	85	151	171	186	200	168
	deciduous broadleaf forest	52	132	150	175	200	152

Deciduous broadleaf forest in summer

As shown in Table 4-34, F_g in Wang's model is larger than that in Wright & Zhang's model (mean, 0.83 pg m^{-2} s^{-1}>0.48 pg m^{-2} s^{-1}) and the reason is similar to that for evergreen needleleaf forest in summer. In F_g, χ_g is not related with land cover in both models. V_g in Wang's model is much smaller than that in Wright & Zhang's (section

4.2.2). This is because larger R_{ac0} leads to smaller V_g in Wang's model. The difference between the two models is smaller than that for evergreen needleleaf forest in summer (Table 4-35, 98% vs. 53%).

Evergreen needleleaf forest in winter

As seen in Table 4-34, F_g in Wang's model is larger than that in Wright & Zhang's (mean, 1.04 pg m^{-2} s^{-1}>0.11 pg m^{-2} s^{-1}) and the reason is similar to that for evergreen needleleaf forest in summer. In F_g, V_g in Wang's model is smaller than that in Wright & Zhang's (section 4.2.2). Lower ambient temperature results in smaller χ_g in Wang's model and lower surface air temperature leads to smaller χ_g in Wright & Zhang's. However, the reduction of χ_g in Wright & Zhang's is larger. χ_g in Wang's model is much larger than that in Wright & Zhang's (section 4.3.2). The difference between the two models is larger than that for evergreen needleleaf forest in summer (Table 4-35, 98% vs. 168%).

Deciduous broadleaf forest in winter

As shown in Table 4-34, F_g in Wang's model is larger than that in Wright & Zhang's model (mean, 0.74 pg m^{-2} s^{-1}>0.12 pg m^{-2} s^{-1}) and the reason is similar to that for evergreen needleleaf forest in summer. The difference between the two models is larger than that for deciduous broadleaf forest in summer (Table 4-35, 53% vs. 152%), and the reason is the same as that for evergreen needleleaf forest in winter.

Summary

Regardless of season and land cover, F_g in Wang's model is larger than that in Wright & Zhang's (mean, 0.98 pg m^{-2} s^{-1}>0.31 pg m^{-2} s^{-1}). The difference in F_g between the two models is dominant by χ_g. For different land cover and the same season, the difference between the two models is smaller for deciduous broadleaf forest (98% vs. 53% in summer, 168% vs. 152% in winter), because larger R_{ac0} leads to smaller V_g in Wang's model. V_g in Wang's model is much smaller than that in Wright & Zhang's. χ_g in Wang's is larger than that in Wright & Zhang's, however χ_g is not related with land cover. As shown in Table 4-36, land cover is significant in the difference between the two models (p=0.001).

Table 4-36. Analysis of variance (ANOVA) of the difference in soil emission flux between the two models.

Parameter	p-value
season	0.001
land cover	0.001
season*land cover	0.001

For the same land cover and different seasons, greater difference between the two models is in winter (98% vs. 168% for evergreen needleleaf forest, 53% vs. 152% for deciduous broadleaf forest). This is because lower ambient temperature results in smaller χ_g in Wang's model and lower surface air temperature leads to smaller χ_g in Wright & Zhang's. The reduction of χ_g is larger in Wright & Zhang's. χ_g in Wang's model is much larger than that in Wright & Zhang's. V_g in Wang's model is smaller than that in Wright & Zhang's. As seen in Table 4-36, season is significant in the difference between the two models (p=0.001).

4.4.3 Cuticle emission flux (F_c)

Wright & Zhang assumed that F_c to be zero and Wang considered it. As seen in Table 4-37, F_c in Wang's model in all cases is negligible, compared with F_{st} (Table 4-31) and F_g (Table 4-34). In all cases, F_c accounts for 0-1.6% (mean of 0.07%) of the total emission flux.

Table 4-37. Cuticle emission flux (pg m^{-2} s^{-1}) in Wang's model in the two seasons.

Season	Land cover	Minimum	First quartile	Median	Third quartile	Maximum	Mean
summer	evergreen needleleaf forest	0	0	0	0.001	0.018	0.001
	deciduous broadleaf forest	0	0	0	0.001	0.009	0.001
winter	evergreen needleleaf forest	0	0	0	0.004	0.01	0.004
	deciduous broadleaf forest	0	0	0	0.001	0.003	0.001

4.4.4 Deposition flux (F_d)

In both models, F_d is a product of V_d and GEM concentration in the air (χ_{atm}). χ_{atm} is the same in the two models, thus F_d in the two models is controlled by V_d.

Evergreen needleleaf forest in summer

a) F_d in the two models

Table 4-38 shows F_d in the two models. Negative sign represents downward flux. F_d in the two models has similar diurnal trend with high values during daytime and low values during nighttime (Fig. 4-48 and Table E1). V_d in Wang's model is larger than that in Wright & Zhang's model (mean, 640μm/s>576μm/s). χ_{atm} is the same in the two models. However, F_d is similar in the two models (Fig. 4-49).

Table 4-38. Deposition flux (F_d, pg m^{-2} s^{-1}) for the two models in the two seasons.

Season	Land cover	Model	Minimum	First quartile	Median	Third quartile	Maximum	Mean
summer	evergreen needleleaf forest	Wang	-3.29	-1.18	-0.62	-0.33	-0.002	-0.78
		Wright & Zhang	-2.91	-1.02	-0.63	-0.34	-0.005	-0.7
	deciduous broadleaf forest	Wang	-3.5	-1.41	-0.4	-0.19	-0.001	-0.75
		Wright & Zhang	-3.13	-1.25	-0.68	-0.32	-0.005	-0.79
winter	evergreen needleleaf forest	Wang	-3.76	-1.23	-0.7	-0.46	-0.001	-0.84
		Wright & Zhang	-3.19	-1.07	-0.74	-0.41	-0.004	-0.77
	deciduous broadleaf forest	Wang	-3.23	-0.77	-0.43	-0.25	-0.007	-0.57
		Wright & Zhang	-2.86	-0.85	-0.63	-0.36	-0.004	-0.66

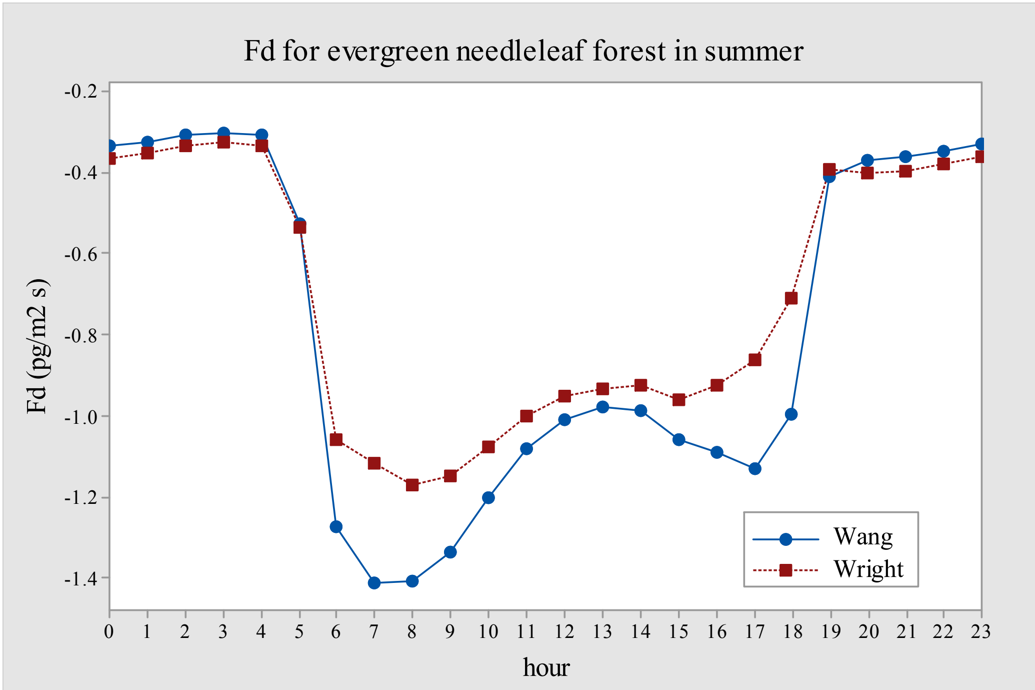

Figure 4-48. Diurnal trend for deposition flux in the two models for evergreen needleleaf forest in summer.

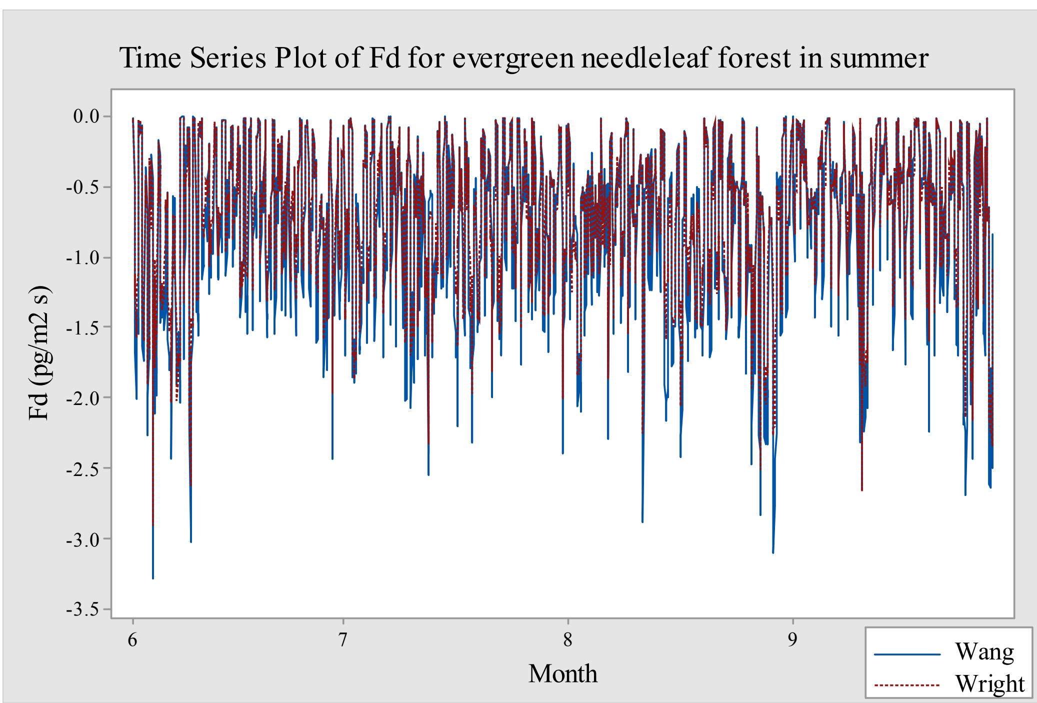

Figure 4-49. Time series for deposition flux in the two models for evergreen needleleaf forest in summer.

b) The difference between the two models and why

As shown in Table 4-39, the difference between the two models ranges from -116% to 168% and mean of absolute difference is 15%. The difference is dependent on V_d. The difference in F_d is similar to that in V_d (section 4.2.3).

Table 4-39. Difference (%) in deposition flux for the two models in the two seasons.

Season	Land cover	Minimum	First quartile	Median	Third quartile	Maximum	Mean of absolute difference (%)
summer	evergreen needleleaf forest	-116	-6	-1	16	168	15
	deciduous broadleaf forest	-155	-48	-29	7	175	36
winter	evergreen needleleaf forest	-137	-5	-0.3	22	82	20
	deciduous broadleaf forest	-146	-69	-30	4	71	41

For other three cases

F_d in Wang's model is similar to that in Wright & Zhang's (Table 4-38). F_d is dependent on V_d. The difference in F_d between the two models is similar to that in V_d.

Summary

Regardless of season and land cover, F_d in Wang's model is similar to that in Wright & Zhang's model (mean, -0.74 pg $m^{-2}s^{-1}$ vs. -0.73 pg $m^{-2}s^{-1}$). The difference between the two models is similar to that in difference in V_d. For different land cover and the same season, the difference between the two models is larger for deciduous broadleaf forest (15% vs. 36% in summer, 20% vs. 41% in winter). For the same land cover and different seasons, the difference between the two models is similar (15% vs. 20% for evergreen needleleaf forest, 36% vs. 41% for deciduous broadleaf forest). Table 4-40 shows that both season and land cover are significant in the difference between the two models (p=0.001).

Table 4-40. Analysis of variance (ANOVA) of the difference in deposition flux between the two models.

Parameter	p-value
season	0.001
land cover	0.001
season*land cover	0.001

4.4.5 Net flux

Evergreen needleleaf forest in summer

a) Net flux in the two models

Table 4-41 shows net flux in the two models. Negative sign stands for net deposition flux and positive sign represents net emission flux. Net flux in the two models has similar diurnal trends with high values during daytime and low values during nighttime (Fig. 4-50 and Table E1). But net flux in Wang's model has a valley value at 7:00 because larger deposition (Fig. 4-48). F_d is similar in the two models (section 4.4.4). F_c is negligible in Wang's model and is not considered by Wright & Zhang (section 4.4.3). F_g in Wang's model is much larger than that in Wright & Zhang's (mean, 1.27 pg m^{-2} s^{-1}>0.47 pg m^{-2} s^{-1}). F_{st} in Wang's model is smaller than that in Wright & Zhang's model (mean, 0.01 pg m^{-2} s^{-1}<0.41 pg m^{-2} s^{-1}). Overall, net flux in Wang's model is larger than that in Wright's model (mean, 0.5 pg m^{-2} s^{-1}>0.18 pg m^{-2} s^{-1}), reflecting that net flux between the two models is mainly affected by F_g.

Table 4-41. Net flux (pg m^{-2} s^{-1}) for the two models in the two seasons.

Season	Land cover	Model	Minimum	First quartile	Median	Third quartile	Maximum	Mean
summer	evergreen needleleaf forest	Wang	-2.49	-0.01	0.32	1.12	2.91	0.5
		Wright & Zhang	-2.44	-0.12	0.02	0.51	1.54	0.18
	deciduous broadleaf forest	Wang	-2.89	-0.32	0.08	0.57	2.53	0.1
		Wright & Zhang	-1.85	-0.05	0.05	0.66	2	0.29
winter	evergreen needleleaf forest	Wang	-1.61	-0.001	0.16	0.5	1.87	0.21
		Wright & Zhang	-2.25	-0.82	-0.57	-0.34	0.08	-0.59
	deciduous broadleaf forest	Wang	-1.43	-0.001	0.18	0.38	1.59	0.18
		Wright & Zhang	-2.04	-0.65	-0.49	-0.32	-0.004	-0.49

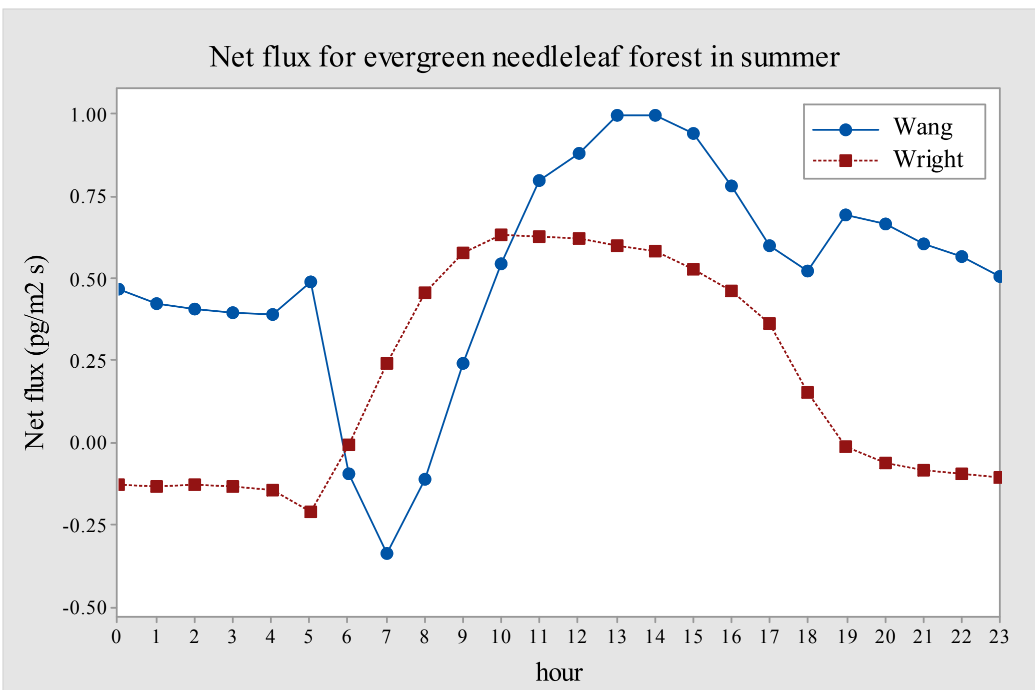

Figure 4-50. Diurnal trend for net flux in the two models for evergreen needleleaf forest in summer.

Castro and Moore (2016) conducted a GEM flux measurements at a site surrounded by deciduous forests during July 2009 to 6 July 2010. They found that GEM emission flux is larger than GEM deposition flux in summer (mean, 16.8 ng m^{-2} h^{-1}>15.5 pg m^{-2} s^{-1}). In winter, GEM emission flux is smaller than GEM deposition flux in summer (mean, 13.9 ng m^{-2} h^{-1}>15.2 pg m^{-2} s^{-1}). Their measurements indicated that GEM net flux was emission in summer and deposition in winter.

b) The difference between the two models and why

As seen in Table 4-42, the difference between the two models ranges from -99874% to 111608% and mean of absolute difference is 882%. The difference in net flux between the two models is mainly caused by F_{st} and F_g. F_g in Wang's model is much larger than that in Wright & Zhang's (mean, 1.27 pg m^{-2} s^{-1}>0.47 pg m^{-2} s^{-1}). F_{st} in Wang's model is smaller than that in Wright & Zhang's model (mean, 0.01 pg m^{-2} s^{-1}<0.41 pg m^{-2} s^{-1}).

Table 4-42. Difference (%) in net flux for the two models in the two seasons.

Season	Land cover	Minimum	First quartile	Median	Third quartile	Maximum	Mean of absolute difference (%)
summer	evergreen needleleaf forest	-99874	-62	70	207	111608	882
	deciduous broadleaf forest	-142634	-83	69	241	313273	914
winter	evergreen needleleaf forest	-101274	-411	-160	-397	285765	1698
	deciduous broadleaf forest	-502272	-580	-263	-57	185056	2245

Deciduous broadleaf forest in summer

F_d is similar in the two models (section 4.4.4). F_c is negligible for Wang's model and is not considered by Wright & Zhang (section 4.4.3). F_g in Wang's model is larger than that in Wright & Zhang's (mean, 0.83 pg m^{-2} s^{-1}>0.48 pg m^{-2} s^{-1}), however the difference is smaller compared with that for evergreen needleleaf forest in summer. F_{st} in Wang's model is smaller than that in Wright & Zhang's (mean, 0.01 pg m^{-2} s^{-1}<0.59 pg m^{-2} s^{-1}). As in Table 4-41, net flux for Wang's model is smaller than that for Wright & Zhang's model (mean, 0.1 pg m^{-2} s^{-1}<0.29 pg m^{-2} s^{-1}).This is because reduction of F_g is larger in Wang's model. The difference between the two models is similar to that for evergreen needleleaf forest in summer (Table 4-42, 882% vs. 914%).

Evergreen needleleaf forest in winter

F_d is similar in the two models (section 4.4.4). F_c is negligible in Wang's model and is not considered by Wright & Zhang (section 4.4.3). F_g in Wang's model is larger than that in Wright & Zhang's model (mean, 1.04 pg m^{-2} s^{-1}>0.11 pg m^{-2} s^{-1}). F_{st} in Wang's model (mean, 0.01 pg m^{-2} s^{-1}) is similar to that in Wright & Zhang's model (mean, 0.06 pg m^{-2} s^{-1}). As seen in Table 4-41, net flux in Wang's model is emission flux (mean, 0.21 pg m^{-2} s^{-1}) and that in Wright & Zhang's is deposition flux (mean, -0.59 pg m^{-2} s^{-1}). This is because of large F_g in Wang's and small F_g in Wright & Zhang's. The difference between the two models is greater than that for evergreen needleleaf forest in summer (Table 4-42, 882% vs. 1698%).

Deciduous broadleaf forest in winter

Similar to that for evergreen needleleaf forest in winter, as in Table 4-41, net flux in Wang's model is emission flux (mean, 0.18 pg m^{-2} s^{-1}) and that in Wright & Zhang's is deposition flux (mean, -0.49 pg m^{-2} s^{-1}). This is also caused by large F_g in Wang's (mean, 0.74 pg m^{-2} s^{-1}) and small F_g in Wright & Zhang's (mean, 0.12 pg m^{-2} s^{-1}). The difference between the two models is larger than that for evergreen needleleaf forest in winter (Table 4-42, 1698% vs. 2245%).

Summary

For evergreen needleleaf forest in summer, net flux in Wang's model is larger than that in Wright & Zhang's model (mean, $0.5\ pg\ m^{-2}\ s^{-1} > 0.18\ pg\ m^{-2}\ s^{-1}$) because of large F_g in Wang's. For deciduous broadleaf forest in summer, net flux in Wang's model is smaller than that in Wright & Zhang's model (mean, $0.1\ pg\ m^{-2}\ s^{-1} < 0.29\ pg\ m^{-2}\ s^{-1}$) because F_g in Wang's is smaller. Regardless of land cover in winter, net flux in Wang's is emission flux (mean, 0.2 pg m^{-2} s^{-1}), and that in Wright & Zhang's is deposition flux (mean, -0.54 pg m^{-2} s^{-1}). This is due to large F_g in Wang's and small F_g in Wright & Zhang's model. The difference in net flux between the two models is mainly affected by F_g.

For different land cover and the same season, greater difference is for deciduous broadleaf forest (882% vs. 914% in summer, 1698% vs. 2245% in winter). For the same land cover and different seasons, larger difference is in winter (882% vs. 1698% for evergreen needleleaf forest, 914% vs. 2245% for deciduous broadleaf forest). As seen in Table 4-43, both season and land cover are significant in the difference between the two models.

Table 4-43. Analysis of variance (ANOVA) of the difference in net flux between the two models.

Parameter	p-value
season	0.068
land cover	0.007
season*land cover	0.004

CHAPTER 5 CONCLUSIONS AND RECOMMENDATIONS

5.1 Conclusions

In this study, two bidirectional air-surface exchange models for GEM were compared over evergreen needleleaf forest and deciduous broadleaf forest with the two models run under the same meteorological condition in the summer of June 2010—September 2010 and the winter of December 2010—March 2011. Resistances, velocities, GEM compensation point concentrations, and fluxes estimated by the two models were compared and the following conclusions were found.

For evergreen needleleaf forest in summer, the net emission flux in Wang's model was greater than that in Wright & Zhang's model (0.5 pg $m^{-2}s^{-1}$>0.18 pg $m^{-2}s^{-1}$). For deciduous broadleaf forest in summer, smaller net emission flux was in Wang's model (0.1 pg $m^{-2}s^{-1}$<0.29 pg $m^{-2}s^{-1}$). Regardless of land cover in winter, net flux in Wang's was emission flux (0.21 pg $m^{-2}s^{-1}$ and 0.18 pg $m^{-2}s^{-1}$) while that in Wright & Zhang's was deposition flux (0.59 pg $m^{-2}s^{-1}$ and 0.49 pg $m^{-2}s^{-1}$).

There are five categories for the difference in diurnal trend of output from the two models: (1) a similar diurnal trend and similar value for quasi-laminar resistance, in-canopy aerodynamic resistance, stomata emission velocity, soil emission velocity, deposition velocity, and deposition flux; (2) a similar diurnal trend and different values for aerodynamic resistance, stomata resistance, GEM compensation point concentration in soil, and soil emission flux; (3) a similar diurnal trend and small difference at a few hours of the day for stomata resistance and stomata emission flux; (4) different diurnal trends and similar value for soil resistance and net flux; and (5) different diurnal trends and different values for GEM compensation point concentration in stomata.

The magnitude of the differences in resistances, velocities, GEM compensation point concentrations, and fluxes between the two models was quantified. Small differences (<35%) between the two models were found in quasi-laminar resistance, cuticle resistance, and soil resistance. Median differences (≥35% and <100%) were found in aerodynamic resistance, soil emission velocity, deposition velocity, and deposition flux. Large differences (≥100%) between the two models were found in stomata resistance, in-canopy aerodynamic resistance, stomata emission velocity, GEM compensation point concentration in stomata, GEM compensation point concentration in soil, stomata emission flux, soil emission flux, and net flux.

The dominant factors causing the large differences between the two models were identified: the discrepancies in

(1) stomata resistance and stomata emission velocity were caused by a) stomata resistance constant values for no exchange flux when stomata is closed, b) the setting of diffusivities (water vapor and GEM diffusivities), c) the calculation of visible solar radiation reaching leaves, and d) when the correction factor by water vapor pressure deficit (f_D) being less than 0.1 in Wang's model, otherwise this correction factor is the same in the two models;

(2) in-canopy aerodynamic resistance were caused by the setting of a reference value for in-canopy aerodynamic resistance (R_{ac0}) (250 s/m in Wang's model and 60-100 s/m in Wright & Zhang's model);

(3) GEM compensation point concentrations in stomata and stomata emission flux were because Wang's model considered GOM chemically-reducing to GEM, GOM washing off from leaves, GOM fixing on the leaves, and GEM partitioning between air and

leaves, all of which were not considered in Wright & Zhang's model;

(4) GEM compensation point concentrations in soil and soil emission flux were because Wang's model considered GOM chemically-reducing to GEM and GEM partitioning between air and soil, all of which were not considered in Wright & Zhang's model;

(5) net flux were due to soil emission flux. For other components of net flux, deposition fluxes were similar in the two models; stomata emission fluxes were different in the two models, but their values were small; cuticle emission flux was negligible in Wang's model and was zero in Wright & Zhang's model.

The difference in all output, except aerodynamic resistance, between the two models is related to the land cover. The difference in all output, except quasi-laminar resistance, soil resistance, and GEM compensation point concentration in soil, between the two models is associated with the season.

For aerodynamic resistance, quasi-laminar resistance, stomata resistance, in-canopy aerodynamic resistance and GEM compensation point concentration in stomata, Wright & Zhang's model is more appropriate. However, for GEM compensation point concentration in soil, Wang's model is more appropriate. For soil resistance, neither of the two models is appropriate because Wang's model did not considered the effect of frozen soil on GEM exchange and Wright & Zhang's model did not considered the effect of wet soil on GEM exchange. Overall, Wright & Zhang's model is more appropriate for GEM exchange flux, because the estimated net deposition flux in winter is reasonable.

5.2 Recommendations

In this study, the difference between the two models was analyzed for two tall canopies, evergreen needleleaf forest and deciduous broadleaf forest, where both LAI values and seasonal variability of LAI are similar in the two land covers. Future studies could investigate the difference between the two models for a low canopy with a different of LAI, such as crops or grass. In this study, the two models were run under the same meteorological conditions in summer and winter, while future studies could compare the two models in all four seasons. Future studies should compare fluxes estimated by the two models and the measured GEM exchange flux. One of the major limitations in both models is the infinite mercury pool in stomata and soil, which may not be unreasonable. Future studies may want to set the mercury pool in stomata and soil as finite values. In future studies, wet soil may be considered in Wright & Zhang's model and surface temperature below -1 °C may be considered in Wang's model.

REFERENCES

Bash, J.O., 2010. Description and initial simulation of a dynamic bidirectional air surface exchange model for mercury in Community Multiscale Air Quality (CMAQ) model. J. Geophys. Res., 115, D06305, doi:10.1029/2009JD012834.

Boening, D.W., 2000. Ecological effects, transport, and fate of mercury: a general review. Chemosphere, 40, 1335–1351.

Castro, M. and Moore, C., 2016. Importance of Gaseous Elemental Mercury Fluxes in Western Maryland. Atmosphere, 7, 110. doi: 10.3390/atmos7090110.

Cole, A.S., Steffen, A., Eckley, C.S., Narayan, J., Pilote, M., Tordon, R., Graydon, J.A., St. Louis, V.L., Xu, X., and Bran-fireun, B.A., 2014. A survey of mercury in air and precipitation across Canada: patterns and trends. Atmosphere, 5, 635–668.

EPA (Environmental Protection Agency), 1997. Mercury Study Report to Congress. EPA -452/R-97, United States. https://cfpub.epa.gov/ols/catalog/advanced_brief_record.cfm?&FIELD1=SUBJECT&INPUT1=Mercury%20Toxicology%20United%20States%2E&TYPE1=EXACT&LOGIC1=AND&COLL=&SORT_TYPE=MTIC&item_count=21. Accessed April, 2019.

EPA (Environmental Protection Agency), 2017. Biomonitoring Mercury. https://www.epa.gov/sites/production/files/2017-09/documents/ace3_mercury_updates_081017_508.pdf. Accessed May, 2019.

Erisman, J.W., Pul, V.A., and Wyers, P., 1994. Parametrization of surface resistance for the quantification of atmospheric deposition of acidifying pollutants and ozone. Atmospheric Environment, 28, 2595–2607.

Fuchs, N.A., 1964. The Mechanics of Aerosols. Pergamon, Oxford, New York.

Fu, X.W., Feng, X.B., Sommar, J., and Wang, S.F., 2012. A review of studies on atmospheric mercury in China. Sci. Total Environ., 421–422, 73–81.

Gaffney, J.S. and Marley, N.A., 2014. In-depth review of atmospheric mercury: sources, transformations, and potential sinks. Energy and Emission Control Technologies, 2, 1–21.

Gallagher, M.W., Nemitz, E., Dorsey, J.R., Fowler, D., Sutton, M.A., Flynn, M., and Duyzer, J., 2002. Measurements and parameterizations of small aerosol deposition velocities to grassland, arable crops, and forest: Influence of surface roughness length on deposition. J. Geophys. Res., 107, 4154. doi:10.1029/2001JD000817.

Hicks, B.B., Baldocchi, D.D., Meyers, T.P., Hosker, R.P., Jr., and Matt, D.R, 1987. A preliminary multiple resistance routine for deriving dry deposition velocities from measured quantities. Water, Air, and Soil Pollution, 36, 311–330.

Kerkweg, A., Buchholz, J., Ganzeveld, L., Pozzer, A., Tost, H., and Jöckel, P., 2006. Technical Note: An implementation of the dry removal processes DRY DEPosition and SEDImentation in the Modular Earth Submodel System (MESSy). Atmos. Chem. Phys., 6, 4617–4632.

Lamaud, E., Fontan, J., Lopez, A., and Druilhet, A., 1994. Parametrization of the dry deposition velocity of submicronic aerosol particles. International Conference on Air Pollution – Proceedings, Barcelona, Spain, 27–29 September 1994, 2, 433–440.

Padro, J., 1996. Summary of ozone dry deposition velocity measurements and model estimates over vineyard, cotton, grass and deciduous forest in summer. Atmospheric Environment, 30, 2363–2369.

Peters, K. and Eiden, R., 1992. Modelling the dry deposition velocity of aerosol particles to a spruce forest. Atmospheric Environment, 26, 2555–2564.

Petroff, A. and Zhang, L., 2010. Development and validation of a size-resolved particle dry deposition scheme for application in aerosol transport models. Geosci. Model Dev., 3, 753–769. doi:10.5194/gmd-3-753-2010.

Pirrone, N., Cinnirella, S., Feng, X., Finkelman, R.B., Friedli, H.R., Leaner, J., Mason, R., Mukherjee, A.B., Stracher, G.B., Streets, D.G., and Telmer, K., 2010. Global mercury emissions to the atmosphere from anthropogenic and natural sources. Atmos. Chem. Phys., 10, 5951–5964.

Pirrone, N., Hedgecock, I.M., and Forlano L, 2000. Role of the Ambient Aerosol in the Atmospheric Processing of semi-volatile contaminants: A parameterized numerical model (GASPAR). Journal of Geophys. Res., 105, D8, 9773–9790.

Poissant, L., Amyot, M., Pilote, M., and Lean, D., 2000. Mercury water-air exchange over the Upper St. Lawrence River and Lake Ontario. Environ. Sci. Technol., 34, 3069–3078.

Prestbo, E.M. and Gay, D.A., 2009. Wet deposition of mercury in the U.S. and Canada, 1996–2005: Results and analysis of the NADP mercury deposition network (MDN). Atmos. Environ., 43, 4223–4233.

Ruijgrok, W., Davidson, C.I., and Nicholson, K.W., 1995. Dry deposition of particles implications and recommendations for mapping of deposition over Europe. Tellus 47B, 587–601.

Ruijgrok, W., Tieben, H., and Eisinga, P., 1997. The dry deposition of particles to a forest canopy: A comparison of model and experimental results. Atmos. Environ., 31, 399–415.

Schroeder, W.H. and Munthe, J., 1998. Atmospheric mercury – An overview. Atmos. Environ., 32, 809–822.

Schwede, D., Zhang, L., Vet, R., and Lear, G., 2011. An intercomparison of the deposition models used in the CASTNET and CAPMoN networks. Atmos. Environ., 45, 1337–1346.

Slinn, W.G.N., 1982. Predictions for particle deposition to vegetative surfaces. Atmos. Environ., 16, 1785–1794.

UNEP (United Nations Environment Programme), 2013. Global Merucry Assessment, 2013 – Sources, Emissions, Releases, and Environmental Transport. UNEP Division of Technology, Industry and Economics, Chemicals Branch International Environment House.

van Hove, L.W.A., Heeres, P., and Bossen, M.E., 2002. The annual variation in stomatal ammonia compensation point of rye grass (Lolium perenne L.) leaves in an intensively managed grassland. Atmos. Environ., 36, 2965–2977.

Wang, X., Lin, C.-J., and Feng, X., 2014. Sensitivity analysis of an updated bidirectional air-surface exchange model for elemental mercury vapor, Atmos. Chem. Phys., 14, 6273–6287.

Wesely, M.L., 1989. Parameterization of surface resistances to gaseous dry deposition in regional-scale numerical models. Atmos. Environ., 23, 1293–1304.

Wesely, M.L., Cook, D.R, Hart, R.L., and Speer, R.E., 1985. Measurements and parameterization of particulate sulfur dry deposition over grass. J. Geophys. Res., 90, 2131–2143.

Wesely, M.L. and Hicks, B.B., 1977. Some factors that affect the deposition rates of sulfur dioxide and similar gases on vegetation. Journal of the Air Pollution Control Association, 27, 1110–1116.

Wesely, M.L. and Hicks, B.B., 2000. A review of the current status of knowledge on dry deposition. Atmos. Environ., 34, 2261–2282.

Wright, L.P. and Zhang, L., 2015. An approach estimating bidirectional air-surface exchange for gaseous elemental mercury at AMNet sites. J. Adv. Model. Earth Syst., 7, 35–49.

Wright, L.P., Zhang, L., and Marsik, F.J., 2016. Overview of mercury dry deposition, litterfall, and throughfall studies. Atmos. Chem. Phys., 16, 13399–13416.

Wu, M., Liu, X., Zhang, L., Wu, C., Lu, Z., Ma, P., Wang, H., Tilmes, S., Mahowald, N., Matsui, H., and Easter, R.C., 2018a. Impacts of aerosol dry deposition on black carbon spatial distributions and radiative effects in the Community Atmosphere Model CAM5. Journal of Advances in Modeling Earth Systems, 10, 1150–1171.

Wu, Z., Schwede, D.B., Vet, R., Walker, J.T., Shaw, M., Staebler, R., and Zhang L., 2018b. Evaluation and intercomparison of five dry deposition algorithms in North America. Journal of Advances in Modeling Earth Systems. Journal of Advances in Modeling Earth Systems, 10, 1571–1586.

Xu, X., Yang, X., Miller, D.R., Helble, J.J., and Carley, R.J., 1999. Formulation of bidirectional atmosphere-surface exchanges of elemental mercury. Atmos. Environ., 33, 4345–4355.

Zhang, L., Brook, J., and Vet, R., 2002a. On Ozone dry deposition With emphasis on non-stomatal uptake and wet canopies. Atmos. Environ., 36, 4787–4799.

Zhang, L., Brook, J.R., and Vet, R., 2003. A revised parameterization for gaseous dry deposition in air-quality models. Atmos. Chem. Phys., 3, 2067–2082.

Zhang, L., Cheng, I., Wu, Z., Harner, T., Schuster, J., Charland, J., Muir, D., and Parnis, J. M. 2015. Dry deposition of polycyclic aromatic compounds to various land covers in the Athabasca oil sands region. Journal of Advances in Modeling Earth Systems, 7, 1339–1350.

Zhang, L., Gong, S., Padro, J., and Barrie, L.A., 2001. A size-segregated particle dry deposition scheme for an atmospheric aerosol module. Atmos. Environ., 35, 549–560.

Zhang, L. and He, Z., 2014. Technical Note: An empirical algorithm estimating dry deposition velocity of fine, coarse and giant particles. Atmos. Chem. Phys., 14, 3729–3737.

Zhang, L., Lyman, S., Mao, H., Lin, C.-J., Gay, D.A., Wang, S., Gustin, M.S., Feng, X., and Wania, F., 2017. A synthesis of research needs for improving the understanding of atmospheric mercury cycling. Atmos. Chem. Phys., 17, 9133–9144.

Zhang, L., Moran, M.D., Makar, P.A., Brook, J.R., and Gong, S.L., 2002b. Modelling gaseous dry deposition in AURAMS: a unified regional air-quality modelling system. Atmos. Environ., 36, 537– 560.

Zhang, L., Wang, S., Wu, Q., Wang, F., Lin, C.-J., Zhang, L., Hui, M., Yang, M., Su, H., and Hao, J., 2016a. Mercury transformation and speciation in flue gases from anthropogenic emission sources: a critical review. Atmos. Chem. Phys., 16, 2417–2433.

Zhang, L., Wright, L.P., and Asman, W.A.H., 2010. Bidirectional air-surface exchange of atmospheric ammonia—A review of measurements and a development of a big-leaf model for applications in regional-scale air-quality models. J. Geophys. Res., 115, D20310, doi: 10.1029/2009JD013589.

Zhang, L., Wu, Z., Cheng, I., Wright, L.P., Olson, M.L., Gay, D.A., Risch, M.R., Brooks, S., Castro, M.S., Conley, G.D., Edgerton, E.S., Holsen, T.M., Luke, W., Tordon, R., and Weiss-Penzias, P., 2016b. The Estimated Six-Year Mercury Dry Deposition Across North America. Environ. Sci. Technol., 50, 12864−12873.

APPENDICES

Appendix A: Comparison of output from Matlab to original output from Fortran

Because Fortran software is not available in University of Windsor and Matlab software is available, the original Fortran code of Wright and Zhang (2015) was recompiled as the Matlab code. Therefore, it is necessary to compare output from Matlab to original output from Fortran. The two codes are run with meteorological data of GA40 site under 26 land cover in Zhang et al. (2003) during Jun. 2009-Sep. 2009 and Dec. 2009-Apr. 2010.

The analysis of percentage of errors in net flux is shown in Table A1. The percentage of error is calculated as

$$\text{Error}=\frac{|\text{Flux}_{\text{Matlab}}-\text{Flux}_{\text{Fortran}}|}{|\text{Flux}_{\text{Fortran}}|}*100 \qquad \text{(A1)}$$

There are three hours with errors larger than 1%. Then the net fluxes of three hours are listed in Table A2 for checking. Although the errors of the hours are larger than 1%, it can be seen that these errors are all caused by round-off. Compared with mean net flux of -6.43 pg m-2s-1, these three errors are small enough. Apart from these three errors, the largest error is 0.325% and is acceptable.

From Figure A1 and Figure A2, the results from Matlab are acceptable and the Matlab code can be used as a replacement of original Fortran code to simulate GEM bidirectional exchange flux. In order to analyze the distribution of errors more clearly, the errors are scaled to a new set of errors without three errors larger than 1%. From Figure A1, almost all the errors concentrate around zero. Then, the frequency was scaled to 5000 for better identification the distribution of errors near zero, as in Figure A2.

Table A1. Analysis of errors in Hg net flux calculated by Matlab.

Error in Hg net fluxes from Fortran and Matlab	Total number of Hg fluxes	Total number of errors exceeding the threshold	Percentage (%)
>1%		3	0.004
>0.1%		15	0.018
>0.01%	84994	441	0.52
>0.001%		6054	7.12
>0.0001%		8862	10.4

Table A2. Data with error>1%

Values from Fortran	Values from Matlab	Error (%)
0.00087	0.00088	1.15
0.00030	0.00029	3.33
-0.00062	-0.00063	1.61

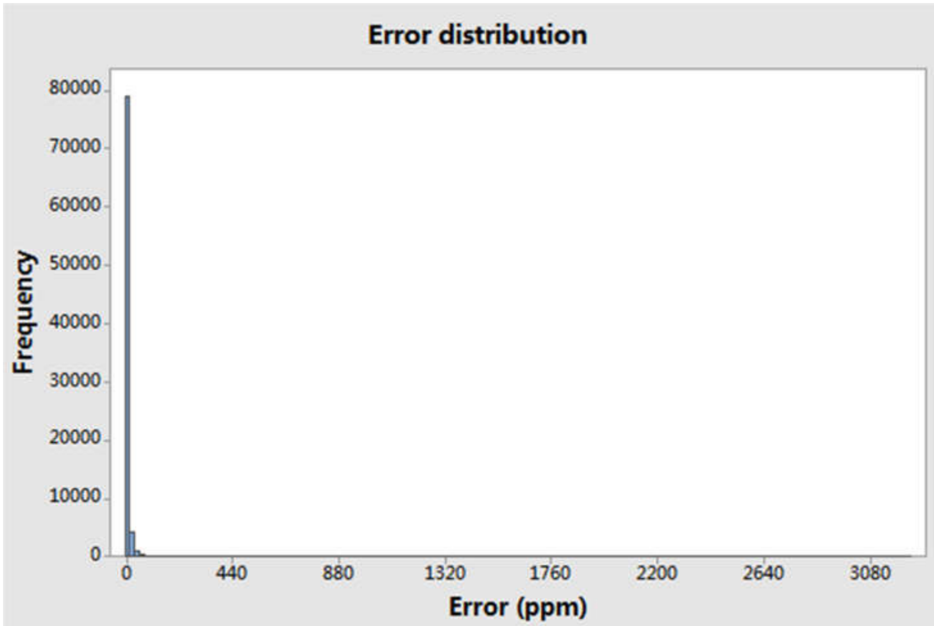

Figure A1. Distribution of errors in ppm.

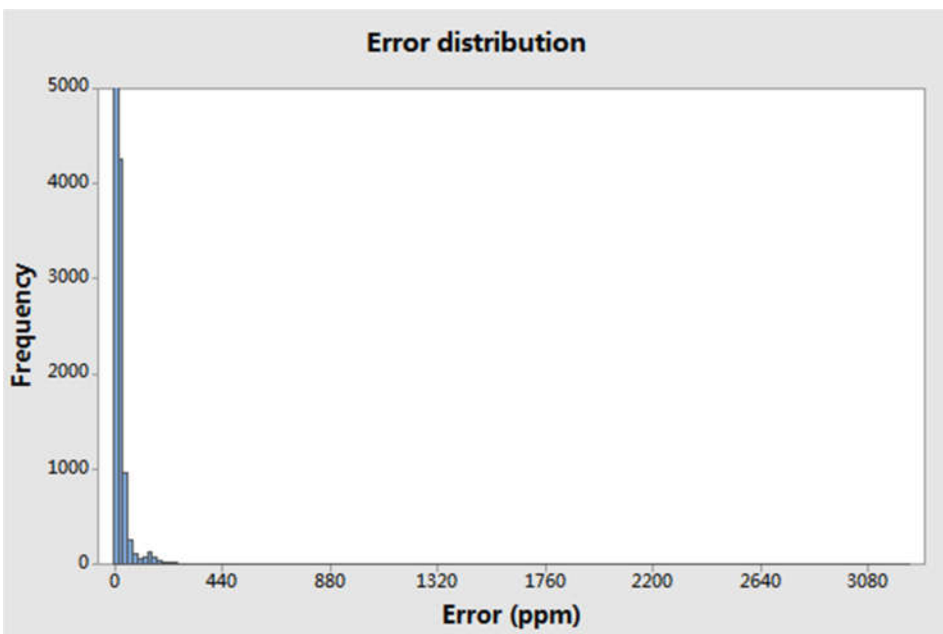

Figure A2. Distribution of errors in ppm with scaled frequency.

Appendix B: Flow chart for the two models

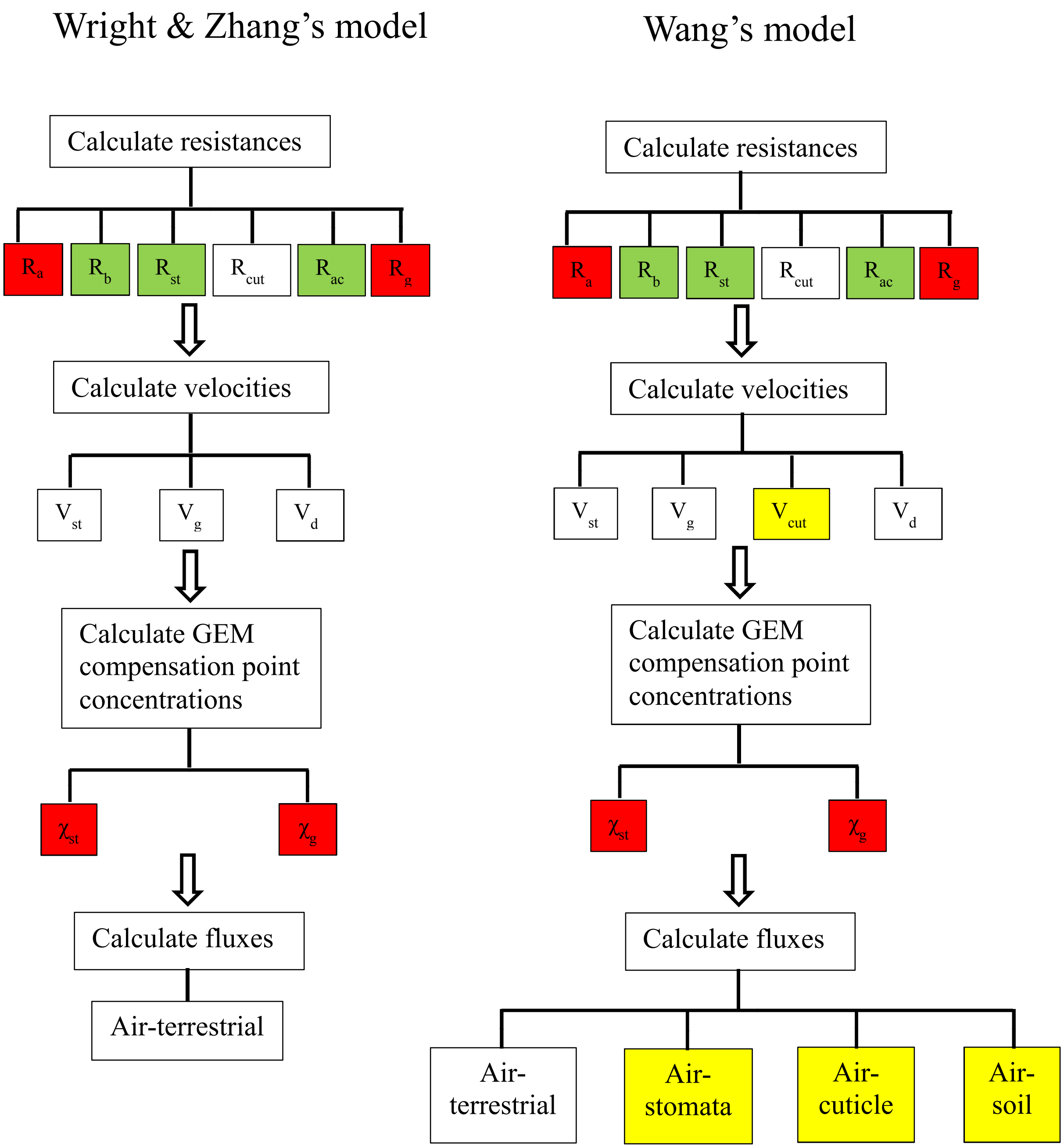

Figure B. Flow chart for the two models.

* ■ : equations were different in the two models

: equations were the same and some parameters were different in the two models

: considered by only one model

Appendix C: Parameterization of the two models

Table C1. Parameterization of resistances

Resistances	Wright & Zhang' model	Wang's model
aerodynamic resistance (R_a)	$R_a=\frac{\ln\left(\frac{Z_R}{Z_0}\right)-\Psi_H}{ku_*}$	$R_a=\frac{U}{u_*^2}$
qasi-laminar resistance (R_b)	$R_b=\frac{2}{ku_*}\left(\frac{VI}{DI}\right)^{2/3}$	
cuticle resistance (R_{cut})	$R_{cutd}=\frac{R_{cutd0}}{e^{0.03RH}LAI^{1/4}u_*}$ $R_{cutw}=\frac{R_{cutw0}}{LAI^{1/2}u_*}$	
stomata resistance (R_{st})	$R_{st}=\frac{1}{G_{st}(PAR)\ f_T\ f_D\ f_\psi}\ \frac{DV}{DI}$ where $f_D=1-b_{vpd}D$	
in-canopy aerodynamic resistance (R_{ac})	$R_{ac}=\frac{R_{ac0}\ LAI^{\frac{1}{4}}}{u_*^2}$	
soil resistance (R_g)	$\frac{1}{R_g}=\frac{\alpha}{R_g(SO_2)}+\frac{\beta}{R_g(O_3)}$	

*Note. Z_R is reference height; Z_0 is roughness height; Ψ_H is stability correction factor; k is a constant of 0.4; U is wind speed; u_* is friction velocity; VI is air diffusivity; DI is GEM diffusivity; R_{cutd} is dry cuticle resistance; R_{cutw} is wet cuticle resistance; R_{cutd0} is reference value for R_{cutd}; RH is relative humidity; R_{cutw0} is reference value for R_{cutw}; $G_{st}(PAR)$ is the unstressed canopy stomata conductance; f_T is correction factor for air temperature; f_D is correction factor for water vapor pressure deficit of air; f_ψ is correction factor for water stress of plant; DV is water vapor diffusivity; b_{vpd} is empirical water vapour pressure deficit constant; D is vapor pressure deficit; R_{ac0} is reference value of R_{ac}; α is a constant of zero; β is a constant of 0.1; $R_g(SO_2)$ is SO_2 soil resistance; and $R_g(O_3)$ is O_3 soil resistance.

Table C2. Parameterization of velocities

Velocities	Equations
stomata emission velocity (V_{st})	$V_{st}=\frac{1}{R_{st}}\ \frac{1}{R_a+R_b}\ (\frac{1}{R_a+R_b}+\frac{1}{R_{st}}+\frac{1}{R_{cut}}+\frac{1}{R_{ac}+R_g})^{-1}=\frac{1}{R_{st}}\ \frac{1}{R_a+R_b}\ R_t$
soil emission velocity (V_g)	$V_g=\frac{1}{R_{ac}+R_g}\ \frac{1}{R_a+R_b}\ (\frac{1}{R_a+R_b}+\frac{1}{R_{st}}+\frac{1}{R_{cut}}+\frac{1}{R_{ac}+R_g})^{-1}=\frac{1}{R_{ac}+R_g}\ \frac{1}{R_a+R_b}\ R_t$
cuticle emission velocity (V_{cut})	$V_{cut}=\frac{1}{R_{cut}}\ \frac{1}{R_a+R_b}\ (\frac{1}{R_a+R_b}+\frac{1}{R_{st}}+\frac{1}{R_{cut}}+\frac{1}{R_{ac}+R_g})^{-1}=\frac{1}{R_{cut}}\ \frac{1}{R_a+R_b}\ R_t$
deposition velocity (V_d)	$V_d=\frac{-1}{R_a+R_b}+(\frac{1}{R_a+R_b})^2\ (\frac{1}{R_a+R_b}+\frac{1}{R_{st}}+\frac{1}{R_{cut}}+\frac{1}{R_{ac}+R_g})^{-1}=\frac{1}{R_a+R_b}(\frac{R_t}{R_a+R_b}-1)$

*Note. $R_t=(\frac{1}{R_a+R_b}+\frac{1}{R_{st}}+\frac{1}{R_{cut}}+\frac{1}{R_{ac}+R_g})^{-1}$

The equations are the same in the two models.

Table C3. Parameterization of GEM compensation point concentrations

GEM compensation point concentrations	Wright & Zhang' model	Wang's model
in stomata (χ_{st})	$\chi_{st}=\frac{8.9803\times10^{9}}{T}\times\Gamma_{st}\times\exp\left(-\frac{8353.8}{T}\right)\times8.2041$	$\chi_{st}=\frac{[Hg_s^0]}{LAP}$ $[Hg_s^0]=(1\text{-}f_{fixed})([Hg]\text{-}[Hg_c^{II+}])$ where $[Hg_c^{II+}]=\frac{[Hg_w^{II+}]}{1\text{-}f_{rxn}\text{-}f_{fixed}}$
on cuticle (χ_c)	—	$\chi_c=\frac{[Hg_c^0]}{LAP}$ $[Hg_c^0]=(f_{rxn}\text{-}f_{fixed})[Hg_c^{II+}]$ where $[Hg_c^{II+}]=\frac{[Hg_w^{II+}]}{1\text{-}f_{rxn}\text{-}f_{fixed}}$
in the soil (χ_g)	$\chi_g=\frac{8.9803\times10^{9}}{T_s}\times\Gamma_g\times\exp\left(-\frac{8353.8}{T_s}\right)\times8.2041$	$\chi_g=\frac{[Hg_g^0]\ H}{f_{oc}\ K_{oc}}$ where $[Hg_g^0]=f_{rxn}[Hg_g^{II+}]$

*Note. T is ambient temperature; Γ_{st} is emission potential of stomata; $[Hg_s^0]$ is dissolved elemental mercury in stomata; f_{fixed} is the fraction of GOM fixed into tissue; [Hg] is total gaseous mercury depositing on foliage; $[Hg_c^{II+}]$ is dry deposited GOM loading on cuticle; $[Hg_w^{II+}]$ is GOM concentration washed-off from leaf; f_{rxn} is the fraction of GOM potentially photoreduced to GEM; $[Hg_c^0]$ is GEM bound to foliar cuticle surface; LAP is leaf–air partitioning coefficient for GEM between leaves and air; Γ_g is emission potential of soil; T_s is surface temperature; $[Hg_g^0]$ is GEM bound to organic matter; H is Henry's law constant in soil condition; f_{oc} is the fraction of organic carbon in topsoil (0-5cm); K_{oc} is soil organic carbon to water partitioning coefficient; $[Hg_g^{II+}]$ is GOM content in the soil.

Appendix D: General statistics of input data

Table D1. General statistic of input meteorology data before merging.

Input parameters (unit)	Seasons	Range	Mean	Median
surface air temperature (° C)	summer	10.1-37	26.5	26.1
	winter	-11.5-25.8	6.1	5.7
ambient temperature (°C)	summer	12.6-35.5	26.8	26.9
	winter	-11.4-25	6.9	6.4
relative humidity (%)	summer	14.9-100	67.9	68.1
	winter	22.2-99.9	68.7	69.6
soil volumetric water content (m^3/m^3)	summer	0.11-0.44	0.19	0.17
	winter	0.12-0.48	0.2	0.18
wind speed (evergreen needleleaf forest, m/s)	summer	0.26-4.8	1.74	1.74
	winter	0.28-7.17	2.68	2.61
wind speed (deciduous broadleaf forest, m/s)	summer	0.26-4.78	1.72	1.72
	winter	0.29-7.87	2.93	2.85
u_* (evergreen needleleaf forest, m/s)	summer	0.001-0.8	0.27	0.28
	winter	0.001-1.19	0.42	0.42
u_* (deciduous broadleaf forest, m/s)	summer	0.001-0.8	0.27	0.28
	winter	0.001-1	0.35	0.35
LAI (evergreen needleleaf forest)	summer	4.54-5.52	5.05	5.14
	winter	0.74-2.23	1.01	0.85
LAI (deciduous broadleaf forest)	summer	4.64-5.75	5.3	5.34
	winter	0.6-1	0.72	0.67
barometric pressure (mbar)	summer	970-990	981	970
	winter	962-998	984	984

solar radiation (W/m^2)	summer	0-867	217	62
	winter	0-781	120	0
precipitation (mm/hour)	summer	0-57	3	0
	winter	0-46	2	0
snow depth (cm)	summer	0	0	0
	winter	0-16.6	0.69	0
fraction of cloud (fraction)	summer	0-1	0.3	0.2
	winter	0-1	0.36	0.14
cosine value of zenith angle (dimensionless)	summer	0-0.98	0.33	0.18
	winter	0-0.86	0.18	0

Table D2. General statistic of input meteorology data after merging.

Input parameters (unit)	Seasons	Range	Mean	Median
surface air temperature (°C)	summer	10.1-37	26.3	25.9
	winter	-11.5-25.3	5.1	4.3
ambient temperature (°C)	summer	10.7-36.6	26.3	26
	winter	-11.5-24.9	5.6	4.4
relative humidity (%)	summer	14.9-1	68.8	69.5
	winter	23.2-99.9	68.9	69.9
soil volumetric water content (m^3/m^3)	summer	0.11-0.44	0.2	0.17
	winter	0.12-0.44	0.2	0.17
wind speed (evergreen needleleaf forest, m/s)	summer	0.26-4.8	1.72	1.71
	winter	0.28-7.04	2.68	2.62
wind speed (deciduous broadleaf forest, m/s)	summer	0.26-4.78	1.7	1.69
	winter	0.29-7.74	2.93	2.86
u_* (evergreen needleleaf forest, m/s)	summer	0.001-0.8	0.27	0.27
	winter	0.001-1.17	0.42	0.42
u_* (deciduous broadleaf forest, m/s)	summer	0.001-0.8	0.27	0.27
	winter	0.001-0.98	0.35	0.35
LAI (evergreen needleleaf forest)	summer	4.54-5.52	5.05	5.14
	winter	0.75-1.86	0.93	0.84
LAI (deciduous broadleaf forest)	summer	4.64-5.75	5.3	5.34
	winter	0.6-0.95	0.7	0.66
barometric pressure (mbar)	summer	970-990	981	982
	winter	963-998	984	985
solar radiation (W/m^2)	summer	0-866.9	213.4	40.1

	winter	0-751.3	115.9	0
precipitation (mm/hour)	summer	0-57	3	0
	winter	0-39	2	0
snow depth (cm)	summer	0	0	0
	winter	0-16.6	0.78	0
fraction of cloud (fraction)	summer	0-1	0.29	0.15
	winter	0-1	0.35	0.12
cosine value of zenith angle (dimensionless)	summer	0-0.98	0.32	0.11
	winter	0-0.83	0.17	0

Appendix E: Comparison of the two models.

Table E1. Comparison of diurnal trends in the two models.

variables	evergreen needleleaf forest (summer)	evergreen needleleaf forest (winter)	deciduous broadleaf forest (summer)	deciduous broadleaf forest (winter)
R_a	similar diurnal trend and different values			
R_b	similar diurnal trend and similar value			
R_{st}	similar diurnal trend and small difference at a few hours	similar diurnal trend and different values	similar diurnal trend and small difference at a few hours	similar diurnal trend and different values
R_{cut}	the same in the two models			
R_{ac}	similar diurnal trend and similar value			
R_g	different diurnal trends and similar value			
V_{st}	similar diurnal trend and similar value			
V_g	similar diurnal trend and similar value			
V_d	similar diurnal trend and similar value			
χ_{st}	different diurnal trends and different values			
χ_g	similar diurnal trend and different values			
F_{st}	similar diurnal trend and small difference at a few hours			
F_g	similar diurnal trend and different values			
F_d	similar diurnal trend and similar value			
net flux	different diurnal trends and similar value			

Table E2. Percentage of difference between the two models.

variables	evergreen needleleaf forest (summer)	evergreen needleleaf forest (winter)	deciduous broadleaf forest (summer)	deciduous broadleaf forest (winter)
R_a	36	32	36	32
R_b	15	19	15	19
R_{st}	98	108	104	113
R_{cut}	0	0	0	0
R_{ac}	0	0	89	122
R_g	28	32	28	32
V_{st}	98	108	104	113
V_g	16	24	67	64
V_d	15	20	37	40
χ_{st}	189	110	187	93
χ_g	110	174	110	174
F_{st}	190	148	190	142
F_g	98	168	53	152
F_d	15	20	36	41
net flux	882	1698	914	2245

Table E3. P-values for land cover, season, and interaction in the difference between the two models.

Variables	Season	Land use	Season*LUC
R_a	0.926	0.052	0.026
R_b	0.001	0.99	0.99
R_{st}	0.001	0.001	0.002
R_{ac}	0.001	0.001	0.001
R_g	0.001	0.99	0.99
V_{st}	0.001	0.001	0.002
V_g	0.001	0.001	0.001
V_d	0.001	0.001	0.001
χ_{st}	0.001	0.001	0.001
χ_g	0.001	0.99	0.99
F_{st}	0.001	0.001	0.097
F_g	0.001	0.001	0.001
F_d	0.001	0.001	0.001
net flux	0.068	0.007	0.004

Table E4. Which model is better.

variables	which model is better	reasons
R_a	Wright & Zhang	• consider both mechanical and thermal turbulence • the cap prevent extreme large values
R_b	Wright & Zhang	• consider the effect of ambient temperature on air diffusivity and GEM diffusivity
R_{st}	Wright & Zhang	Wang • input barometric pressure Wright & Zhang • calculate visible solar radiation from input solar radiation • correction factor for water vapor pressure deficit of air (f_D) ≥ 0.1 • the dependence of diffusivity on ambient temperature
R_{ac}	Wright & Zhang	• consider canopy growth
R_g	neither (add wet soil in Wright & Zhang' model)	Wang • consider wet soil Wright & Zhang • consider surface temperature below -1^0C
χ_{st}	Wright & Zhang	• diurnal trend with high values during daytime
χ_g	Wang	Wright & Zhang • zero when soil is covered by snow Wang • photo-reduced from GOM • related with organic carbon content in soil and Henry's low

Appendix F: ANOVA analysis for output from the two models

Table F1. ANOVA results for resistance in the two models.

Resistances	Parameters	p-values or R-sq values in Wang's model	p-values or R-sq values in Wright & Zhang's model
R_a	Season	0.025	0.001
	LUC	0.539	0.097
	Season*LUC	0.414	0.051
	R-sq (%)	0.05	0.38
	R-sq (adj) (%)	0.03	0.36
R_b	Season	0.001	0.001
	LUC	0.447	0.432
	Season*LUC	0.334	0.323
	R-sq (%)	0.29	0.24
	R-sq (adj) (%)	0.27	0.21
R_{st}	Season	0.001	0.001
	LUC	0.001	0.03
	Season*LUC	0.321	0.004
	R-sq (%)	1.34	2.97
	R-sq (adj) (%)	1.31	2.94
R_{cut}	Season	0.001	0.001
	LUC	0.001	0.001
	Season*LUC	0.001	0.001
	R-sq (%)	1.49	1.48
	R-sq (adj) (%)	1.46	1.46
R_{ac}	Season	0.001	0.001
	LUC	0.001	0.766
	Season*LUC	0.169	0.994
	R-sq (%)	0.23	0.2
	R-sq (adj) (%)	0.21	0.17
R_g	Season	0.264	0.001
	LUC	0.99	0.99
	Season*LUC	0.99	0.99
	R-sq (%)	0.01	9.99
	R-sq (adj) (%)	0	9.96

Table F2. ANOVA results for velocity in the two models.

Velocities	Parameters	p-values or R-sq values in Wang's model	p-values or R-sq values in Wright & Zhang's model
V_{st}	Season	0.001	0.001
	LUC	0.001	0.001
	Season*LUC	0.001	0.001
	R-sq (%)	4.12	9.73
	R-sq (adj) (%)	4.09	9.71
V_{cut}	Season	0.001	N.A.
	LUC	0.001	
	Season*LUC	0.073	
	R-sq (%)	13.37	
	R-sq (adj) (%)	13.35	
V_g	Season	0.001	0.001
	LUC	0.001	0.001
	Season*LUC	0.001	0.103
	R-sq (%)	17.06	12.27
	R-sq (adj) (%)	17.03	12.25
V_d	Season	0.001	0.001
	LUC	0.001	0.286
	Season*LUC	0.001	0.001
	R-sq (%)	3.58	2.61
	R-sq (adj) (%)	3.56	2.58

Table F3. ANOVA results for GEM compensation point concentration in the two models.

GEM compensation point concentrations	Parameters	p-values or R-sq values in Wang's model	p-values or R-sq values in Wright & Zhang's model
χ_{st}	Season	0.001	0.001
	LUC	0.001	0.001
	Season*LUC	0.001	0.001
	R-sq (%)	29.91	66.67
	R-sq (adj) (%)	29.88	66.66
χ_{cut}	Season	0.001	N.A.
	LUC	0.054	
	Season*LUC	0.054	
	R-sq (%)	8.89	
	R-sq (adj) (%)	8.87	
χ_{g}	Season	0.001	0.001
	LUC	0.99	0.99
	Season*LUC	0.99	0.99
	R-sq (%)	74.37	63.94
	R-sq (adj) (%)	74.36	63.93

Table F4. ANOVA results for flux in the two models.

Fluxes	Parameters	p-values or R-sq values in Wang's model	p-values or R-sq values in Wright & Zhang's model
F_{st}	Season	0.001	0.001
	LUC	0.001	0.001
	Season*LUC	0.001	0.001
	R-sq (%)	1.01	22.92
	R-sq (adj) (%)	0.98	22.9
F_{cut}	Season	0.001	N.A.
	LUC	0.001	
	Season*LUC	0.001	
	R-sq (%)	8.1	
	R-sq (adj) (%)	8.07	
F_g	Season	0.001	0.001
	LUC	0.001	0.297
	Season*LUC	0.001	0.718
	R-sq (%)	8.37	30.02
	R-sq (adj) (%)	8.34	30
F_d	Season	0.001	0.001
	LUC	0.001	0.132
	Season*LUC	0.001	0.001
	R-sq (%)	2.59	1.09
	R-sq (adj) (%)	2.56	1.06
total emission flux	Season	0.001	0.001
	LUC	0.001	0.001
	Season*LUC	0.001	0.001
	R-sq (%)	8.3	31.57
	R-sq (adj) (%)	8.27	31.55
net flux	Season	0.001	0.001
	LUC	0.001	0.001
	Season*LUC	0.001	0.78
	R-sq (%)	5.09	45.46
	R-sq (adj) (%)	5.06	45.44

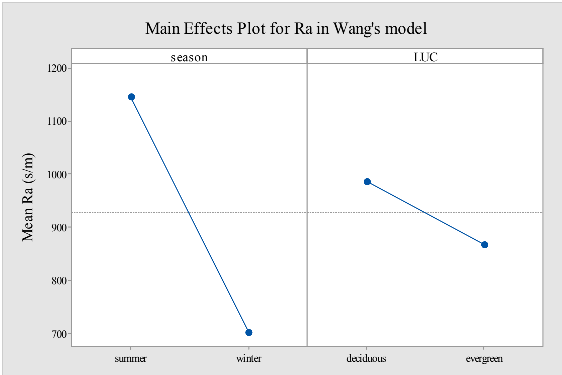
Main Effects Plot for Ra in Wang's model
season
LUC
Mean Ra (s/m)
1200
1100
1000
900
800
700
summer
winter
deciduous
evergreen

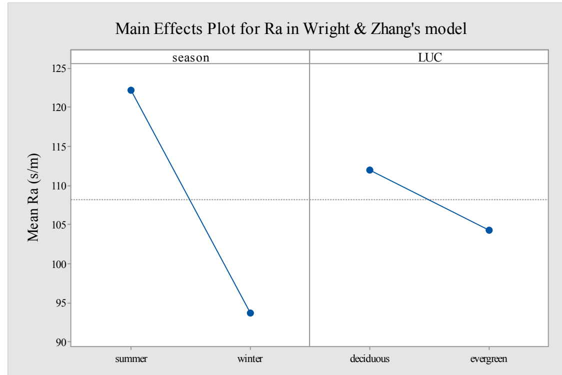
Main Effects Plot for Ra in Wright & Zhang's model
season
LUC
Mean Ra (s/m)
125
120
115
110
105
100
95
90
summer
winter
deciduous
evergreen

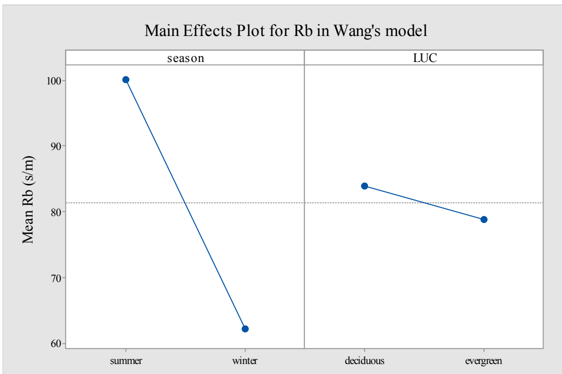
Main Effects Plot for Rb in Wang's model
season
LUC
Mean Rb (s/m)
100
90
80
70
60
summer
winter
deciduous
evergreen

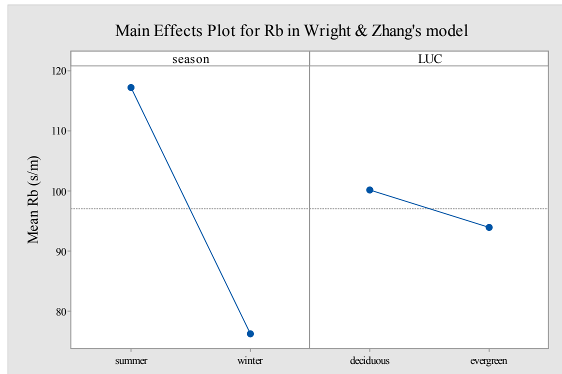
Main Effects Plot for Rb in Wright & Zhang's model
season
LUC
Mean Rb (s/m)
120
110
100
90
80
summer
winter
deciduous
evergreen

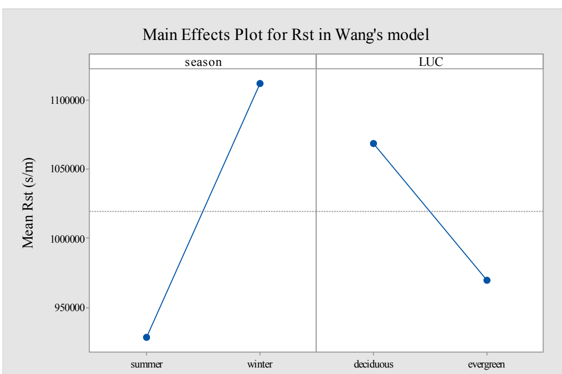
Main Effects Plot for Rst in Wang's model
season
LUC
Mean Rst (s/m)
1100000
1050000
1000000
950000
summer
winter
deciduous
evergreen

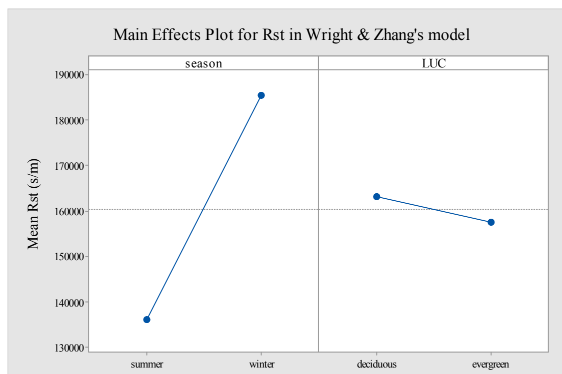
Main Effects Plot for Rst in Wright & Zhang's model
season
LUC
Mean Rst (s/m)
190000
180000
170000
160000
150000
140000
130000
summer
winter
deciduous
evergreen

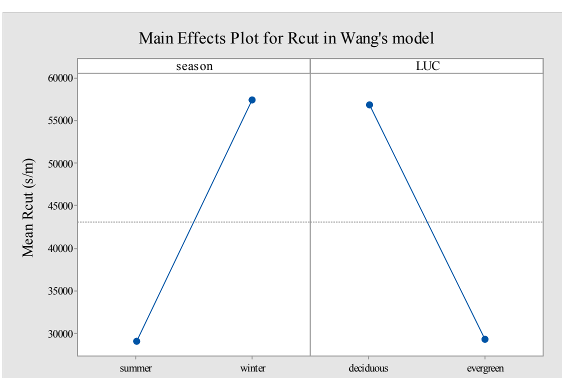
Main Effects Plot for Rcut in Wang's model
season
LUC
Mean Rcut (s/m)
60000
55000
50000
45000
40000
35000
30000
summer
winter
deciduous
evergreen

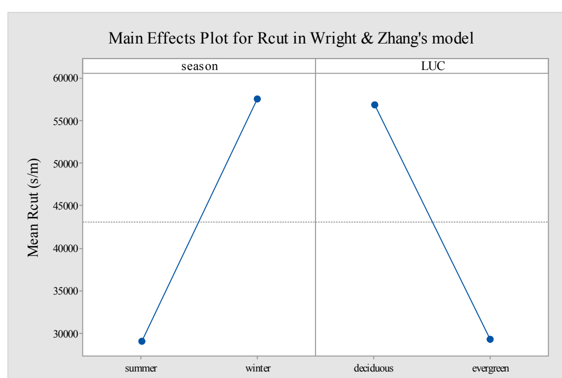
Main Effects Plot for Rcut in Wright & Zhang's model
season
LUC
Mean Rcut (s/m)
60000
55000
50000
45000
40000
35000
30000
summer
winter
deciduous
evergreen

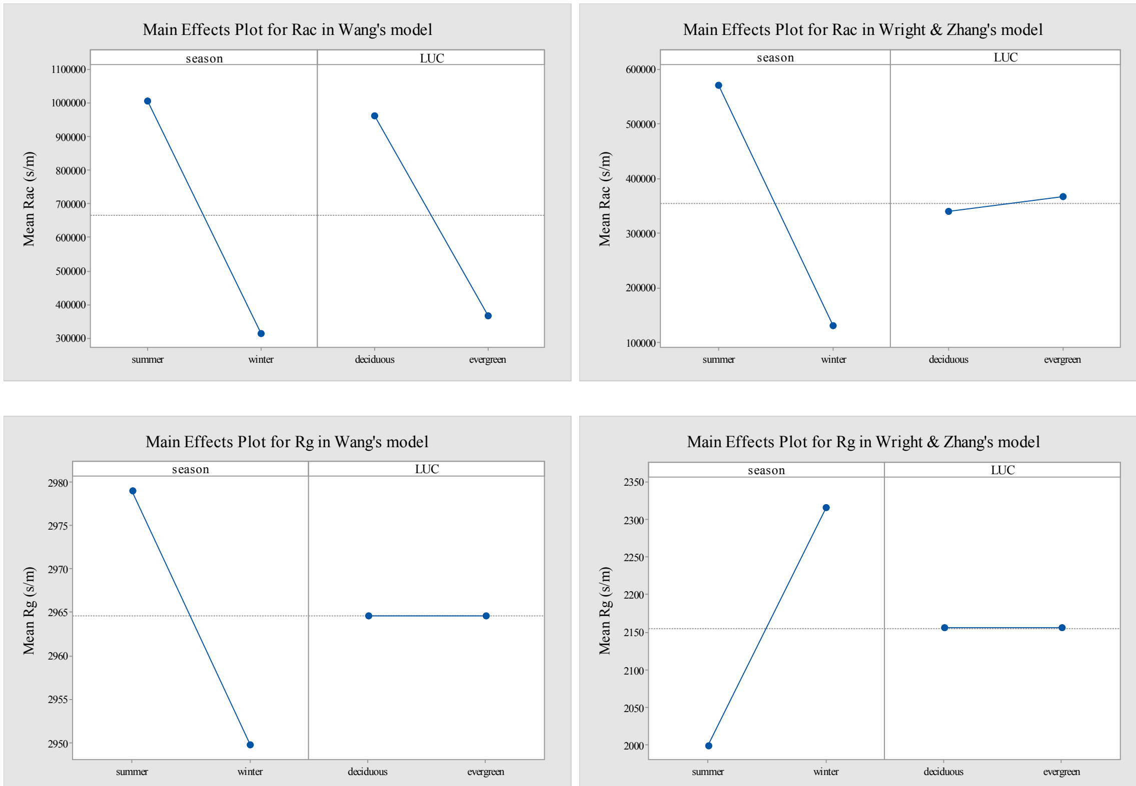

Figure F1. Main effects plot for resistance in the two models.

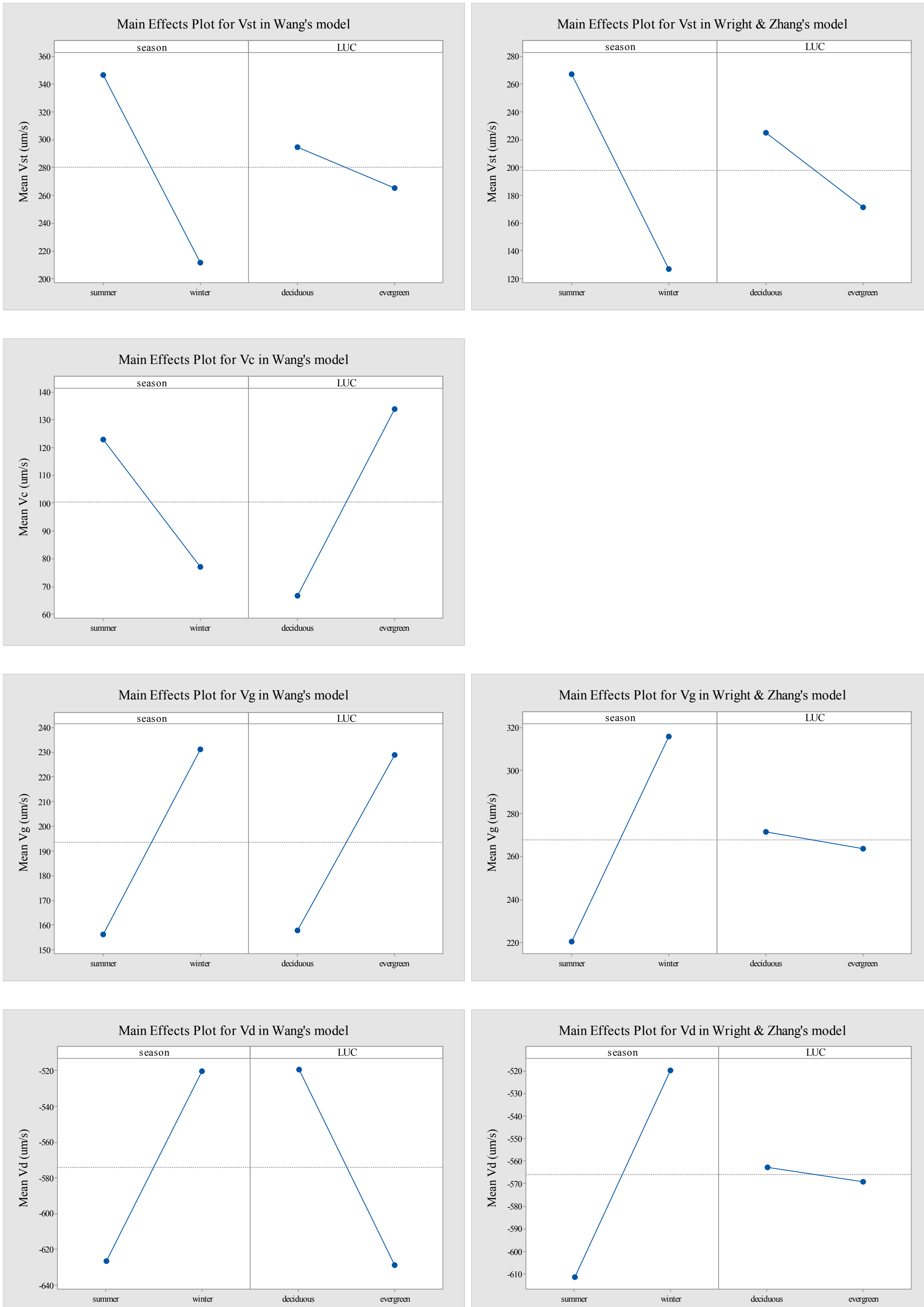

Figure F2. Main effects plot for velocity in the two models.

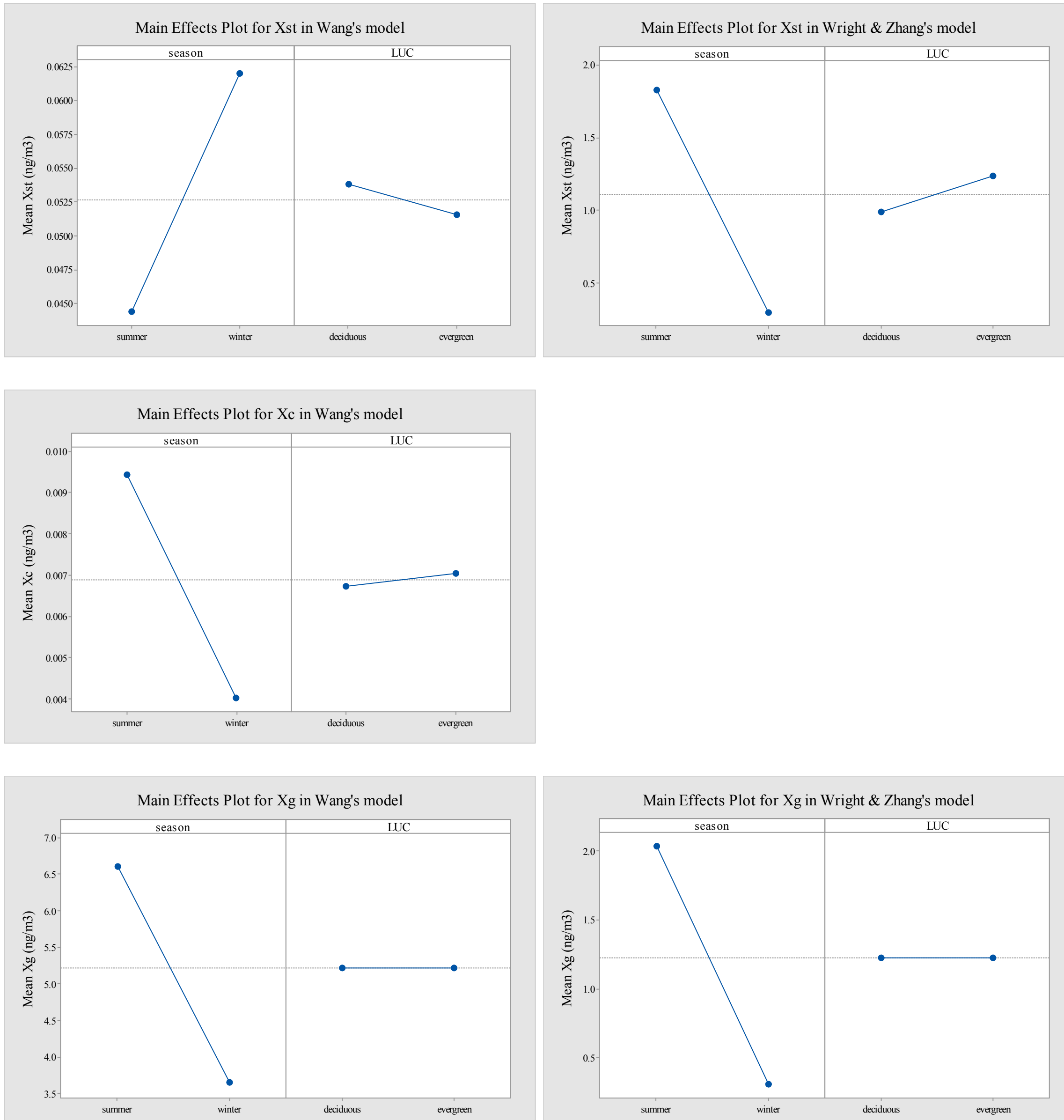

Figure F3. Main effects plot for GEM compensation point concentration in the two models.

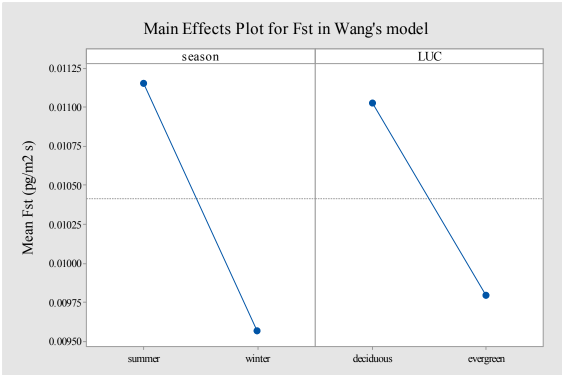
Main Effects Plot for Fst in Wang's model
season
LUC
Mean Fst (pg/m2 s)
0.01125
0.01100
0.01075
0.01050
0.01025
0.01000
0.00975
0.00950
summer
winter
deciduous
evergreen

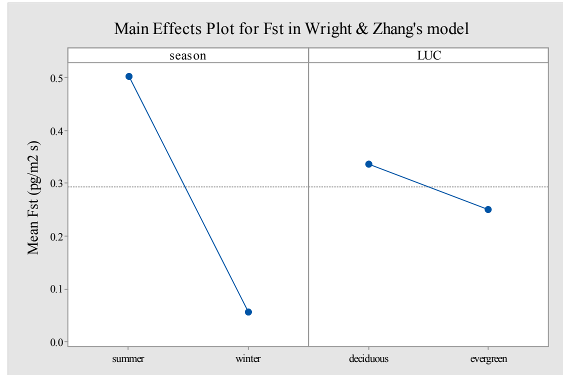
Main Effects Plot for Fst in Wright & Zhang's model
season
LUC
Mean Fst (pg/m2 s)
0.5
0.4
0.3
0.2
0.1
0.0
summer
winter
deciduous
evergreen

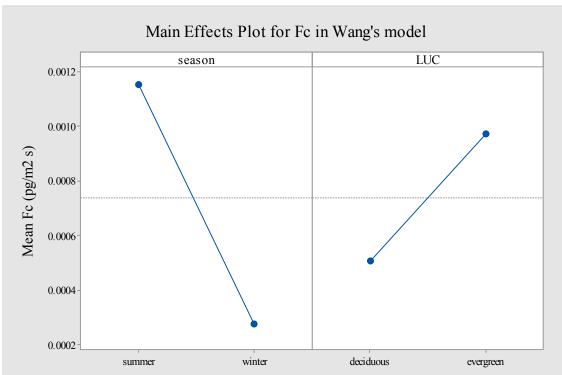
Main Effects Plot for Fc in Wang's model
season
LUC
Mean Fc (pg/m2 s)
0.0012
0.0010
0.0008
0.0006
0.0004
0.0002
summer
winter
deciduous
evergreen

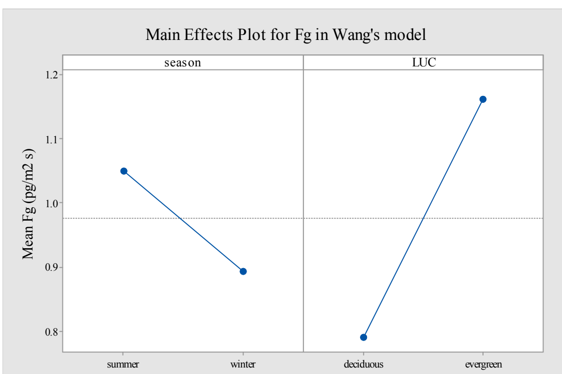
Main Effects Plot for Fg in Wang's model
season
LUC
Mean Fg (pg/m2 s)
1.2
1.1
1.0
0.9
0.8
summer
winter
deciduous
evergreen

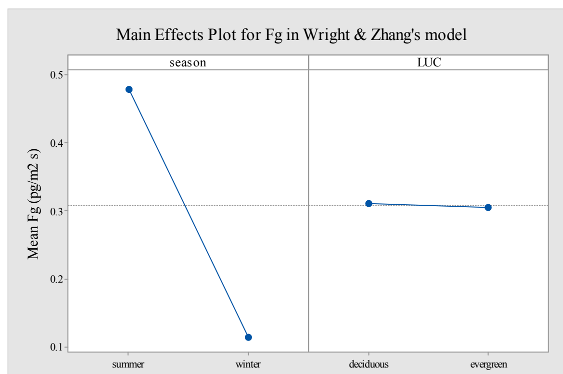
Main Effects Plot for Fg in Wright & Zhang's model
season
LUC
Mean Fg (pg/m2 s)
0.5
0.4
0.3
0.2
0.1
summer
winter
deciduous
evergreen

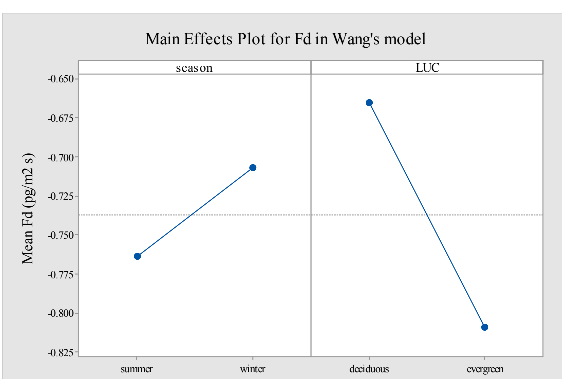
Main Effects Plot for Fd in Wang's model
season
LUC
Mean Fd (pg/m2 s)
-0.650
-0.675
-0.700
-0.725
-0.750
-0.775
-0.800
-0.825
summer
winter
deciduous
evergreen

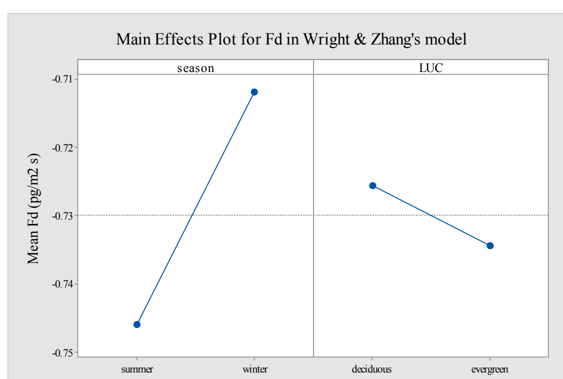
Main Effects Plot for Fd in Wright & Zhang's model
season
LUC
Mean Fd (pg/m2 s)
-0.71
-0.72
-0.73
-0.74
-0.75
summer
winter
deciduous
evergreen

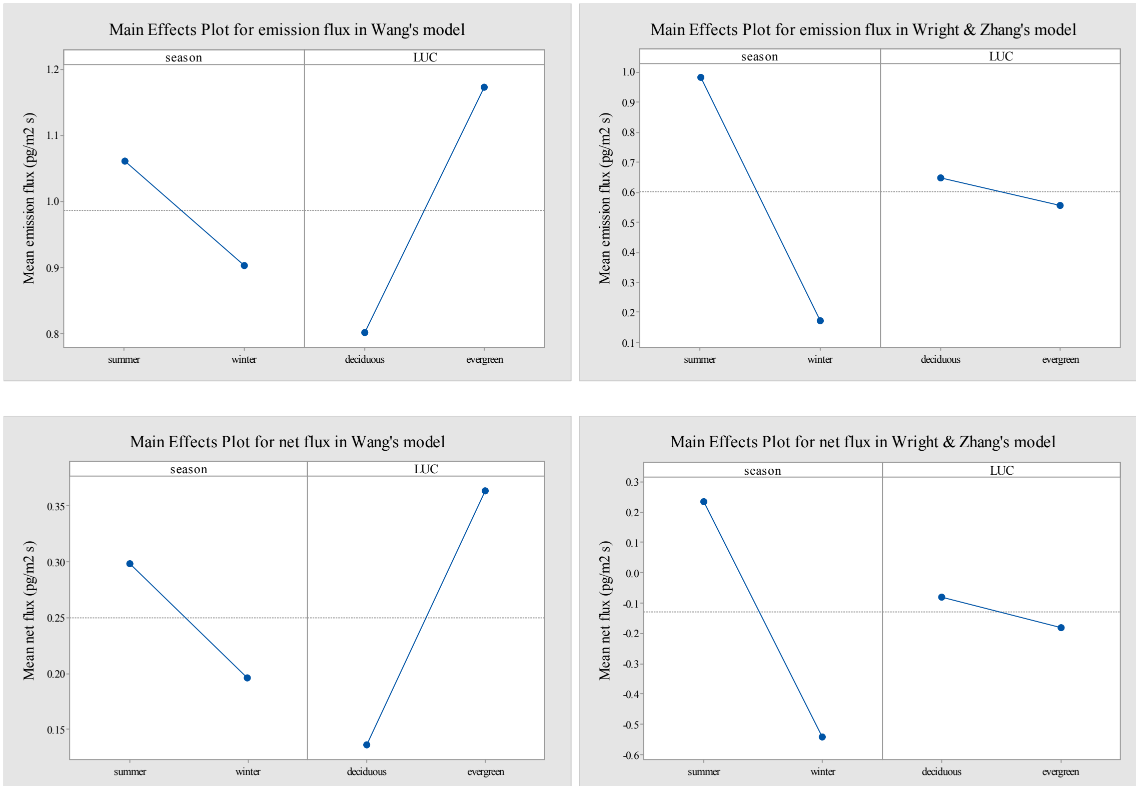

Figure F4. Main effects plot for flux in the two models.

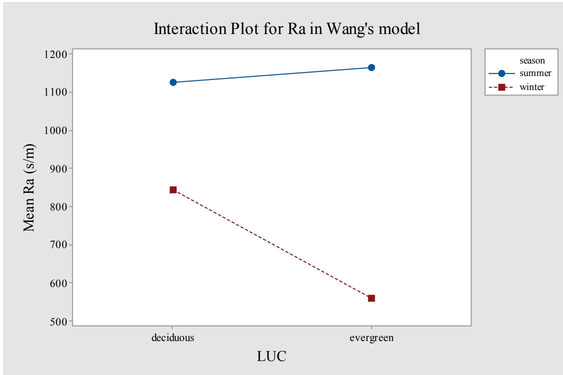
Interaction Plot for Ra in Wang's model
Mean Ra (s/m)
1200
1100
1000
900
800
700
600
500
deciduous
evergreen
LUC
season
summer
winter

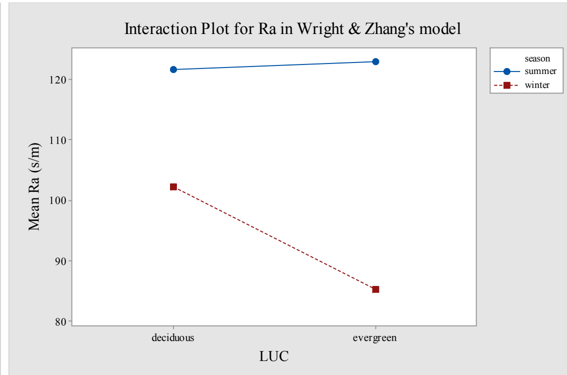
Interaction Plot for Ra in Wright & Zhang's model
Mean Ra (s/m)
120
110
100
90
80
deciduous
evergreen
LUC
season
summer
winter

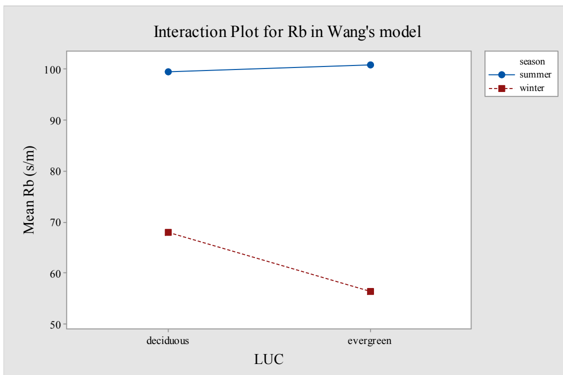
Interaction Plot for Rb in Wang's model
Mean Rb (s/m)
100
90
80
70
60
50
deciduous
evergreen
LUC
season
summer
winter

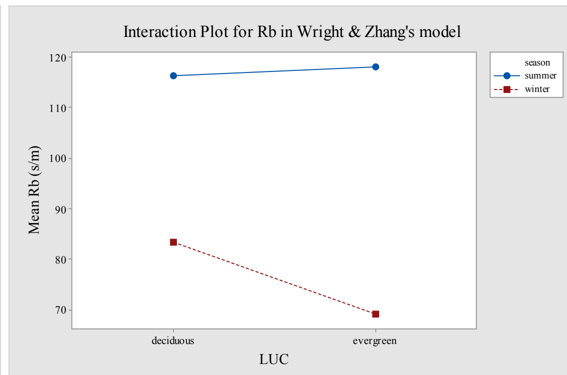
Interaction Plot for Rb in Wright & Zhang's model
Mean Rb (s/m)
120
110
100
90
80
70
deciduous
evergreen
LUC
season
summer
winter

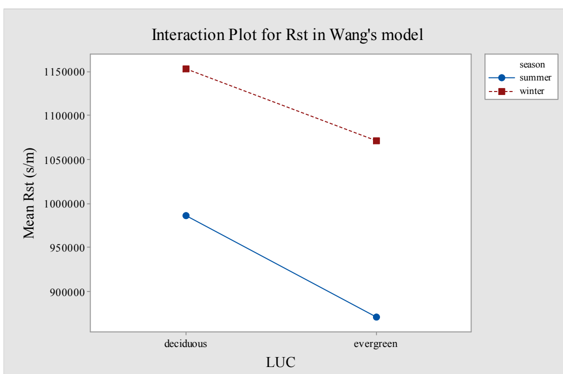
Interaction Plot for Rst in Wang's model
Mean Rst (s/m)
1150000
1100000
1050000
1000000
950000
900000
deciduous
evergreen
LUC
season
summer
winter

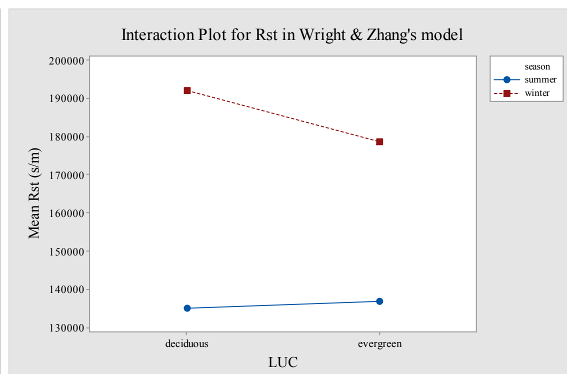
Interaction Plot for Rst in Wright & Zhang's model
Mean Rst (s/m)
200000
190000
180000
170000
160000
150000
140000
130000
deciduous
evergreen
LUC
season
summer
winter

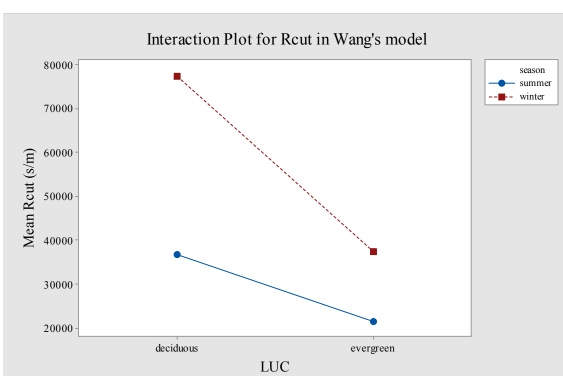
Interaction Plot for Rcut in Wang's model
Mean Rcut (s/m)
80000
70000
60000
50000
40000
30000
20000
deciduous
evergreen
LUC
season
summer
winter

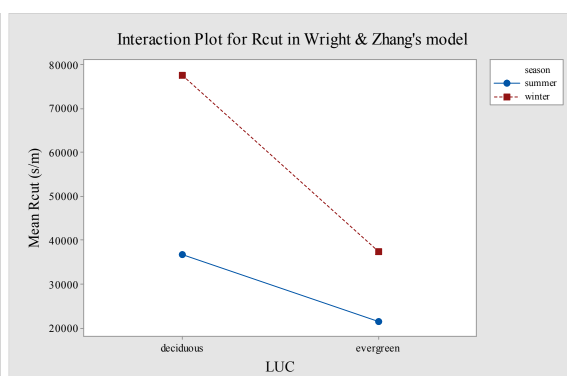
Interaction Plot for Rcut in Wright & Zhang's model
Mean Rcut (s/m)
80000
70000
60000
50000
40000
30000
20000
deciduous
evergreen
LUC
season
summer
winter

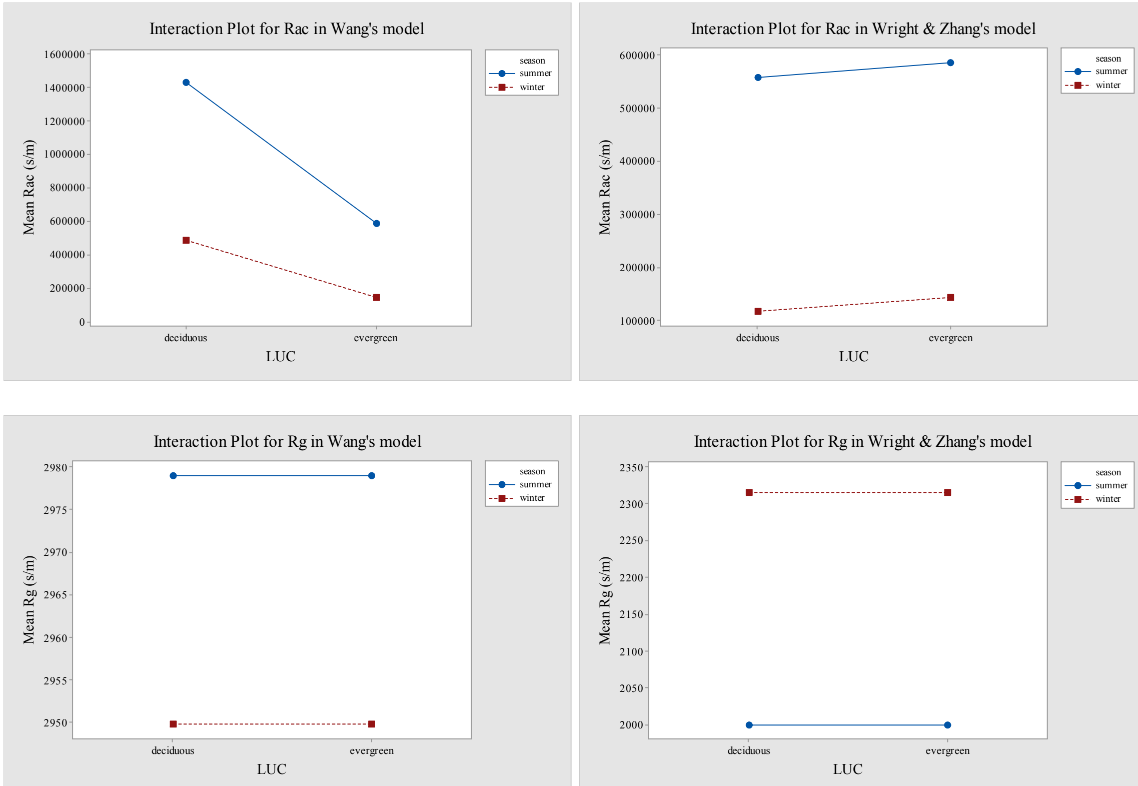

Figure F5. Interaction plot for resistance in the two models.

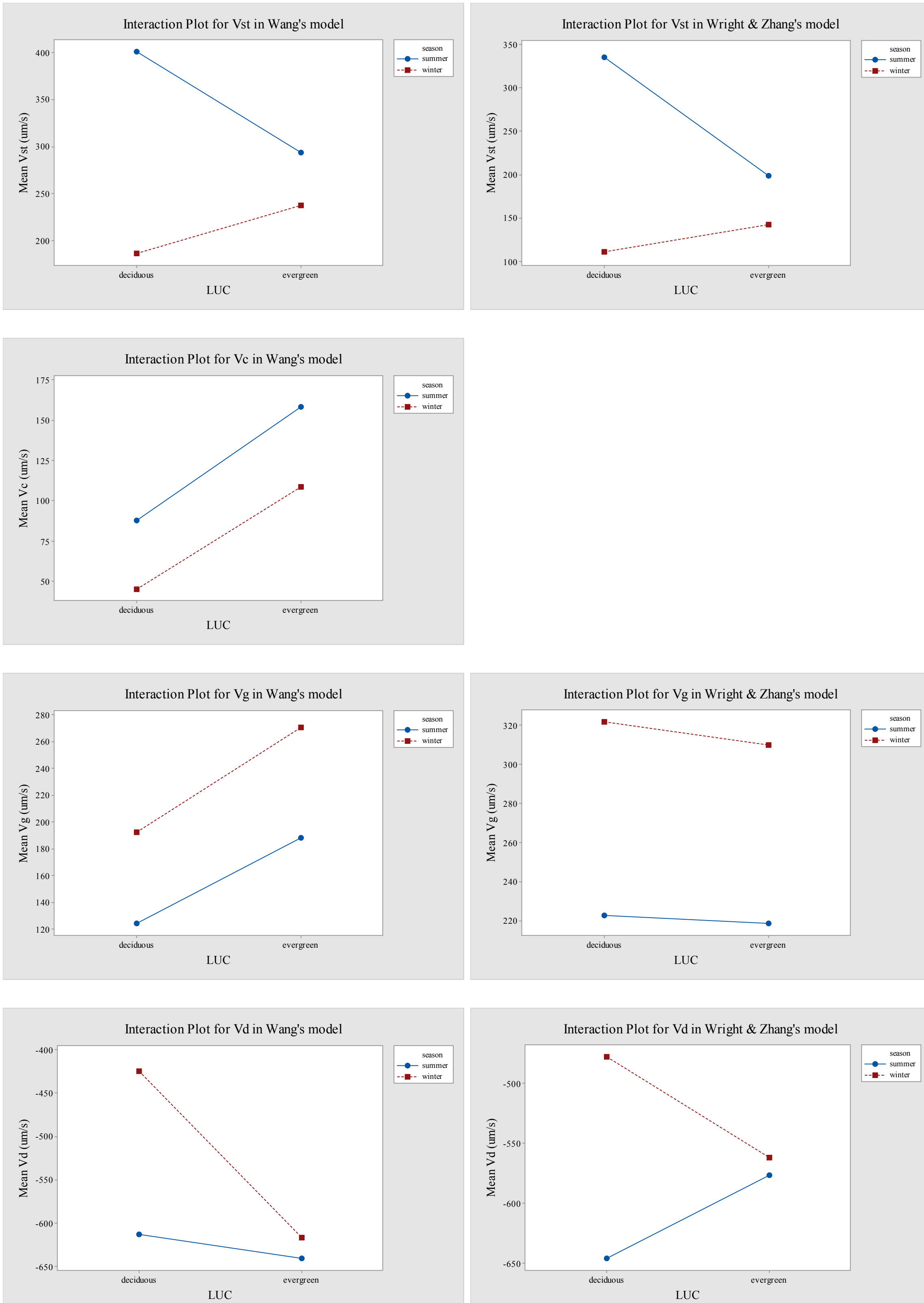

Figure F6. Interaction plot for velocity in the two models.

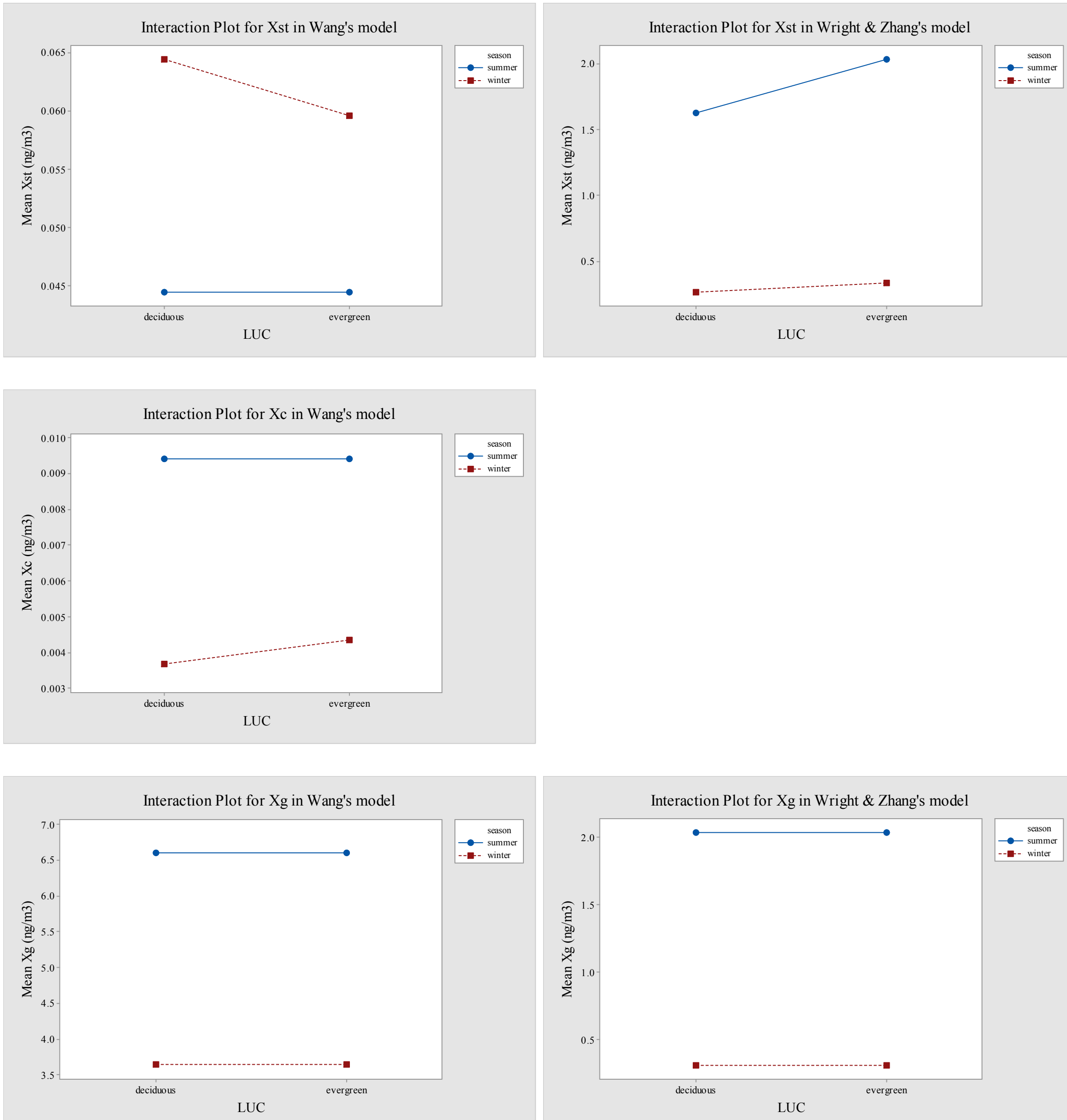

Figure F7. Interaction plot for GEM compensation point concentration in the two models.

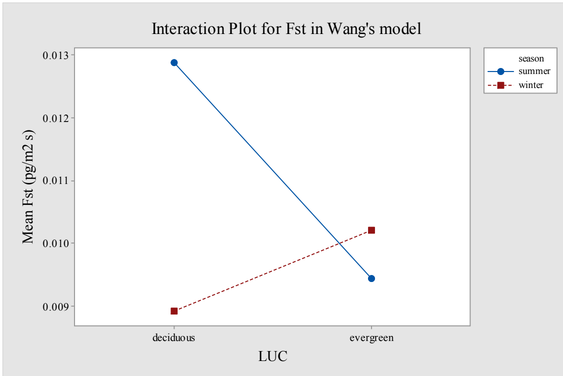
Interaction Plot for Fst in Wang's model
Mean Fst (pg/m2 s)
0.013
0.012
0.011
0.010
0.009
deciduous
evergreen
LUC
season
summer
winter

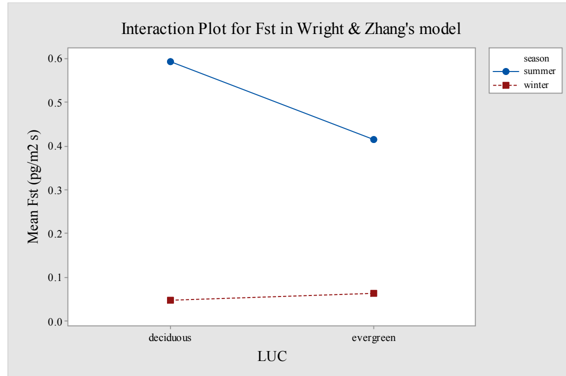
Interaction Plot for Fst in Wright & Zhang's model
Mean Fst (pg/m2 s)
0.6
0.5
0.4
0.3
0.2
0.1
0.0
deciduous
evergreen
LUC
season
summer
winter

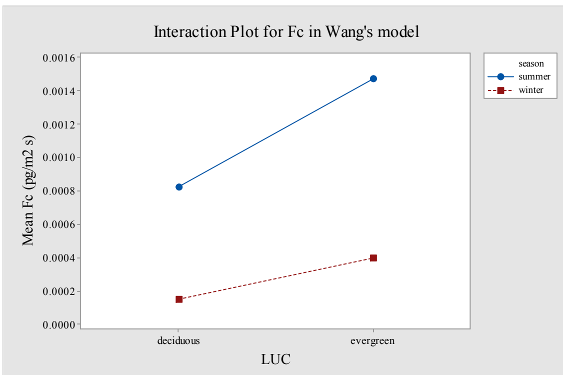
Interaction Plot for Fc in Wang's model
Mean Fc (pg/m2 s)
0.0016
0.0014
0.0012
0.0010
0.0008
0.0006
0.0004
0.0002
0.0000
deciduous
evergreen
LUC
season
summer
winter

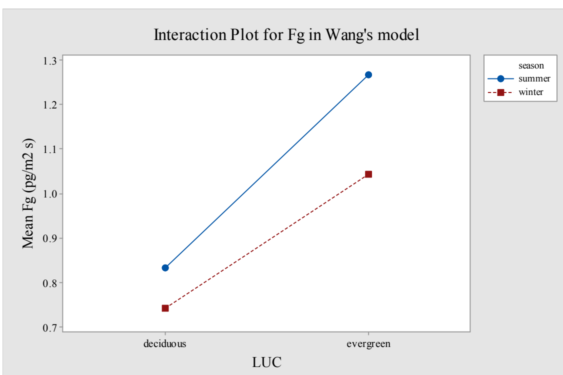
Interaction Plot for Fg in Wang's model
Mean Fg (pg/m2 s)
1.3
1.2
1.1
1.0
0.9
0.8
0.7
deciduous
evergreen
LUC
season
summer
winter

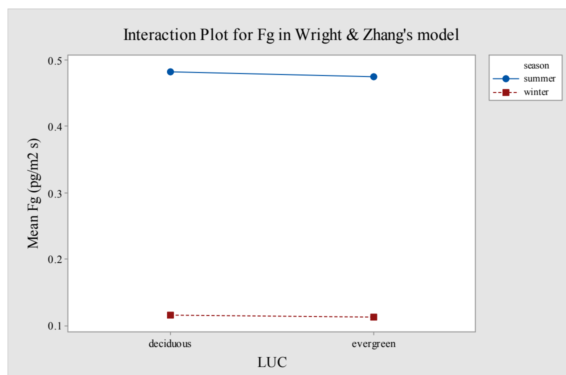
Interaction Plot for Fg in Wright & Zhang's model
Mean Fg (pg/m2 s)
0.5
0.4
0.3
0.2
0.1
deciduous
evergreen
LUC
season
summer
winter

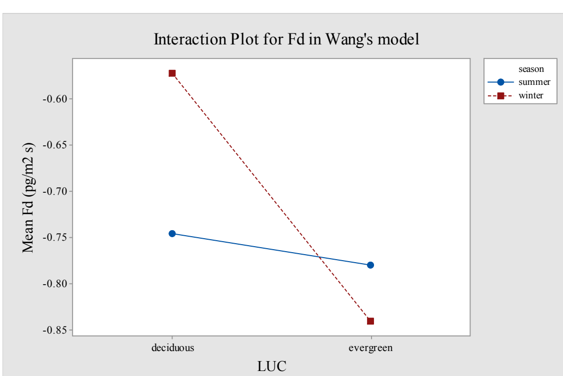
Interaction Plot for Fd in Wang's model
Mean Fd (pg/m2 s)
-0.60
-0.65
-0.70
-0.75
-0.80
-0.85
deciduous
evergreen
LUC
season
summer
winter

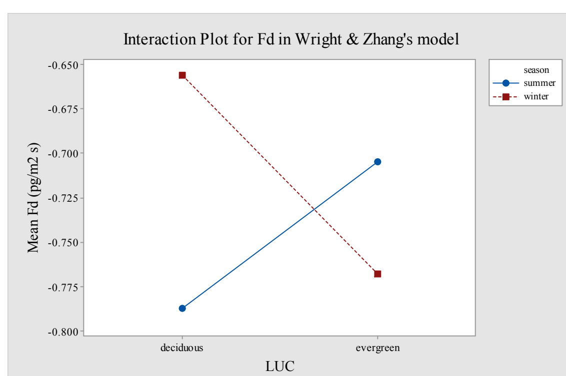
Interaction Plot for Fd in Wright & Zhang's model
Mean Fd (pg/m2 s)
-0.650
-0.675
-0.700
-0.725
-0.750
-0.775
-0.800
deciduous
evergreen
LUC
season
summer
winter

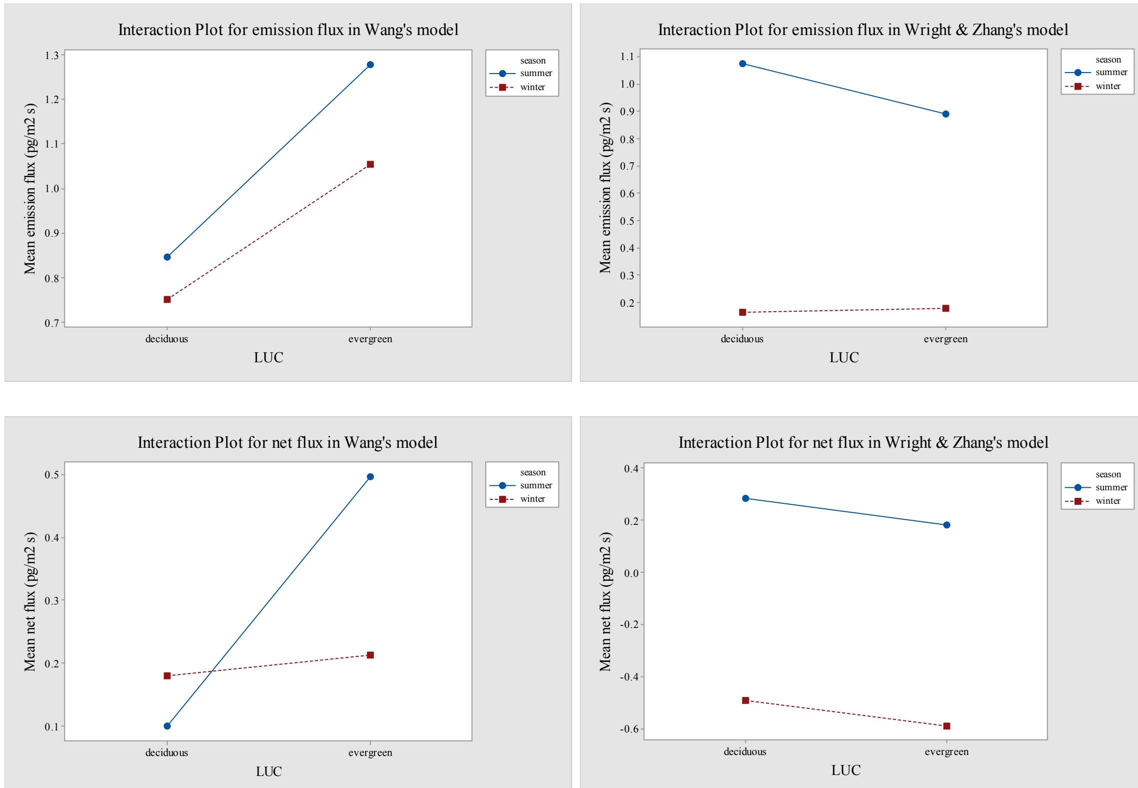

Figure F8. Interaction plot for flux in the two models.

Appendix G: ANOVA analysis for the difference between the two models

Table G1. ANOVA results for the difference in resistance between the two models.

Resistances	Parameters	p-values or R-sq values in the difference (Wang-Wright)/ (Wang+Wright)/2*100%
R_a	Season	0.926
	LUC	0.052
	Season*LUC	0.026
	R-sq (%)	0.08
	R-sq (adj) (%)	0.05
R_b	Season	0.001
	LUC	0.99
	Season*LUC	0.99
	R-sq (%)	69.97
	R-sq (adj) (%)	69.96
R_{st}	Season	0.001
	LUC	0.001
	Season*LUC	0.002
	R-sq (%)	0.69
	R-sq (adj) (%)	0.66
R_{ac}	Season	0.001
	LUC	0.001
	Season*LUC	0.001
	R-sq (%)	99.96
	R-sq (adj) (%)	99.96
R_g	Season	0.001
	LUC	0.99
	Season*LUC	0.99
	R-sq (%)	1.72
	R-sq (adj) (%)	1.7

Table G2. ANOVA results for the difference in velocity between the two models.

Velocities	Parameters	p-values or R-sq values in the difference (Wang-Wright)/ (Wang+Wright)/2*100%
V_{st}	Season	0.001
	LUC	0.001
	Season*LUC	0.002
	R-sq (%)	0.67
	R-sq (adj) (%)	0.64
V_g	Season	0.001
	LUC	0.001
	Season*LUC	0.001
	R-sq (%)	38.89
	R-sq (adj) (%)	38.87
V_d	Season	0.001
	LUC	0.001
	Season*LUC	0.001
	R-sq (%)	18.78
	R-sq (adj) (%)	18.76

Table G3. ANOVA results for the difference in GEM compensation point concentration between the two models.

GEM compensation point concentrations	Parameters	p-values or R-sq values in the difference (Wang-Wright)/ (Wang+Wright)/2*100%
χ_{st}	Season	0.001
	LUC	0.001
	Season*LUC	0.001
	R-sq (%)	56.68
	R-sq (adj) (%)	56.66
χ_g	Season	0.001
	LUC	0.99
	Season*LUC	0.99
	R-sq (%)	73.21
	R-sq (adj) (%)	73.2

Table G4. ANOVA results for the difference in flux between the two models.

Fluxes	Parameters	p-values or R-sq values in the difference (Wang-Wright)/ (Wang+Wright)/2*100%
F_{st}	Season	0.001
	LUC	0.001
	Season*LUC	0.097
	R-sq (%)	20.91
	R-sq (adj) (%)	20.89
F_g	Season	0.001
	LUC	0.001
	Season*LUC	0.001
	R-sq (%)	74.07
	R-sq (adj) (%)	74.06
F_d	Season	0.001
	LUC	0.001
	Season*LUC	0.001
	R-sq (%)	19.37
	R-sq (adj) (%)	19.35
total emission flux	Season	0.001
	LUC	0.001
	Season*LUC	0.001
	R-sq (%)	55.23
	R-sq (adj) (%)	55.22
net flux	Season	0.068
	LUC	0.007
	Season*LUC	0.004
	R-sq (%)	0.18
	R-sq (adj) (%)	0.15

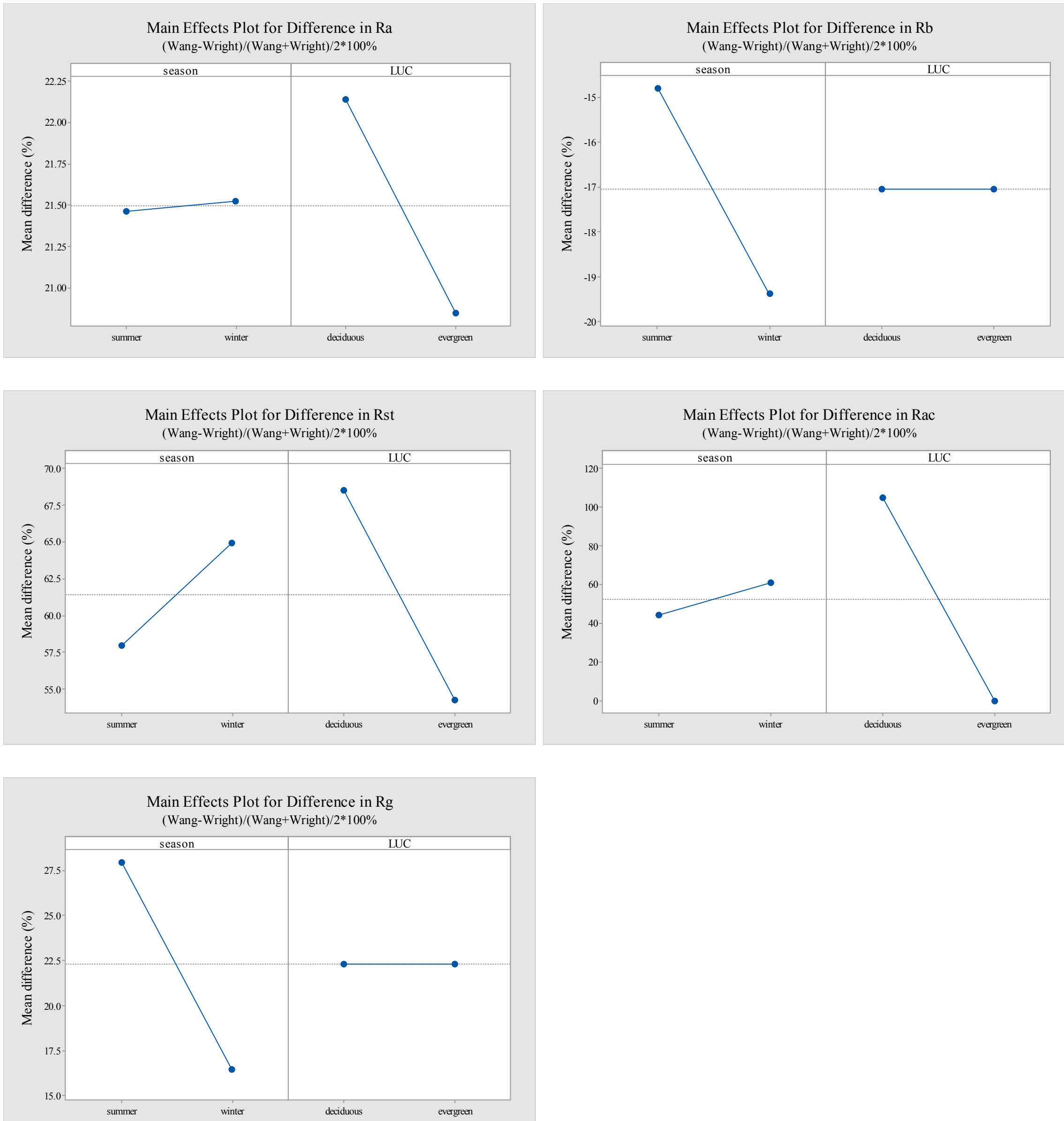

Figure G1. Main effects plot for the difference in resistance.

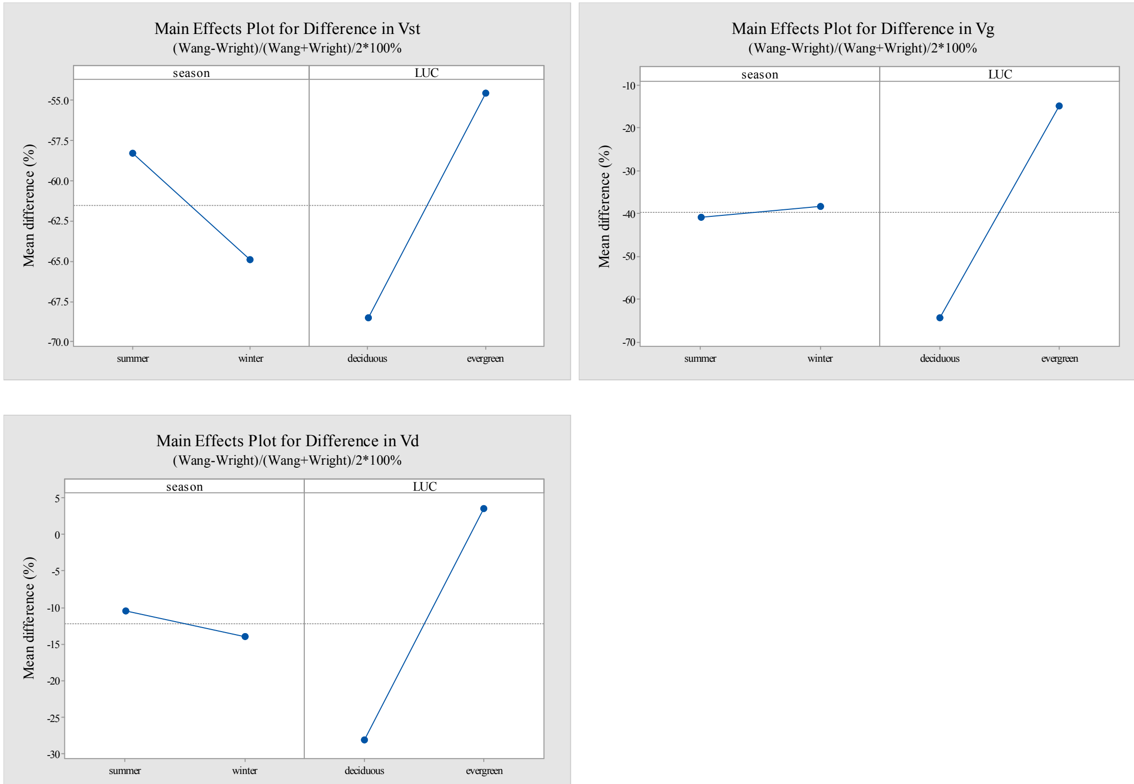

Figure G2. Main effects plot for the difference in velocity.

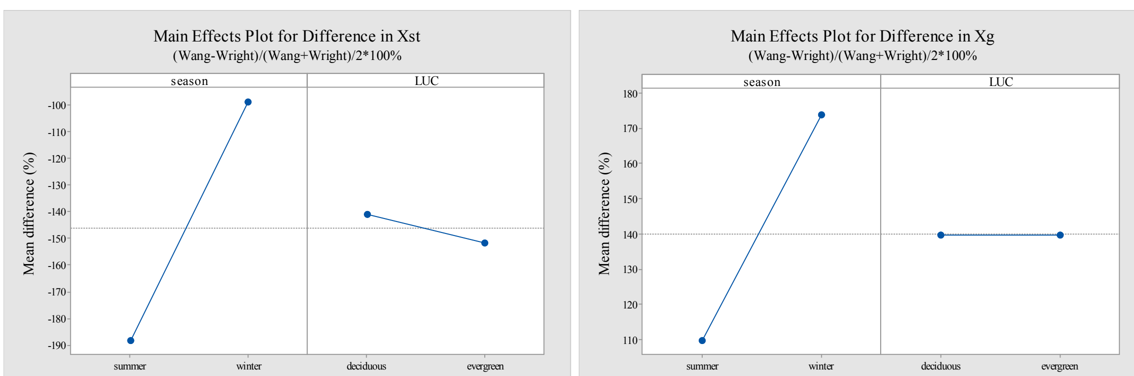

Figure G3. Main effects plot for the difference in GEM compensation point concentration.

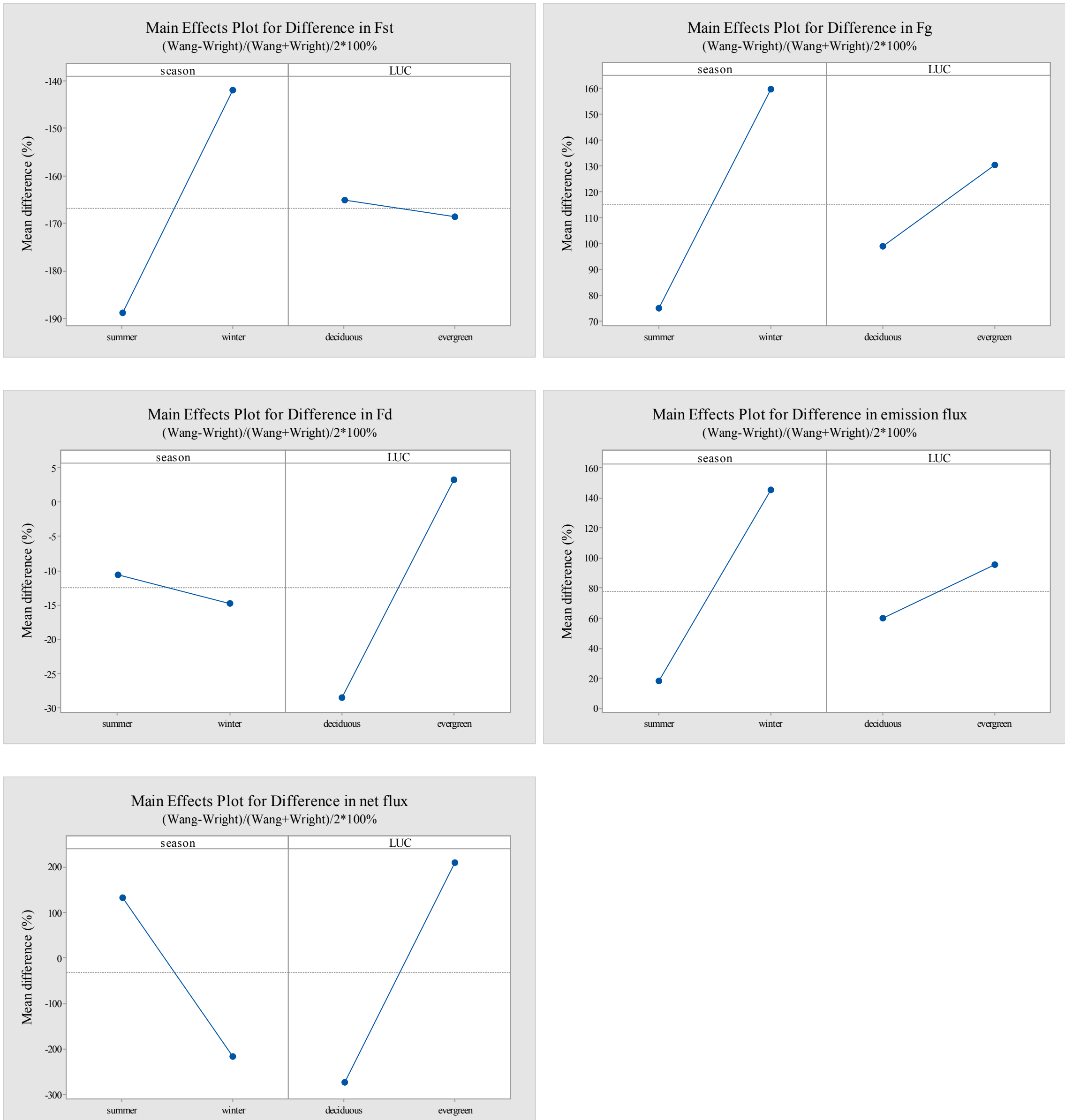

Figure G4. Main effects plot for the difference in flux.

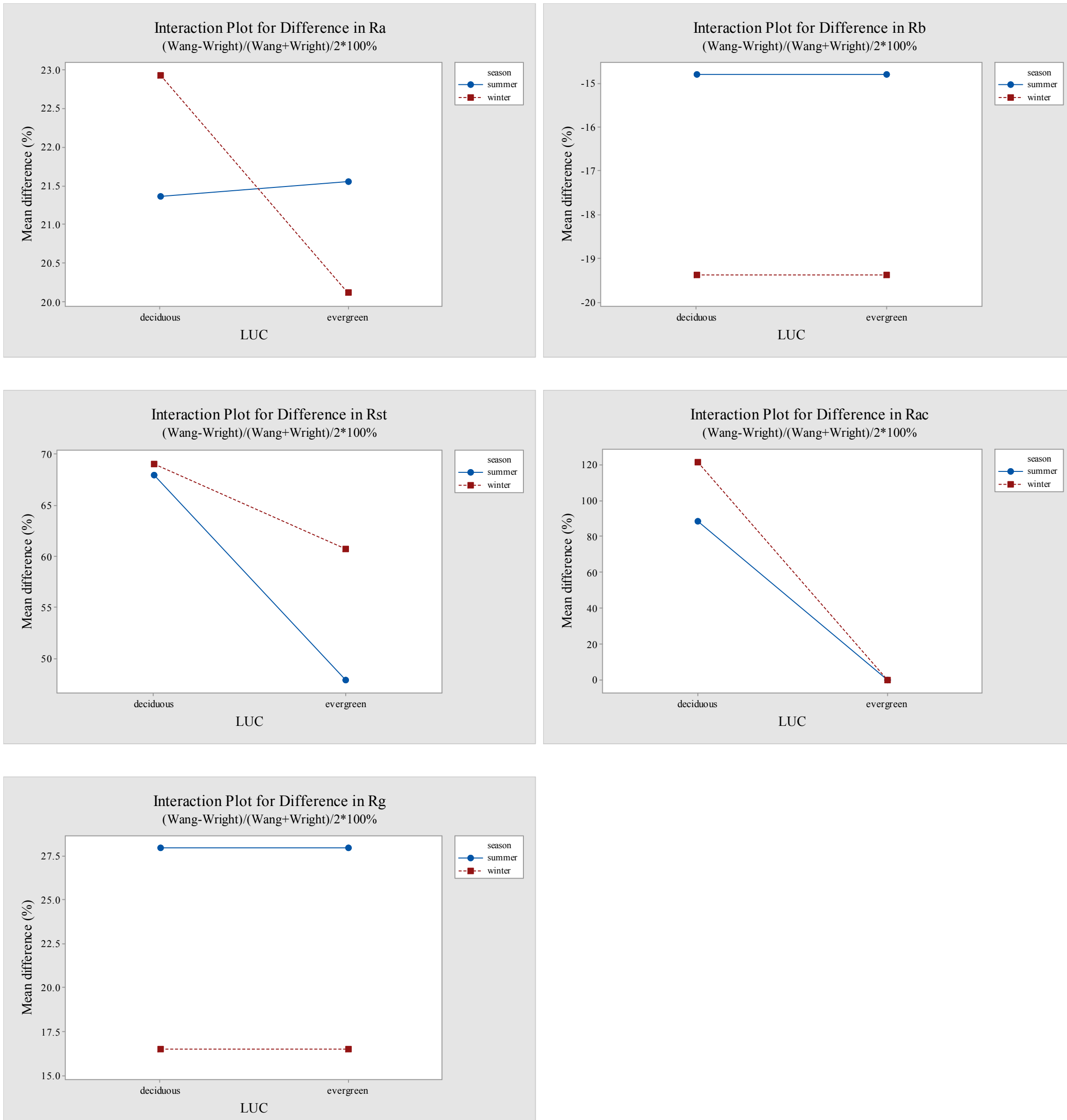

Figure G5. Interaction plot for the difference in resistance.

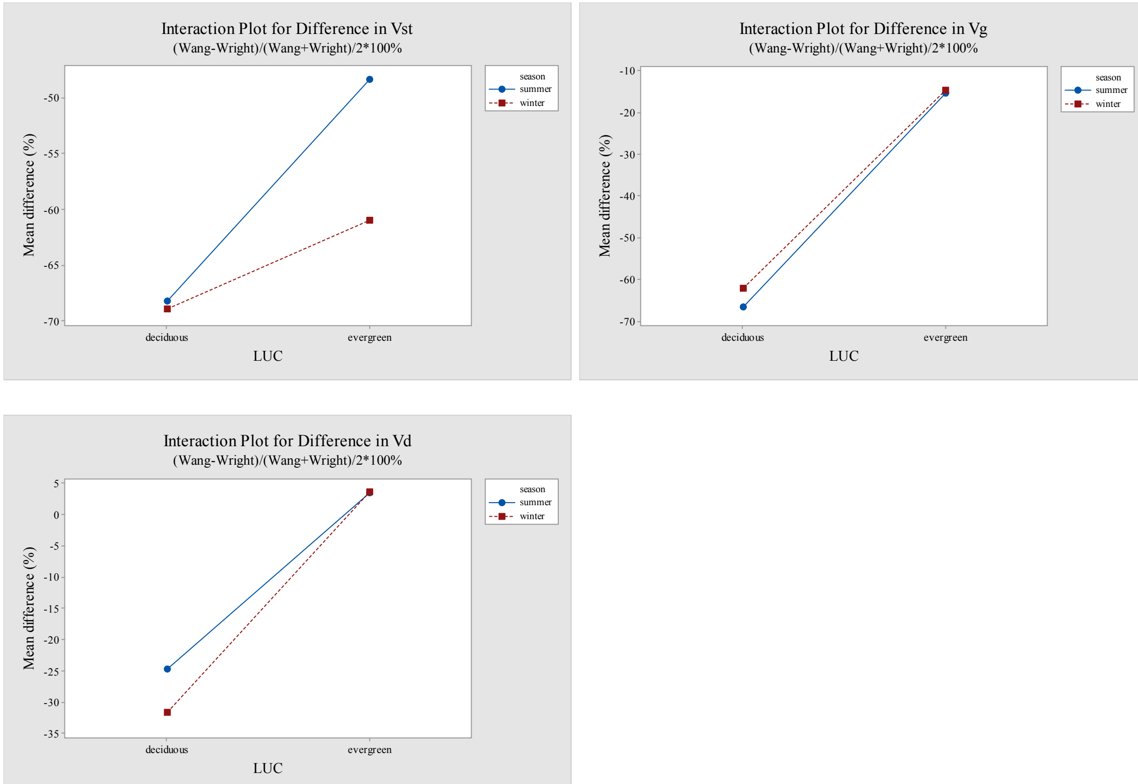

Figure G6. Interaction plot for the difference in velocity.

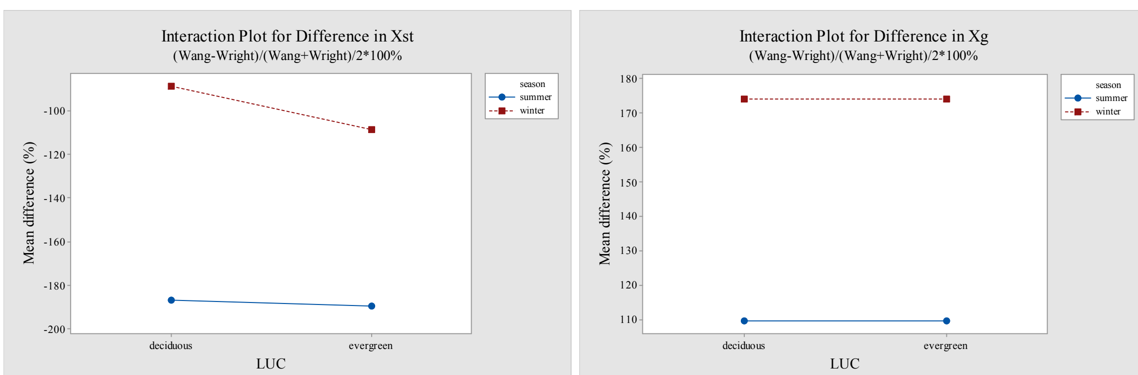

Figure G7. Interaction plot for the difference in GEM compensation point concentration.

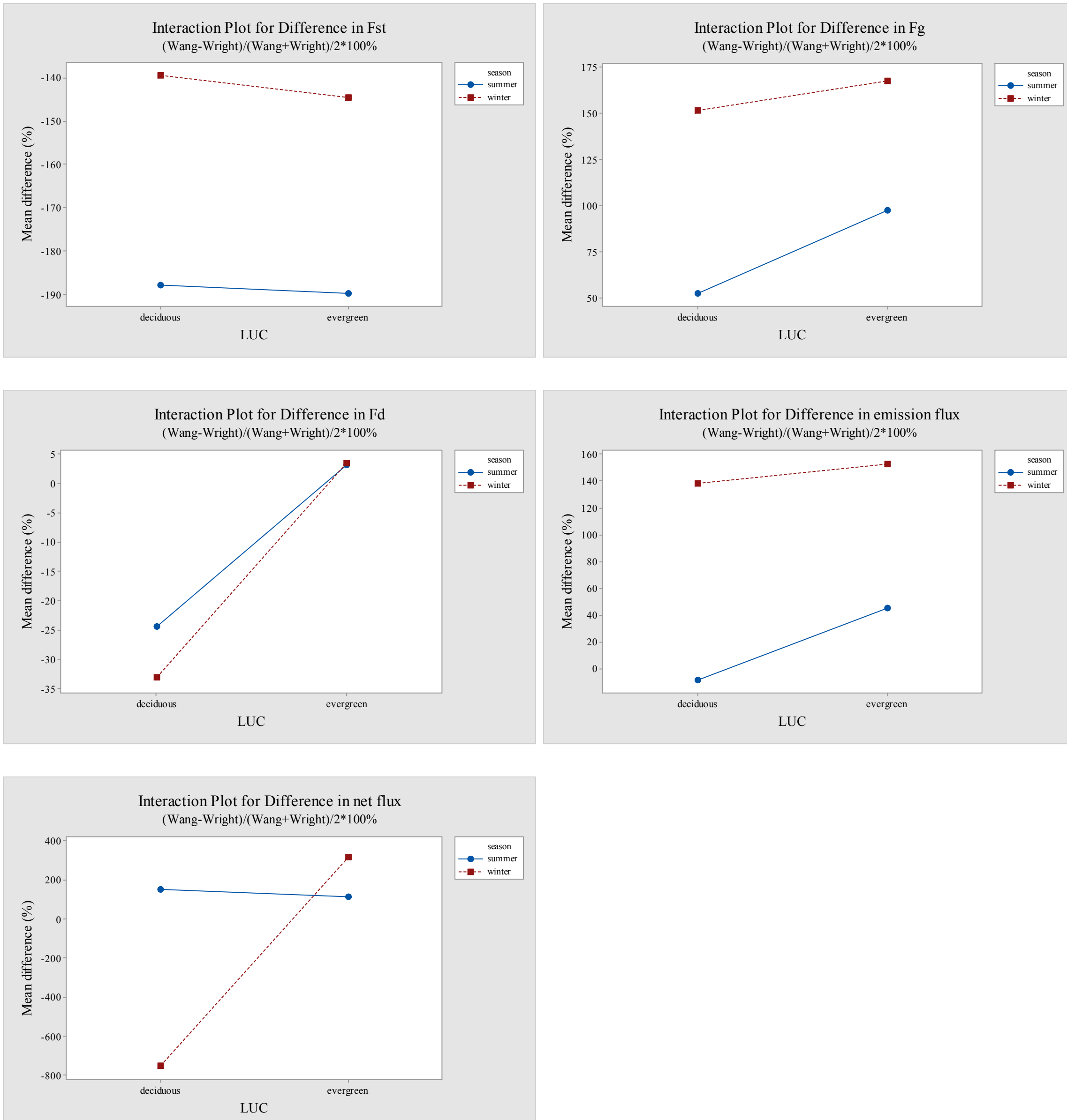

Figure G8. Interaction plot for the difference in flux.

VITA AUCTORIS

NAME:	Jingliang Hao
PLACE OF BIRTH:	China
YEAR OF BIRTH:	1994
EDUCATION:	Nanjing University of Information Science & Technology, B.Sc., Atmospheric Physics, Nanjing, Jiangsu, 2013-2017